Journal of Atomic, Molecular, and Optical Physics

Recent Advances in Spectroscopy of Hydrogen-Bonded Systems

Guest Editors: Marek J. Wójcik, Paul Blaise, Henryk Flakus, and Joanna Sadlej

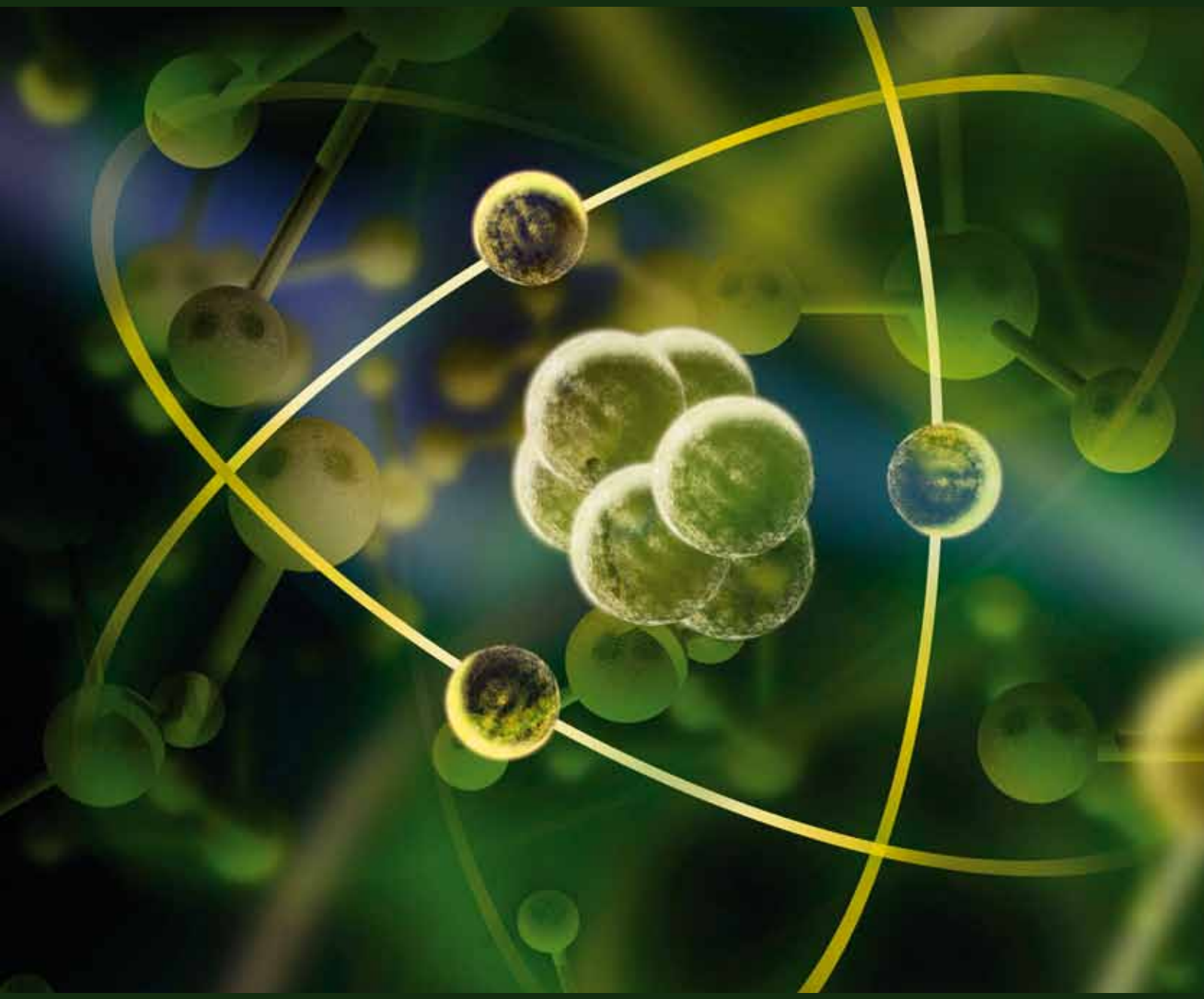

Recent Advances in Spectroscopy of Hydrogen-Bonded Systems

Journal of Atomic, Molecular, and Optical Physics

Recent Advances in Spectroscopy of Hydrogen-Bonded Systems

Guest Editors: Marek J. Wójcik, Paul Blaise, Joanna Sadlej, and Henryk Flakus

Copyright © 2012 Hindawi Publishing Corporation. All rights reserved.

This is a special issue published in "Journal of Atomic, Molecular, and Optical Physics." All articles are open access articles distributed under the Creative Commons Attribution License, which permits unrestricted use, distribution, and reproduction in any medium, provided the original work is properly cited.

Editorial Board

Miron Ya Amusia, Israel
Dimitris G. Angelakis, Singapore
Vanderlei Bagnato, Brazil
Yehuda B. Band, Israel
André D. Bandrauk, Canada
Raul A. Baragiola, USA
Klaus R. Bartschat, USA
Shih I. Chu, USA
John Costello, Ireland
Derrick S. F. Crothers, UK
Nir Davidson, Israel
Edward E. Eyler, USA
Z. Ficek, Australia
Dong-Sheng Guo, USA
Keli Han, China
Jan Petter Hansen, Norway
Mark D. Havey, USA
Hanspeter Helm, Germany
Elliot P. Kanter, USA
George C. King, UK
Paul Kleiber, USA
Predrag S. Krstic, USA
Gregory Lapicki, USA
Boris A. Malomed, Israel
Nigel J. Mason, UK
J. W. McConkey, Canada
Alan Migdall, USA
Takamasa Momose, Canada
Robert Moshammer, Germany
Juan Gonzalo Muga, Spain
Ivo Nezbeda, Czech Republic
Cleanthes A. Nicolaides, Greece
R. F. O'Connell, USA
Anil K. Pradhan, USA
Ali Hussain Reshak, Czech Republic
Roberto Daniel Rivarola, Argentina
M. Rosenbluh, Israel
Hari P. Saha, USA
H. Schmidt, Sweden
Vladimir M. Shabaev, Russia
Robert Spreeuw, The Netherlands
Andris Stelbovics, Australia
Thomas H. Stohlker, Germany
Steven Stolte, China
Kalle-Antti Suominen, Finland
Colm T. Whelan, USA
Jim F. Williams, Australia
Jory A. Yarmoff, USA
Jianping Yin, China

Contents

Hindawi Publishing Corporation
Journal of Atomic, Molecular, and Optical Physics
Volume 2012, Article ID 174236, 1 page
doi:10.1155/2012/174236

Editorial

Recent Advances in Spectroscopy of Hydrogen-Bonded Systems

Marek J. Wójcik,[1] Paul Blaise,[2] Joanna Sadlej,[3] and Henryk Flakus[4]

[1] *Faculty of Chemistry, Jagiellonian University, Ingardena 3, 30-060 Krakow, Poland*
[2] *Laboratoire "Mathématiques et Physique" (LAMPS), Université de Perpignan, 52 Avenue Paul Alduy, 66860 Perpignan Cedex, France*
[3] *Faculty of Chemistry, University of Warsaw, Pasteura 1, 02-093 Warsaw, Poland*
[4] *Institute of Chemistry, University of Silesia, Szkolna 9, 40-006 Katowice, Poland*

Correspondence should be addressed to Marek J. Wójcik, wojcik@chemia.uj.edu.pl

Received 13 August 2012; Accepted 13 August 2012

Copyright © 2012 Marek J. Wójcik et al. This is an open access article distributed under the Creative Commons Attribution License, which permits unrestricted use, distribution, and reproduction in any medium, provided the original work is properly cited.

Hydrogen bond plays a crucial role in many areas of physics, chemistry, and biology. This issue compiles five exciting papers presenting the state of the art in spectroscopic and computational aspects of hydrogen-bonded systems in three original research articles and two reviews.

These papers will stimulate the continuing efforts to understand molecular interactions in hydrogen-bonded complexes, liquids and solids, the development of experimental and theoretical strategies to treat hydrogen-bonded systems, and the new evaluation of outcomes.

The papers describe new methods for characterization of spectra, advances in molecular description of molecular interactions in hydrogen-bonded systems, new insights into molecular models, and current concepts in the treatment of small and large hydrogen-bonded systems. The topics include recent developments in experimental and theoretical studies of hydrogen-bonded systems, advances in theoretical models of hydrogen bonds, spectroscopy of hydrogen bonds in excited electronic states, proton transfer in hydrogen-bonded complexes, photophysics of hydrogen-bonded systems, polymorphism, and dynamical aspects of hydrogen bonding.

In the paper by A. Gorski et al., the authors discuss polymorphism, hydrogen bond properties, and vibrational structure of 1*H*-pyrrolo[3,2-*h*]quinoline dimers performing analysis of IR and Raman spectra, combined with DFT calculations. Theoretical investigation of the cooperativity in the $CH_3CHO \cdot 2H_2O$, $CH_2FCHO \cdot 2H_2O$, and $CH_3CFO \cdot 2H_2O$ systems is presented in the paper by A. K. Chandra and T. Zeegers-Huyskens. Temperature and H/D isotopic effects in the IR spectra of the hydrogen bond in solid-state 2-furanacetic acid and 2-furanacrylic acid are discussed in the paper by H. Flakus and A. Jarczyk.

L. Sobczyk et al. review proton transfer equilibria and critical behavior of H-bonding. They analyze the hydrogen bond properties of the acid-base systems depending on the ability of the proton transfer in the formulation of the Brönsted approach. M. J. Wójcik et al. present theoretical studies of dynamic interactions in excited states of hydrogen-bonded systems. They present model for vibrational interactions in the hydrogen-bonded dimer of benzoic acid in electronically excited state which is used for theoretical simulation of the O–H stretching IR absorption bands and calculate tunneling splittings for vibrationally excited states in electronically excited tropolone.

By compiling these papers, we hope to enrich our readers and researchers with respect to the modern problems of spectroscopy of hydrogen-bonded systems.

Marek J. Wójcik
Paul Blaise
Joanna Sadlej
Henryk Flakus

Hindawi Publishing Corporation
Journal of Atomic, Molecular, and Optical Physics
Volume 2012, Article ID 125471, 17 pages
doi:10.1155/2012/125471

Research Article

Temperature and H/D Isotopic Effects in the IR Spectra of the Hydrogen Bond in Solid-State *2-Furanacetic Acid* and *2-Furanacrylic Acid*

Henryk T. Flakus and Anna Jarczyk-Jędryka

Institute of Chemistry, University of Silesia, 9 Szkolna Street, 40-006 Katowice, Poland

Correspondence should be addressed to Henryk T. Flakus, flakus@ich.us.edu.pl

Received 1 March 2012; Revised 16 June 2012; Accepted 4 July 2012

Academic Editor: Joanna Sadlej

Copyright © 2012 H. T. Flakus and A. Jarczyk-Jędryka. This is an open access article distributed under the Creative Commons Attribution License, which permits unrestricted use, distribution, and reproduction in any medium, provided the original work is properly cited.

Polarized IR spectra of *2-furanacetic acid* and of *2-furanacrylic acid* crystals were measured at 293 K and 77 K in the ν_{O-H} and ν_{O-H} band frequency ranges. The corresponding spectra of the two individual systems strongly differ, one from the other, by the corresponding band shapes as well as by the temperature effect characterizing the bands. The crystal spectral properties remain in a close relation with the electronic structure of the two different molecular systems. We show that a vibronic coupling mechanism involving the hydrogen bond protons and the electrons on the π-electronic systems in the molecules determines the way in which the vibrational exciton coupling between the hydrogen bonds in the carboxylic acid dimers occurs. A strong coupling in *2-furanacrylic acid* dimers prefers a "*tail-to-head-*" type *Davydov coupling* widespread by the π-electrons. A weak *through-space* coupling in *2-furanacetic acid* dimers is responsible for a "*side-to-side-*" type coupling. The relative contribution of each exciton coupling mechanism in the dimer spectra generation is temperature and the molecular electronic structure dependent. This explains the observed difference in the temperature-induced evolution of the compared spectra.

1. Introduction

Infrared spectroscopy still constitutes a basic tool in the research of the hydrogen bond dynamics. The ν_{X-H} bands measured in the highest frequency range of the mid-infrared attributed to the proton stretching vibrations in X–H$\cdots$Y hydrogen bonds are the source of wealth data system in this matter. Complex fine structure patterns of these bands are considered as the result of anharmonical coupling mechanisms involving the proton stretching vibrations and other normal vibrations occurring in associated molecular systems, mainly the low-frequency X$\cdots$Y hydrogen bridge stretching vibrational motions [1–5]. The band contour shapes are extremely susceptible on the influences exerted by diverse physical factors, such as changes of temperature, changes in the matter state of condensation, pressure, and solvents [1–5].

Among the contemporary theories of the IR spectra of the hydrogen bond, formed in molecular systems, quantitative theoretical models elaborated for the description of the ν_{X-H} band generation mechanisms are of the particular importance. There are two most advanced quantitative theoretical models, namely, the "*strong-coupling*" theory [6–8] (the elder theory) and the "*relaxation*" (*linear response*) theory, the novel model [9, 10]. Both models are of a purely vibrational nature. Over the last four decades, by using of these theories, IR spectra of diverse hydrogen bond systems have been reproduced satisfactorily. The model calculations concerned quantitative interpretation of spectra of single, isolated hydrogen bonds [7, 11], spectra of cyclic dimeric hydrogen bond systems [7, 12–14], and the IR spectra of hydrogen-bonded molecular crystals [15]. Simultaneously, the H/D isotopic effects observed in the spectra of the deuterium-bonded corresponding systems have been interpreted [7–15].

Nevertheless, despite the doubtless successes achieved in this area, when interpreting the hydrogen bond system spectra, it seems that a number of basic theoretical problems still remain unsolved. It also seems that the main source in the understanding of many spectral phenomena characterizing

systems consisting with a number of mutually coupled hydrogen bonds, in terms of the two different quantitative approaches, is in the early history of these studies. In practice, up to the beginning of the 90s of the 20th century, these studies were restricted to the interpretation of spectra of a number of very simple hydrogen bond systems, mainly to the spectra of cyclic acetic acid dimers formed in the gaseous phase [7, 12–14]. The extension of this research over other, more diversified and complex hydrogen bond aggregates allowed us to recognize numerous puzzling spectral effects attributed to these systems. Interpretation of these effects seemed to be beyond the contemporary quantitative theoretical models of the hydrogen bond IR spectra without assuming that some not revealed yet mechanisms codecide in the spectra generation.

For the last decade, spectroscopy in polarized light of hydrogen-bonded molecular crystals has provided key experimental data in this area. By measuring of polarized IR spectra of spatially oriented molecular crystals, characterized by a rich diversity of hydrogen bond arrangements met in their lattices, the most complete information has been be obtained about the coupling mechanisms involving hydrogen bonds in these systems. It appeared that the investigation of spectra of even so simple mutually interacting hydrogen bond aggregates like cyclic dimers (e.g., carboxylic acid dimers) allowed to reveal new H/D isotopic effects, namely, the H/D isotopic *self-organization* effects. They depend on a nonrandom distribution of protons and deuterons in the crystal lattices of isotopically diluted hydrogen bond systems. These spectral effects may be considered as the manifestation of a new kind of *cooperative interactions* involving hydrogen bonds, that is, the so-called *dynamical cooperative interactions* [16–18]. This revealing has emphasized the role of the vibronic coupling between the electronic and the proton vibrational motions taking place in hydrogen bond aggregates, in the generation of the very nature of the hydrogen bond as the natural phenomenon and in the interhydrogen bond interaction mechanisms [17, 18].

In the lattices of carboxylic acid crystals, centrosymmetric hydrogen bond dimers, present in the $(COOH)_2$ cycles, are frequently met [19, 20]. These dimers are the bearers of the main crystal spectral properties in the frequency ranges of the ν_{O-H} bands attributed to the proton stretching vibrations. One might expect that regardless of the molecular structure of carboxylic acids in their fragments placed outside the carboxyl groups, the ν_{O-H} band contour shapes should be fairly similar one to the other. This presumption is based on the considerations of the classic vibrational analysis, which predicted that the proton stretching vibrations in these molecules practically do not mix with vibrations of other atomic groups [21]. The experiment learns, however, that spectra of diverse carboxylic acid crystals considerably differ, one from the other, with regard to their ν_{O-H} band contour shapes as well as with regard to the temperature effects measured in the spectra. Qualitatively similar conclusion is valid for the ν_{O-D} bands in the spectra of the deuterium-bonded species [22–27]. Our hitherto estimations, resulting from the comparison of the IR crystalline spectra of diverse carboxylic acid molecular systems, ascribe the differences between the compared spectra in relation to the differences in the electronic structure of carboxylic acid molecules. For instance, π-electronic systems of aromatic rings or other larger conjugated π-electronic systems, linked directly to carboxyl groups, strongly change the basic spectral properties of carboxylic acid dimers in comparison with the analogous properties of aliphatic carboxylic acids [22–27]. The generation mechanism of these effects still remains unknown.

This paper deals with IR spectra of the hydrogen bond in crystals of two different carboxylic acids, namely, of *2-furanacetic acid* and *2-furanacrylic acid*. In these crystalline systems, associated molecules form hydrogen-bonded cyclic, centrosymmetric dimers (Complete crystallographic data for *2-furanacetic acid* and (excluding structure factors) have been deposited at the Cambridge Crystallographic Data Centre under the number CCDC-885823. Copies can be obtained free of charge from CCDC, 12 Union Road, Cambridge CB2 1EZ, U.K. (Fax: Int.+1223-336-033; e-mail: deposit@ccdc.cam.ac.uk)). The crystallographic data for 2-furanacrylic acid can be found in [28, 29]. Molecules of these two individual molecular systems differ, one from the other, by their electronic structures. In the latter case, the carboxyl groups are directly linked to the large π-electronic systems. In the *2-furanacetic acid* crystal case, *methylene* groups separate the hydrogen bonds, formed by the associated carboxyl groups, from the π-electronic system of *furan* rings.

The aim of the study reported in this paper was to provide new arguments of experimental nature about the role of the electronic structures of carboxylic acid molecules in the generation of IR spectra of cyclic hydrogen bond dimers. The investigation results presented constitute a part of results obtained in the frames of a wider project, which also assumed measuring of crystalline spectra of other *carboxylic acids*, mainly of *furan* and *thiophene* derivatives. Our choice of these model molecular systems was strongly supported by advantageous well-developed ν_{O-H} and ν_{O-D} band contour shapes in the IR spectra of these systems. We expected that the quantitative analysis of the polarized IR spectra of *2-furanacetic acid* and *2-furanacrylic acid* crystals and also of the spectra of relative carboxylic acid crystals should provide new arguments for the formulation of a new theoretical approach for the description of the hydrogen bond dimer spectra. The understanding of the temperature effects and the generation mechanism of the intensity distribution patterns in the ν_{O-H} and ν_{O-D} bands in the spectra of diverse carboxylic acid crystals are of the particular interest and importance in this project.

2. X-Ray Structures of *2-Furanacetic Acid* and *2-Furanacrylic Acid*

Crystals of *2-furanacetic acid* are monoclinic and the space-symmetry group is $P2_1/c$, $Z = 4$. The lattice constants at 100 K: $a = 13.0525(4)$ Å; $b = 4.85360(10)$ Å; $c = 9.4107(3)$ Å, $\beta = 103.832(3)^\circ$. In a unit cell four translationally nonequivalent molecules form two plain centrosymmetric cyclic hydrogen-bonded dimers (Complete crystallographic data for *2-furanacetic acid* (excluding structure factors) have been

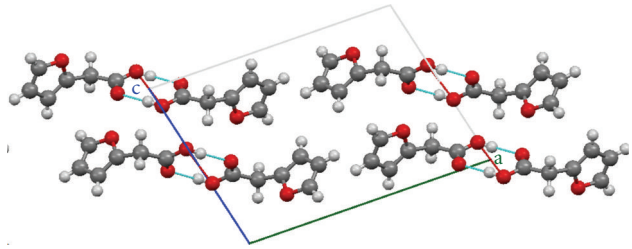

Figure 1: The X-ray structure of *2-furanacetic acid* crystal. Projection of the lattice onto the "*ac*" plane.

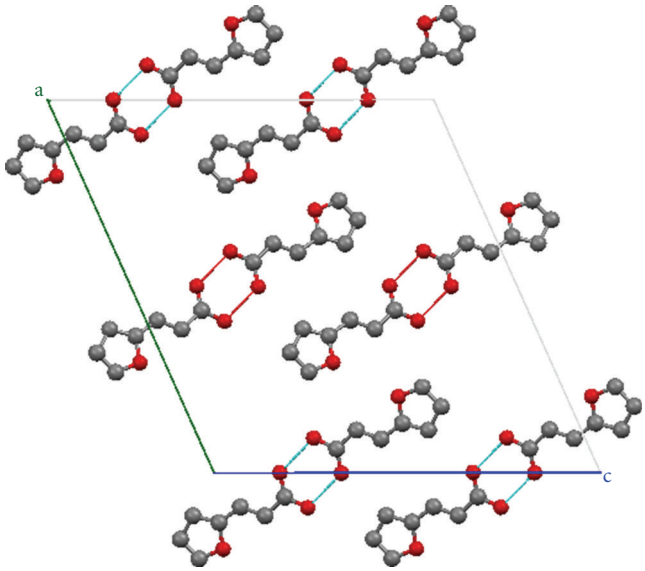

Figure 2: The X-ray structure of *2-furanacrylic acid* crystal. Projection onto the "*ac*" plane.

deposited at the Cambridge Crystallographic Data Centre under the number CCDC-885823). The molecules of *2-furanacetic acid* in the lattice are linked together by the O–H$\cdots$O hydrogen bonds, forming centrosymmetric dimers. A view of the crystal lattice of *2-furanacetic acid* is shown in Figure 1.

Crystals of *2-furanacrylic acid* are also monoclinic, the space-symmetry group is C2/c and Z = 8. The unit cell parameters are a= 18.975 Å; b = 3.843 Å; c = 20.132 Å, β = 113.9°. The molecules of *2-furanacrylic acid* in the lattice are linked together by the O–H$\cdots$O hydrogen bonds, forming cyclic approximately centrosymmetric dimers [28, 29]. The X-ray structure of *2-furanacrylic acid* crystals is shown in Figure 2.

3. Experimental

2-Furanacetic acid (C_4H_3O–CH_2–COOH) and *2-furanacrylic acid* (C_4H_3O–CH=CH–COOH) used for our studies were the commercial substance (Sigma-Aldrich). *2-furanacetic acid* was employed without further purification, while *2-furanacetic acid* was purified by crystallization from its acetone solution. The d_1 deuterium derivatives of the compounds (C_4H_3O–CH_2–COOD and C_4H_3O–CH=CH–COOD) were obtained by evaporation of D_2O solution of each compound at room temperature and under reduced pressure. It was found that the deuterium exchange rate for the COOH groups varied from 60 to 90% and from 70 to 90% for different samples, respectively.

Crystals suitable for further spectral studies were obtained by melting solid samples between two closely compressed spaces CaF_2 windows, followed by a very slow cooling of the liquid film. By that means, reasonably thin crystals could be received, characterized by their maximum absorbance at the ν_{O-H} band frequency range near to 0.5 at room temperature. From the crystalline mosaic, adequate monocrystalline fragments, having dimensions of at least 2×2 mm, were selected and then spatially oriented with the help of a polarization microscope. It was found that in each system case the crystals most frequently developed the "*ac*" crystalline face. These crystals were selected to the experiment by use of a thin, tin plate diaphragm with a 1.5 mm diameter hole, and then IR spectra of these crystalline fragments were measured by a transmission method. Spectral experiments were accomplished at room temperature and also at the temperature of liquid nitrogen, using polarized IR radiation. In each measurement, two different, mutually perpendicular orientations of the incident beam electric field vector "E" were applied, with respect to the developed face of the crystal lattice. The solid-state polarized spectra were measured with a resolution of 2 cm^{-1}, for the normal incidence of the IR radiation beam with respect to the crystalline face. The IR spectra were measured with the Nicolet Magna 560 FT-IR spectrometer. Measurements of the spectra were repeated for ca. 8 crystals of each isotopomer of an individual compound. Spectra were recorded in a similar manner for the deuterium derivatives.

The Raman spectra of polycrystalline samples of *2-furanacetic acid* and 2-furanacrylic acid were measured at room temperature with the use of the Bio-Rad FTS-175C FT-IR spectrometer at the 1 cm^{-1} resolution.

4. Results

The preliminary experimental studies of spectral properties of *2-furanacetic acid* and *2-furanacrylic acid* based on the measurements in CCl_4 solution in the frequency range of the ν_{O-H} proton stretching vibration bands. The results are shown in Figure 3.

In Figure 4 are shown the ν_{O-H} bands from the IR spectra of the polycrystalline acid samples in KBr pellets, measured at 298 K and 77 K, and in Figure 5 the ν_{O-D} bands spectra of the deuterium derivatives samples in the same conditions. The comparatively wealth spectrum of ν_{O-H} and ν_{O-D} bands for *2-furanacrylic acid* molecules may be predictable, based on earlier results for *cinnamic acid* crystals [24], while the ν_{O-H} and ν_{O-D} bands for *2-furanacetic acid* crystals are relatively poorer, similarly as in the *phenylacetic acid* crystal case [25].

Polarized IR spectra of the two crystalline systems measured at the room temperature in the ν_{O-H} band frequency

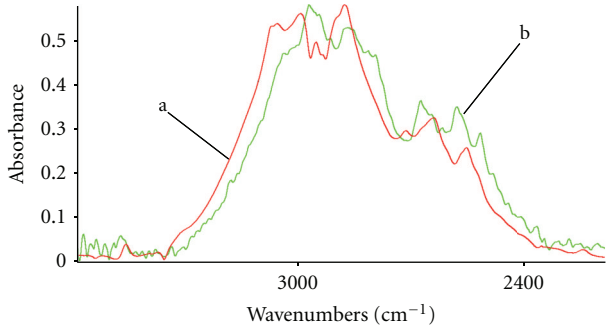

FIGURE 3: The ν_{O-H} band in the IR spectra of (a) *2-furanacetic acid* and (b) 2-furanacrylic acid in CCl_4 solution.

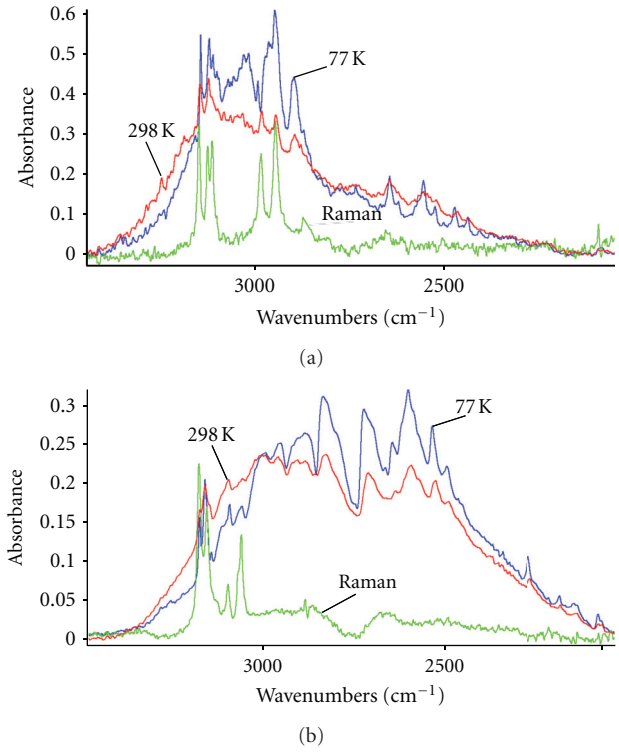

FIGURE 4: The ν_{O-H} bands in the IR spectra of polycrystalline samples of (a) *2-furanacetic acid* and (b) 2-furanacrylic acid, dispersed in KBr pellets. Temperature effect in the spectra. The Raman spectra measured for polycrystalline samples of the compounds at room temperature are also shown.

range are presented in Figure 6, whereas the corresponding low-temperature spectra are shown in Figure 7.

The corresponding spectra of isotopically diluted crystals recorded in the ν_{O-D} band range are shown in Figures 8 and 9.

The temperature effect in the crystalline spectra in the most intense polarized components of the ν_{O-H} bands is shown in Figure 10 and in the ν_{O-D} bands is given in Figure 11.

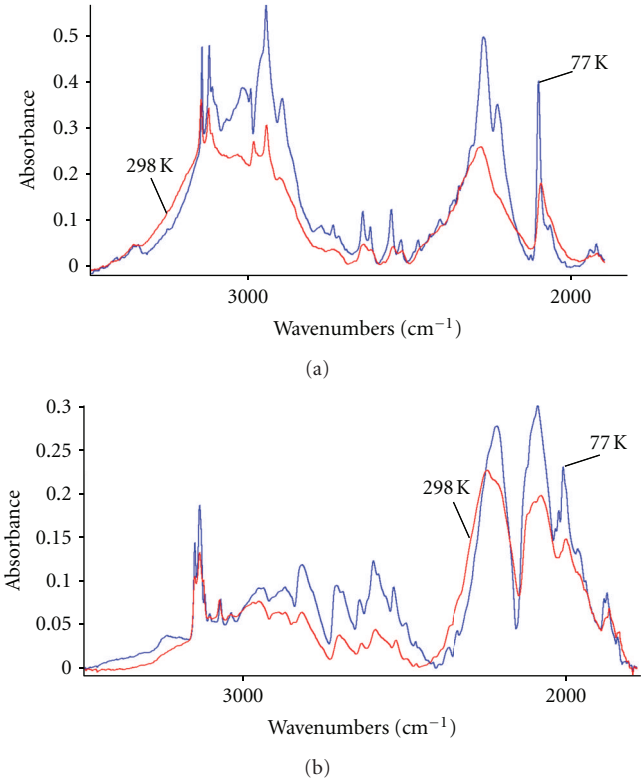

FIGURE 5: The ν_{O-D} bands in the IR spectra of polycrystalline samples of (a) d_1-*2-furanacetic acid* (ca. 45% H and 55% D) and (b) d_1-*2-furanacrylic acid* (ca. 20% H and 80% D) dispersed in KBr pellets. Temperature effect in the spectra.

5. Isotopic Dilution Effects in the Crystalline IR Spectra

On comparing the spectra in Figures 3 and 6–9, it can be noticed that the replacement of the major part of the hydrogen bond protons by deuterons changed the dichroic properties in the "*residual*" ν_{O-H} band substantially. The band shapes no longer depended on the crystal orientation investigated and resembled the spectrum measured for the CCl_4 solution of the compounds. Regardless of the increase in the rates of deuterium substitution in the samples, the "*residual*" ν_{O-H} band still retained its "*dimeric*" character. This is due to the fact that the hydrogen-bonded dimeric spectrum measured in the "*residual*" ν_{O-H} band range is still under the influence of the interhydrogen bond vibrational exciton interactions occurring within each individual carboxylic acid dimer [22–27].

The unusual properties of the "*residual*" ν_{O-H} bands have proved that the distribution of protons and deuterons between the hydrogen bonds of the isotopically diluted crystalline samples is nonrandom and in an individual dimer the coexistence of two identical hydrogen isotope atoms, proton or deuterons, is preferred. As a result, the interhydrogen bond exciton interactions still occur in each dimeric system and consequently the "*residual*" ν_{O-H} bands retain their "*dimeric*" properties. These spectral effects, that is, the so-called H/D isotopic "*self-organization*" effects, are

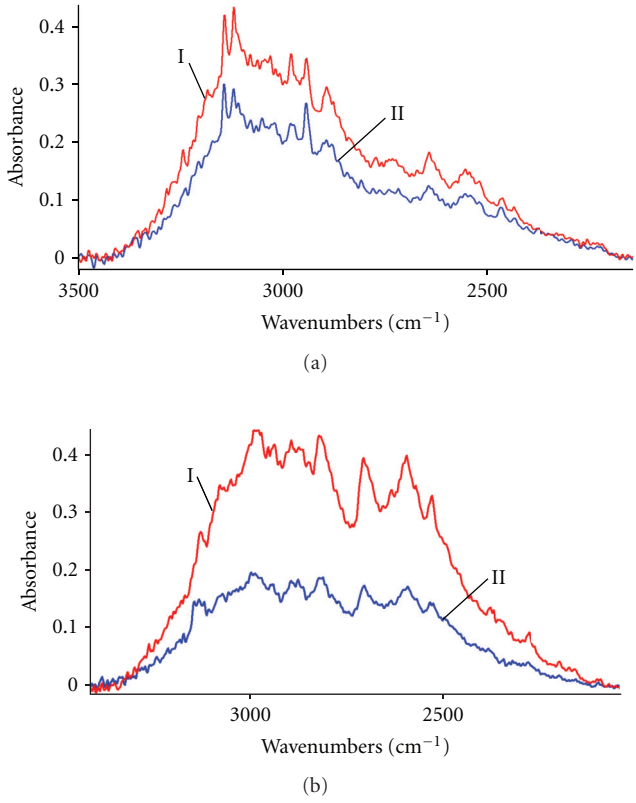

Figure 6: Polarized IR spectra of *2-furanacetic acid* and *2-furanacrylic acid* crystals measured at room temperature in the ν_{O-H} band frequency range for the IR radiation of the normal incidence with respect to the "*ac*" crystal faces. (a) *2-furanacetic acid* crystal. (I) The electric field vector *E* of the incident beam of IR radiation parallel to the *a*-axis (II) The E vector parallel to the c^*-axis (the c^*-symbol denotes the vector in the reciprocal lattice). (b) *2-furanacrylic acid* crystal. (I) The electric field vector E parallel to the *c*-axis. (II) The E vector parallel to the a^*-axis.

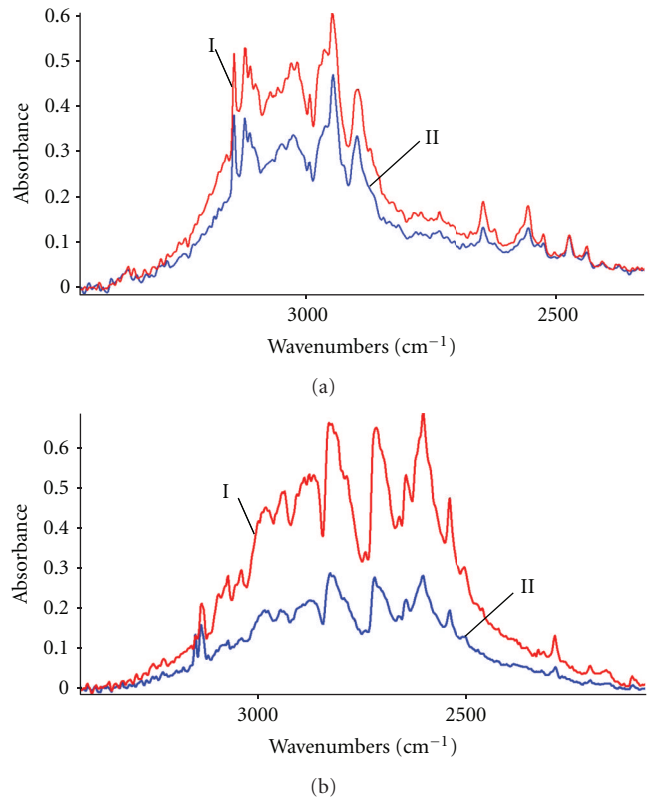

Figure 7: Polarized IR spectra of (a) *2-furanacetic acid* and (b) *2-furanacrylic acid* crystals measured at 77 K in the ν_{O-H} band frequency range. (a) *2-furanacetic acid* crystal. (I) The electric field vector E parallel to the *a*-axis. (II) The *E* vector parallel to the $c*$-axis. (b) 2-furanacrylic acid crystal. (I) The electric field vector *E* parallel to the *c*-axis. (II) The E vector parallel to the a^*-axis.

the attribute of the "*dynamical cooperative interactions*" involving hydrogen bonds in the dimers [16–18].

In the case of high excess of protons in the crystals qualitatively similar spectral effects can be identified in the "*residual*" ν_{O-D} bands, located in the range of 1900–2300 cm^{-1}, as those observed in the "*residual*" ν_{O-H} bands. In the low concentration of deuterons, the "*residual*" ν_{O-D} bands still retain the characteristic linear dichroic effects accompanying them (see Figures 4–9). For the two compared "*residual*" bands, ν_{O-H} and ν_{O-D}, not only the linear dichroic but also the temperature effects appear to be similar to the corresponding effects measured in the spectra of isotopically neat crystals.

This property results from the "*dynamical cooperative interactions*" in the hydrogen-bonded systems which lead to the appearance of the so-called H/D isotopic *self-organization* effects in the hydrogen bond IR spectra [17, 18]. The source of these nonconventional interactions in the hydrogen bond dimers is a vibronic coupling mechanism involving the totally symmetric proton stretching vibrations and the electronic motions in the systems [17, 18]. According to the theory of the "*dynamical cooperative interactions*," the symmetric hydrogen bond dimers of the HH or DD-type, with identical hydrogen isotope atoms, are thermodynamically more stable than the non-symmetric dimers of the HD type. The distribution of the HH- or DD-type dimers in the lattice sites is random. The energy difference between the two forms of dimers, the HH and the HD types was estimated as approximately equal to 1.5 kcal/mole of the dimers. Therefore, the relative concentration of the HD-type dimers is negligibly low and practically nondetectable with the use of the IR spectroscopic methods [16–18].

From the experimental studies presented in Figures 3–11 it also results that hydrogen-bonded cyclic centrosymmetric dimers are the bearers of the crystal spectral properties, since the inter-dimer vibrational exciton interactions are negligibly small.

6. Model

6.1. Carboxylic Acid Dimers the Basic Idea. The problem of the quantitative theoretical treatment of the spectral properties of systems composed with mutually interacting hydrogen bonds still constitute a real challenge in the area of the hydrogen bond research. There are still many problems to solve in this matter, since even the most advanced theories,

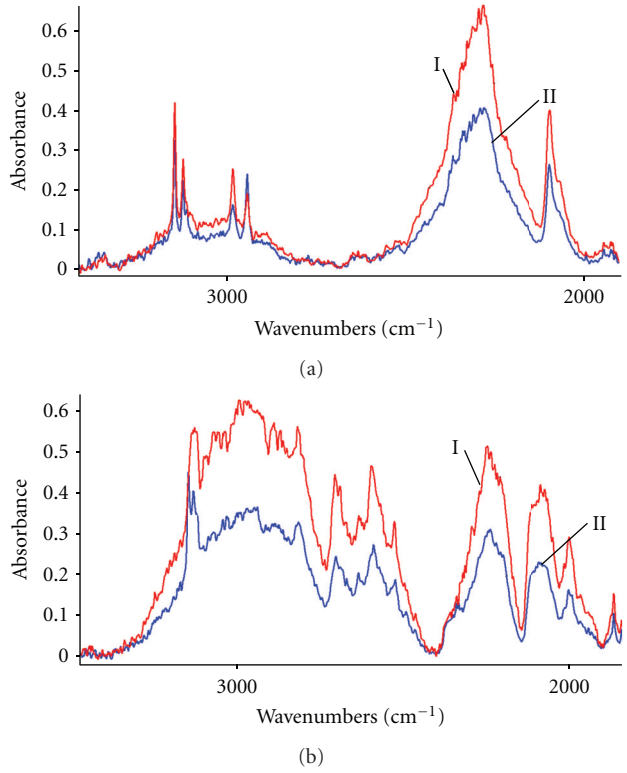

Figure 8: Polarized IR spectra of (a) d_1-*2-furanacetic acid* and (b) d_1-2-furanacrylic acidcrystals measured at room temperature in the ν_{O-D} band frequency range. (a) *2-furanacetic acid* crystal (ca. 10% H and 90% D). (I) The electric field vector E parallel to the a-axis, (II) The E vector parallel to the c^*-axis (b) 2-furanacrylic acid crystal (ca. 65% H and 35% D). (I) The electric field vector E parallel to the c-axis, (II) The E vector parallel to the a^*-axis.

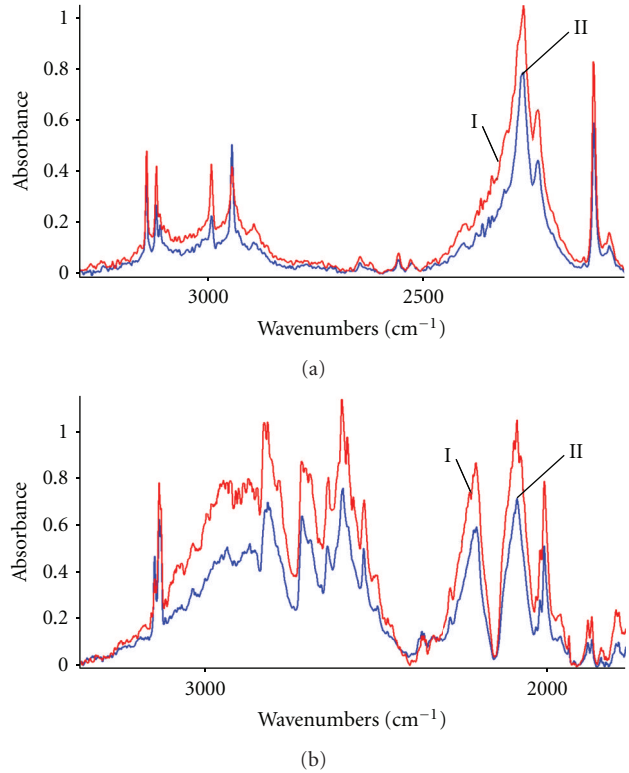

Figure 9: Polarized IR spectra of (a) d_1-*2-furanacetic acid* and (b) d_1-2-furanacrylic acid crystals measured at 77 K in the ν_{O-D} band frequency range. (a) *2-Furanacetic acid* crystal (ca. 10% H and 90% D). (I) The electric field vector E parallel to the a-axis, (II) The E vector parallel to the c^*-axis. (b) 2-Furanacrylic acid crystal (ca 65% H and 35% D). (I) The electric field vector E parallel to the c-axis, (II) The E vector parallel to the a^*-axis.

elaborated for the description of the IR spectra of hydrogen bond systems, are unable to reliably explain a number of effects observed in the dimeric spectra. Despite of spectacular achievements in the quantitative description of the intensity distribution in the ν_{X-H} bands, which are the attribute of the proton stretching vibrations in the X–H$\cdots$Y bridges and in the description of the H/D isotopic effects, the understanding of temperature effects in the spectra seems to be totally incomplete.

Cyclic hydrogen bond dimers, formed by associated carboxyl groups of diverse carboxylic acid molecules, are the most frequently studied model systems investigated in this research area. They exhibit some unusual spectral properties in IR connected with the highly abnormal thermal evolution of the ν_{O-H} and ν_{O-D} band contour shapes. One could expect that the hydrogen bond spectra of diverse carboxylic acid dimers, measured in the ν_{O-H} and ν_{O-D} band frequency ranges, should be fairly similar one to another due to the identical structural units of the molecular dimers, namely, the $(COOH)_2$ rings, in which two hydrogen bonds exist forming hydrogen bond dimers. However, on comparison of the crystalline spectra of diverse carboxylic acids, a considerable variation degree of the analyzed band contour shapes can be found. This fact undoubtedly remains in a close connection with differences in the electronic structures of diverse carboxylic acid molecules. Simultaneously, these spectra strongly differ, one from the other, by temperature effects characterizing them. Also these effects undoubtedly remain in a close relation with the electronic structures of the associating molecules. The basic experimental facts supporting the hypothesis given above are presented in the following.

6.2. Electronic Structure of Carboxylic Acid Molecules versus the Temperature Effects in Their Crystalline IR Spectra. Based on our previous studies, at this point, let us summarize the basic properties of the ν_{O-H} bands in the IR spectra of the hydrogen bond cyclic dimers formed by diverse carboxylic acid molecules, in relation to their electronic structures.

(a) In the case of carboxylic acid molecules in which the aliphatic fragments are connected directly with carboxyl groups (e.g., *aliphatic monocarboxylic acids* [11–13, 30, 31] and *dicarboxylic acids* [22]), the ν_{O-H} bands are characterized by different intensity distribution patterns, when compared with the corresponding band properties in the IR spectra of *arylcarboxylic acids* [23, 26]. In the first case,

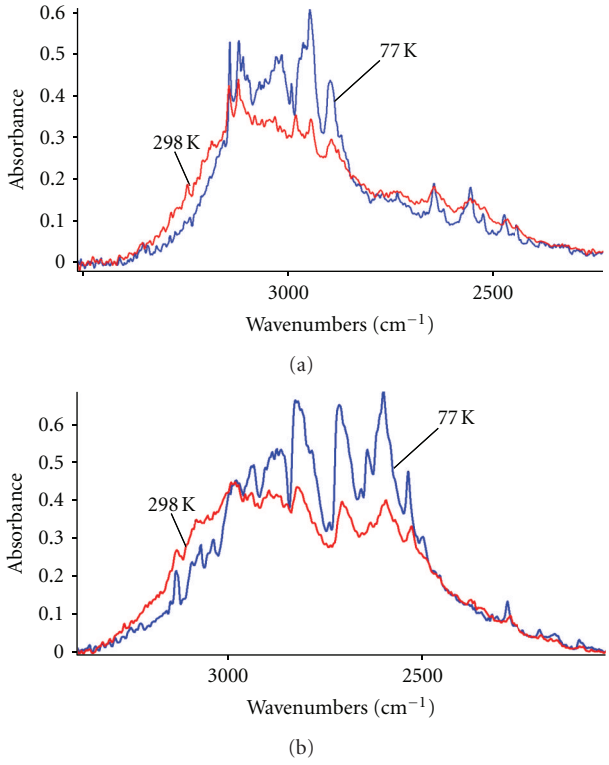

FIGURE 10: The ν_{O-H} bands in the IR spectra of monocrystalline samples of (a) *2-furanacetic acid* and (b) 2-furanacrylic acid. Temperature effect in the spectra.

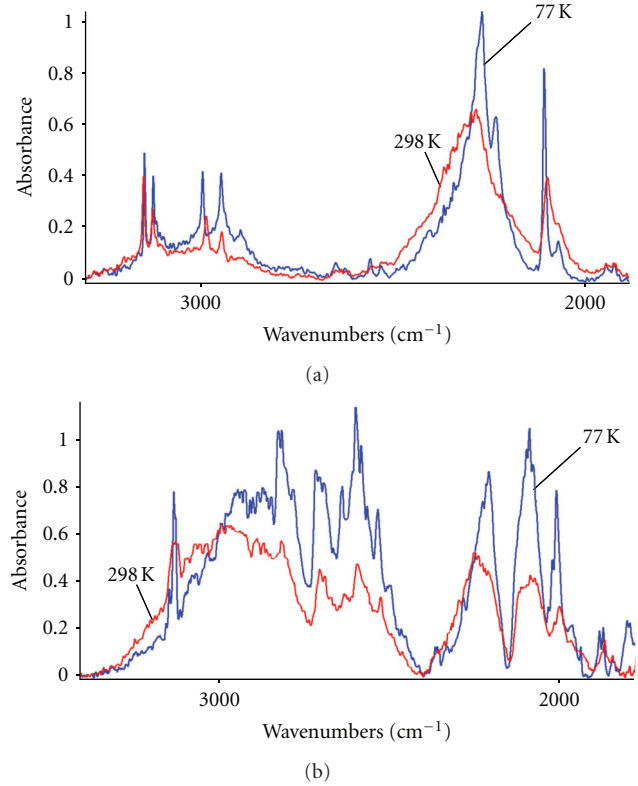

FIGURE 11: The ν_{O-D} bands in the IR spectra of monocrystalline samples of (a) d_1-*2-furanacetic acid* (ca 10% H and 90% D). and (b) d_1-2-furanacrylic acid (ca 65% H and 35% D). Temperature effect in the spectra.

the higher-frequency branch of the ν_{O-H} band is more intense in relation to the intensity of the lower-frequency band branch.

(b) In the case of hydrogen-bonded molecular systems, in which carboxyl groups are directly linked to π-electronic systems (e.g., *arylcarboxylic* [23, 26] and *arylacrylic acids* [24]), the ν_{O-H} band contours are a "*mirror reflection*" of the band shapes of systems from the point "a." In this case, the lower-frequency branch of the band is the most intense one. Similar property characterizes spectra of carboxylic acids with other large π-electronic systems in their molecules, for example, *cinnamic acid* [24], *2-naphthoic acid* [26], and *1-naphthylacrylic acid* [32].

(c) For other carboxylic acids, in which aromatic radicals are separated from carboxyl groups by fragments of aliphatic hydrocarbon chains (e.g., *arylacetic acid* [25, 27] and *styrylacetic acid* [33]), the ν_{O-H} band contour shapes are fairly similar to the corresponding band characteristics from the point "a," that is, to the corresponding spectra of *aliphatic monocarboxylic acids* [30, 31] and *dicarboxylic acids* [22]).

The ν_{O-H} bands in the spectra of the hydrogen bond of carboxylic acid crystals from the "a" and "c" groups, measured at room temperature, are characterized by relatively low intensity of the lower-frequency branch of he band in comparison with the higher-frequency band branch intensity. On the decrease of temperature to 77 K, only a relatively small growth of the relative intensity of the lower-frequency branch of each band can be observed. This band branch still remains of the lower intensity in the low-temperature spectra.

In the case "b," even at room temperature spectra, the ν_{O-H} bands exhibit relatively high intensity of their lower-frequency branch in relation to the higher-frequency branch. On the temperature decrease up to 77 K, a considerable growth of the relative intensity of the lower-frequency branch of each analyzed band can be observed. As the result of the band contour thermal evolution, in the low-temperature spectra of carboxylic acid crystals of this group the lower-frequency branch is of the dominant intensity in the bands.

According to the "*state-of-art*" in our contemporary knowledge about the quantitative description of the IR spectra of the hydrogen bond in carboxylic acid dimers, the following interpretation of the ν_{O-H} band generation mechanisms seemed to be valid: the lower-frequency branch of the ν_{O-H} band is generated by the transition occurring to the Ag-symmetry excited state of the totally symmetric proton stretching vibrations in the dimers. This transition, forbidden by the symmetry rules, becomes allowed via a vibronic mechanism, which is a kind of reverse of the familiar *Herzberg-Teller* mechanism, originally responsible for the promotion of forbidden electronic transitions in UV spectra

of aromatic hydrocarbons [34]. Within this approach of the reverse *Herzberg-Teller* vibronic coupling mechanism, electronic properties of single hydrogen bonds themselves, as well as electronic properties of the whole associated molecules and the proton vibration anharmonicity, are responsible for the magnitude of the forbidden transition promotion effects in the dimeric spectra [35]. The promotion mechanism determines a unique property of centrosymmetric hydrogen bond dimeric system. This effect found no counterpart in the vibrational spectroscopy of single centrosymmetric molecules.

On the other hand, the higher-frequency spectral branch of the band corresponds with the symmetry-allowed transition to the Au-state of the nontotally symmetric proton vibrations in the centrosymmetric hydrogen bond dimers. One should expect that the higher-frequency branch of the ν_{O-H} band, attributed to the allowed transition, should be more intense than the other band branch related with the forbidden transition. Therefore, based on these intuitive predictions, the spectral properties of the carboxylic acid dimers from the "b" group seem to be highly surprising, contradicting the interpretation of the spectra of systems belonging to the "a" and "c" groups. The particular electronic properties of the carboxylic acid molecules from the "c" group can anyway explain the extremely high integral intensity of the forbidden lower-frequency branch of the band and its strong temperature dependence.

In order to propose a reliable explanation of this paradox in our analysis, one should also recall the hydrogen bond IR spectra of other hydrogen bond dimeric systems, including spectra of hydrogen-bonded heterocycles. On comparison of the IR spectra of diverse crystalline systems containing cyclic hydrogen bond dimers as the structural units of their lattices, the following general conclusions can be made: most of centrosymmetric hydrogen bond dimers exhibit regular enough spectral properties characterizing their hydrogen bond spectra. Usually, the ν_{X-H} bands have the lower-frequency (i.e., the "*forbidden*") branch of a lower intensity, even in their low-temperature spectra. However, in some rare cases, for example, *3-hydroxy-4-methyl-2(3H)-thiazolethione* [36], *2-tiopyridone* [37], and *2-pyridone* [38], the ν_{O-H} and ν_{N-H} bands are characterized by an abnormal, that is, by a "*reverse*" intensity distribution patterns in their contours. In the latest cases, the lower-frequency branch of each band is more intense when compared with the higher-frequency band intensities. It fairly resembles the properties of the spectral properties at 77 K of carboxylic acid crystals of the "b" group. In the case of the dimeric spectra of the reverse intensity distribution patterns in the bands, for example, *3-hydroxy-4-methyl-2(3H)-thiazolethione* [36] and *2-tiopirydone* [37], this effect was ascribed previously to the influence of the extreme lengths of the O–H···S and N–H···S hydrogen bonds in the dimeric systems.

The recent considerations, aiming to explain these phenomena, were performed in terms of the *dipole-dipole* model of the vibrational exciton interactions involving the hydrogen bonds in the dimers. In the case of the interpretation of the spectra of *3-hydroxy-4-methyl-2(3H)-thiazolethione* [36] and *2-tiopirydone* [37], the hydrogen bond geometry

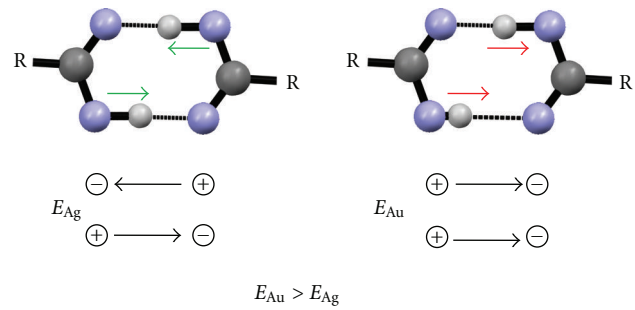

FIGURE 12: The "*side-to*-side" (SS) exciton coupling involving the proton stretching vibrations in a cyclic centrosymmetric hydrogen bond dimer.

was considered to be responsible for the unusual spectral property of these dimers. However, this approach fails in the interpretation of the spectra of *2-pyridone* cyclic dimers [38], in which the N–H···O hydrogen bonds are considerably shorter when compared with the N–H···S bond lengths in *2-thiopyridone* cyclic dimers [37] and their spectra qualitatively fairly resemble the corresponding spectra of *2-pyridone* [38]. On the other hand, even among the hydrogen bond dimers of diverse molecular systems with the N–H···S hydrogen bonds, for which the extreme spectral properties were found, a substantial diversification in the analyzed spectral properties has been found, despite the extremely long hydrogen bonds in these cases. The IR spectra of *2-mercaptobenzothiazole* cyclic dimers [39] exhibit regular properties of the intensity distribution pattern in their ν_{N-H} band contours, similarly as the carboxylic acid dimers in the crystals of the groups "a" an "b," regardless of the extreme N–H···S bond lengths, like these found in *2-thiopyridone* dimers [37].

6.3. Spectra of Cyclic Dimers versus Spectra of Chain Hydrogen Bond Systems. It is surprising that spectra of cyclic hydrogen bond dimers in *3-hydroxy-4-methyl-2(3H)-thiazolethione* [36], *2-thiopyridone* [37], *and 2-pyridone* [38] crystals fairly resemble by their intensity distribution patterns of the ν_{N-H} bands the spectra of chain hydrogen bond systems in a particular group of molecular crystals. In the hydrogen bond spectra of *pyrazole* [40] and *4-thiopyridone* [41] crystals, with hydrogen-bonded molecules forming infinite chains in their lattices, strong linear dichroic effects can be observed, which prove a considerable influence of the exciton interactions involving the adjacent hydrogen bonds in each chain. Figures 12 and 13 explain the source of the differences in the hydrogen bond dimers, the cyclic and the chain ones.

The analysis of this inter-hydrogen-bond coupling, in case of cyclic centrosymmetric dimers and in linear dimers, requires taking into consideration two situations of the vibrational transition moment directions for hydrogen bonds in the dimers. For cyclic dimers, the parallel mutual orientation of the dipole transition moments, the exciton interaction energy E_{Au} in the limits of the *dipole-dipole* model is of the positive sign. The vibrational transition corresponding to such arrangement of the vibration dipole moments is

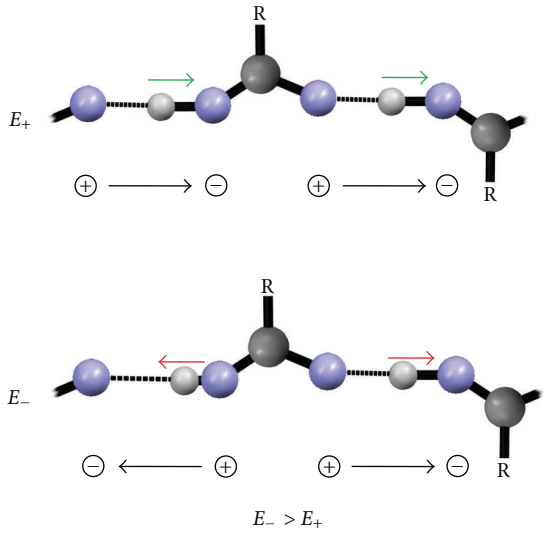

FIGURE 13: The "*head-to-tail*" (TH) exciton coupling involving the proton stretching vibrations in an infinite chain of associated hydrogen bonds.

responsible for generation of the intense, symmetry-allowed, shorter-wave branch of the dimeric spectra. In contrast, when the dipole transition moments are of the antiparallel arrangement (see Figure 12), the energy exciton interaction energy value E_{Ag} is negative, so the band generated by this situation is placed at the lower frequency and it corresponds to the symmetry-forbidden excitation of the totally symmetric proton vibrations. Such sequence of the spectral branches in the hydrogen bond stretching bands is typical for cyclic, centrosymmetric hydrogen bond dimers.

When the vibrating transition moment dipoles in a linear dimer, in the case of the totally symmetric proton vibrations, are oriented axially as "*tail-to-head*" (Figure 5), the sign of the exciton interaction energy value E_+ is negative, so the intense branch corresponding to the symmetry-allowed transition is placed at the lower-frequency range. On the contrary, the forbidden by the symmetry rules spectral branch, situated at the higher frequency, is generated by the antiparallel orientation of the vibrating dipoles (see Figure 13). In this case, the exciton coupling energy E_- is of the positive sign. The sequence and the properties of the branches in the proton stretching vibration bands in the discussed case are reverse to those observed in the IR spectra of hydrogen bond cyclic dimeric systems.

Therefore, the following problem demands explanation: why do some individual cyclic hydrogen bond dimeric systems exhibit similar spectral properties to the corresponding properties of a particular group of crystals with chain structures of hydrogen-bonded associates (*formic acid* [31], *pyrazole* [40], and *4-thiopyridone* [41] crystals). Undoubtedly, this property remains in a close connection with the π-electronic properties of the associating molecules. In the associated molecular systems, vibrational exciton couplings are of the "*tail-to-head*" (TH) type. They involve the adjacent hydrogen bonds within each individual chain in the lattice. The electronic structure of molecules of this group is most probably the key factor governing these interhydrogen bond interactions.

Nevertheless, the majority of crystals with hydrogen-bonded molecular chains in their lattices surprisingly exhibit the spectral properties similar to the analogous properties of cyclic hydrogen bond dimer spectra from the "a" and "c" groups (e.g., *acetic acid* [30], *N-methylthioacetamide* [42], or *acetanilide* [18] crystals). In the latest case the exciton interactions of the "*side-to-side*" (SS) type involve the closely spaced hydrogen bonds where each moiety belongs to a different chain. In molecules of this group, large π-electronic systems are absent. Only *carbonyl* or *thiocarbonyl* groups, each with a small π-electronic system, are present in these molecules.

From the above-presented data, it results that the way of realization of the vibrational exciton interactions in various hydrogen bond aggregates (cyclic dimers, infinite chains), affecting the ν_{X-H} and ν_{X-H} band fine structures, does not directly depend on the hydrogen bond system geometry. It is rather determined by the electronic structure of the associating molecules.

7. Theoretical Approach Proposed

The *dipole-dipole* interaction model, widely used for a simplified description of the exciton interactions between hydrogen bonds, seems to be nonadequate in the explanation of the wide diversity of the spectra of cyclic hydrogen bond dimers. There is some experimental data indicating that these couplings do not always occur as "*through-space*" and they are also widespread by the hydrogen bond electrons as well as by electrons of the molecular skeletons. Therefore, in terms of the theory of molecular vibrational excitons [43, 44], the exciton interaction integrals in some cases may also considerably strongly depend on the electronic coordinates. In advantageous circumstances, resulting from a proper electronic structure of the associating molecules, the proton stretching vibrations can induce electric current oscillating around a cyclic hydrogen bond dimer, or in the other case, oscillating along a hydrogen bond chain. However, only the totally symmetric proton vibrations are able to effectively induce the electric current in the ring or in the chain, while the nontotally symmetric vibrations are inactive in this mechanism, since currents induced in each individual hydrogen bond are annihilated in a dimer. The formalism of the model of the electric current generated by oscillating protons in cyclic hydrogen bond dimers was proposed by *Nafie* three decades ago [45].

In the scope of the considerations given above, it seems justified to treat formally a cyclic hydrogen bond dimer by the following two ways, taking into account the exciton interactions in the system.

(1) As a closed chain in which the adjacent hydrogen bonds are strongly exciton-coupled, similarly as in the chain associates in *pyrazole* [40] and *4-thiopyridone* [41] crystals. This is the coupling of the TH type occurring around the molecular cycle. This

way the coupling occurs via the easy-polarizable electrons on the π-orbitals. Therefore, the cyclic dimer spectrum is fairly similar to the spectrum of a chain system, with a low intensity of the higher-frequency band branch.

(2) As a pair of partially independent hydrogen bonds, which remains only "*through-space*" exciton coupled. It can be considered as a coupling of the SS type, without the generation of the ring electric current in the dimer. This behavior characterizes the associated molecular systems with no large π-electronic systems in their structures, where only small π-electronic systems are present in *carbonyl* and *thiocarbonyl* groups. In these circumstances, the dimeric spectra are of the standard form, with a low intensity of the lower-frequency ν_{X-H} band branch. For the quantitative description of the exciton interactions involving hydrogen bonds, influencing the dimer spectra, the *dipole-dipole* model is sufficiently adequate.

The ν_{X-H} band shapes in the two types of the dimer spectra are related one with the other by the approximate mirror reflection symmetry. In the case 1, the lower-intensity spectral branch appears in the higher-frequency range and is generated by the quasiforbidden vibrational transition in a dimer, occurring to the excited state of the totally symmetric proton stretching vibrations. In case 2 the lower intensity spectral branch appears in the lower-frequency range. It corresponds with the quasi-forbidden vibrational transition in a dimer. The above-presented spectral properties of diverse hydrogen bond cyclic dimers may allow explaining the thermal evolution effects in the hydrogen bond IR spectra of carboxylic acid crystals.

It seems that in order to explain the temperature effects in the IR spectra of cyclic hydrogen bond dimers the following hypothesis concerning the mechanisms of the spectra generation should be accepted: let us assume that two competing mechanisms of vibrational exciton interactions involving hydrogen bonds in cyclic dimers are simultaneously responsible for the formation of the ν_{X-H} band contour shapes. The contribution of each individual mechanism depends on the electronic structure of the associating molecules, on the electronic properties of the heavy atoms forming the hydrogen bridges as well as on temperature.

(A) The first mechanism depends on the "*side-to-side*" (SS)-type vibrational exciton coupling between the hydrogen bonds in cyclic dimers. In this case, the dimer hydrogen bonds interact one with the other as *through-space* via the *van der Waals* forces.

(B) The other mechanism assumes a "*tail-to-head*" (TH)-type exciton coupling involving the hydrogen bonds in the dimers. These interactions occur around the cycles via electrons.

The "B" mechanism seems to be privileged in the case of the particular kind of associated molecules, in which hydrogen bonds couple with large π-electronic systems, for example, for aromatic carboxylic acid molecules. The "A" mechanism seems to dominate in the case of molecular systems with small π-electronic systems, for example, for aliphatic carboxylic acid molecules.

It seems obvious that for an individual hydrogen-bonded dimeric system the contribution of each mechanism is temperature dependent. For molecules with large π-electronic systems directly coupled with the hydrogen bonds, the "B" mechanism should be privileged at very low temperatures. Temperature growth, influencing the increase of atomic vibration amplitudes, should annihilate the electric current induced by the totally symmetric proton vibrations in the cycles. In these circumstances, the role of the "A" mechanism increases, namely, of the "*through-space*" vibrational exciton coupling between the hydrogen bonds in a dimer. This should, therefore, result in a particularly strong temperature-induced evolution of the ν_{X-H} bands, especially in the case of the spectra of *2-thiopyridone* [37] and *2-pyridone* [38] type dimers. Even when the lower-frequency branch of the band is less intense when compared with the higher-frequency one, the temperature decrease till 77 K causes its considerable intensity growth, and in these circumstances the lower-frequency branch becomes more intense than the higher-frequency band branch.

In the spectra of cyclic dimers, with only small π-electronic systems in the associating molecules, the temperature decrease usually does not cause a considerable intensity growth of the lower-frequency band branch. It still remains less intense when compared with the higher-frequency branch of the band. It means that, due to the molecular electronic properties of this group of dimers, the "B" mechanism cannot be activated effectively enough even at very low temperatures.

8. Spectral Consequences of the Model for Carboxylic Acids

From the above assumptions, it results the choice of the proper way of the model calculations of the ν_{X-H} and ν_{X-D} band contours in IR spectra of hydrogen bond dimers. In the limits of the proposed approach, a theoretical spectrum of the model system can be derived, formally treated as a superposition of two component spectra, where each individual spectrum corresponds with a different mechanism of the exciton interactions, SS (A) and TH (B), involving the dimer hydrogen bonds. In terms of the "*strong-coupling*" theory [6–8], in each exciton interaction mechanism case, the ν_{X-H} band in the dimeric spectrum is a superposition of two component bands, "*Plus*" and "*Minus*," each of a different origin.

The "*Plus*" band is generated by the dipole allowed transition to the excited state of the nontotally symmetric proton stretching vibrations in a centrosymmetric dimer, belonging to the Au representation. On the other hand, the "*Minus*" band is connected with the symmetry forbidden transition to the Ag-symmetry state of the totally symmetric proton vibrations in the dimers, activated by a vibronic mechanism [35]. In the case when the mechanism "A" exclusively decides about the dimer spectra generation mechanism, the "*Minus*" band appears in the lower "B" mechanism frequency range in

relation to the "*Plus*" band location. In the other case, when the "B" mechanism governs the dimer spectra generation, the two component bands appear in the reverse sequence than in the case "A." It means that in the case of the "B" mechanism governing the spectra generation, the "*Minus*" band representing the forbidden transition appears in the higher-frequency range than the "*Plus*" band connected with the allowed transition.

9. Model Calculations of the Band Contours

In the two cases, A and B, model calculations, aiming at reconstituting of the "*residual*" ν_{O-H} and ν_{O-D} band shapes, were performed within the limits of the "*strong-coupling*" theory, for a model centrosymmetric O–H$\cdots$O hydrogen bond dimeric system. [6–8, 46]. We assumed that the main ν_{O-H} and ν_{O-D} band shaping mechanism involved strongly anharmonically coupled the high-frequency proton (or deuteron) stretching vibrations and the low-frequency O$\cdots$O hydrogen bridge stretching vibrational motions. Calculation of the hydrogen bond system IR spectra in terms of the "*strong-coupling*" model allows to obtain results fairly comparable with the results of the spectra calculation performed using the "*relaxation*" theory [9, 10, 47–49].

According to the formalism of the "*strong-coupling*" theory [6–8, 46], the ν_{O-H} band shape of a dimer depends on the following system of dimensionless coupling parameters: (i) on the distortion parameter, "b_H", and (ii) on the resonance interaction parameters, "C_O" and "C_1". The "b_H" parameter describes the change in the equilibrium geometry for the low-energy hydrogen bond stretching vibrations, accompanying the excitation of the high-frequency proton stretching vibrations ν_{O-H}. The "C_O" and "C_1" parameters are responsible for the exciton interactions between the hydrogen bonds in a dimer. They denote the subsequent expansion coefficients in the series on developing the resonance interaction integral "C" with respect to the normal coordinates of the $\nu_{O\cdots O}$ low-frequency stretching vibrations of the hydrogen bond. This is in accordance with the formula:

$$C = C_O + C_1 Q_1, \tag{1}$$

where Q_1 represents the totally symmetric normal coordinate for the low-frequency hydrogen bridge stretching vibrations in the dimer. This parameter system is closely related to the intensity distribution in the dimeric ν_{N-H} band. The "b_H" and "C_1" parameters are directly related to the dimeric ν_{N-H} component bandwidth. The "C_O" parameter defines the splitting of the component bands of the dimeric spectrum corresponding to the excitation of the proton vibrational motions of different symmetries, Ag and Au. In its simplest, original version, the "*strong-coupling*" model predicts reduction of the distortion parameter value for the deuterium bond systems according to the relation:

$$b_H = \sqrt{2} b_D. \tag{2}$$

For the " C_O" and "C_1" resonance interaction parameters, the theory predicts the isotopic effect expressed by the 1.0 to $\sqrt{2}$-fold reduction of the parameter values for *D*-bonded dimeric systems.

As the consequence of the "*strong-coupling*" model, the ν_{O-H} and ν_{O-D} band contour fine structures were treated as a superposition of two component bands. They correspond to the excitation of the two kinds of proton stretching vibrations, each exhibiting a different symmetry. In the case of the A exciton coupling mechanism and for the C_i point symmetry group of the model dimer, the excitation of the Ag vibrations in the dimer generates the lower-frequency transition branch of the ν_{O-H} band when the Au vibrations are responsible for the higher-frequency band branch. In the case of the B mechanism, the component subbands appear in reverse sequence.

Here, we consider an identical anharmonic coupling parameter system for the two individual mechanism cases A and B although diversification of the coupling parameter value systems seems to be better justified. We assume the contribution of each mechanism as governed by a *Boltzmann*-type relation. In addition, for the statistical weight parameters of each individual mechanism, $P_A(T)$ and $P_B(T)$, one must distinguish which state is dominant, that is, when the SS (A) state is of the lower energy and the TH (B) state is of a higher energy value and vice versa. In order to reproduce the temperature dependence of experimental spectra particularly for its width and the position of its first moment, we used for the $P_A^{AB}(T)$ exponential temperature dependence according to

$$P_A^{AB}(T) = 1 - \exp\left(-\frac{\alpha^{AB}}{k_B T}\right), \tag{3}$$

where is α^{AB} the activation energy parameter when the SS state is dominant and k_B is the constant of Boltzmann. In such circumstance, $P_B^{AB}(T)$ takes the following expression:

$$P_B^{AB}(T) = \exp\left(-\frac{\alpha^{AB}}{k_B T}\right), \tag{4}$$

It is interesting to note that, in the case of A, for very low temperatures, the statistical weight $P_A^{AB}(T)$ parameter is close to 1.0 and $P_B^{AB}(T)$ is almost equal 0.0. In these circumstances, the SS-type interaction is the basic type of the exciton coupling involving the dimer hydrogen bonds. For high temperatures, the $P_B^{AB}(T)$ parameter values are different from 0.0 and they are intermediate between 0.0 and 1.0 (rather closer to 0.5) and $P_A^{AB}(T)$ approaches 0.5. When the temperature increases, $P_B^{AB}(T)$ also increases. It means that, the TH coupling, occurring via the electric current in the ring is activated in higher temperatures in a magnitude depending of the energy gap between these two states of the vibrationally excited dimer. From our experimental estimations, the energy gap for some dimeric system cases is relatively large and in another cases it may be relatively low.

In the case B, where the TH state is of a lower energy value, we assume the same formula but the energy barrier α^{BA} height is relatively low. In such a circumstance,

the statistical weight parameters, $P_A(T)$ and $P_B(T)$, may be written as follows:

$$P_A^{BA}(T) = \exp\left(-\frac{\alpha^{BA}}{k_B T}\right),$$
$$P_B^{BA}(T) = 1 - \exp\left(-\frac{\alpha^{BA}}{k_B T}\right). \quad (5)$$

As we can see, for very low temperatures, $P_A^{AB}(T)$ may be practically equal to 1.0. For this kind of dimeric systems, the TH-type exciton coupling is the basic natural way in which the inter-hydrogen bond interactions occur. The growth in temperature annihilates this way of the coupling, due to the vanishing of the electronic current induced in the cycles, accompanied by large-amplitude thermal motions of atoms in the dimers. For high temperatures, $P_A^{AB}(T)$ decreases and becomes of an intermediate value between 0.0 and 1.0 (rather closer to 0.5), while the statistical weight $P_A^{AB}(T)$ grows declining from 0.0 up to 0.5. The energy gap between the two states in some molecular cases is usually relatively large, and in other cases it may be relatively small. It depends of the electronic properties of the associating molecules forming the dimers. From our experimental data, it can be concluded that the cases A and B represent the extreme cases of the interhydrogen bond coupling in cyclic hydrogen bond dimers. There are also many systems exhibiting an intermediate behavior. For a relatively small magnitude of the absolute values of the energy barrier height, the two cases A and B are practically nondistinguishable.

The theoretical spectra reconstituting the ν_{O-H} band contours measured at the two different temperatures, 293 K and 77 K, were calculated in terms of the two different individual coupling mechanisms, SS and TH, which generate the two component bands, "*plus*" and "*minus*" in a different sequence. The following coupling parameter values, identical in both molecular system cases, were used.

For the *2-furanacetic acid* crystal spectra: $b_H = 1.6$, $C_0 = 1.5$, $C_1 = -0.2$, $F^+ = 1.0$, $F^- = 0.2$, $\Omega_{O\cdots O} = 100\,\text{cm}^{-1}$, and we used the same parameter system for calculation of the *2-furanacrylic acid* crystal spectra: $b_H = 1.6$, $C_0 = 1.5$, $C_1 = -0.2$, $F^+ = 1.0$, $F^- = 0.2$, $\Omega_{O\cdots O} = 100\,\text{cm}^{-1}$.

The F^+ and F^- symbols denote the statistical weight parameters for the "*plus*" and "*minus*" theoretically derived subspectra contributing at the band formation.

The coupling parameter values used for calculation of the ν_{O-D} band contour shapes were as follows.

For *2-furanacetic acid* crystal, spectrum $b_D = 0.7$, $C_0 = 0.7$, $C_1 = -0.1$, $F^+ = 1.0$, $F^- = 0.2$, $\Omega_{O\ldots O} = 100\,\text{cm}^{-1}$ and for *2-furanacrylic acid* crystal spectrum: $b_H = 0.7$, $C_0 = 0.7$, $C_1 = -0.1$, $F^+ = 1.0$, $F^- = 0.2$, $\Omega_{O\cdots O} = 100\,\text{cm}^{-1}$.

For the *2-furanacetic acid* crystal spectra the statistical weight parameter ratio, $P_A(T)$: $P_B(T)$, for the SS and TH mechanisms was estimated as equal to 1.0 : 0.0 in the case of the room temperature spectrum reconstitution. For the low-temperature spectrum case, this parameter ratio value is very similar and equal to 1.0 : 0.0. Among various parameter ratio values for the SS and TH mechanisms contributing in the band generation, this parameter ratio value allowed for the most adequate reproduction of the temperature effect in the crystal spectra.

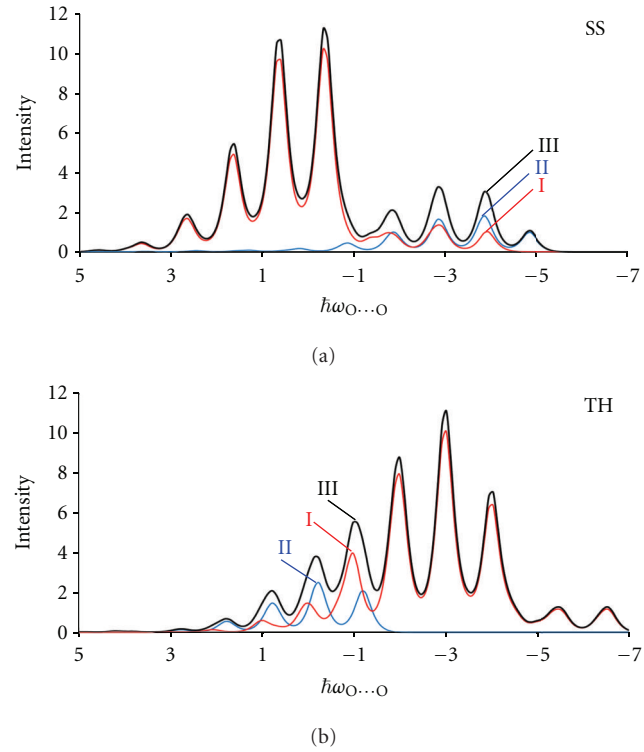

FIGURE 14: The theoretically derived ν_{O-H} band contours calculated in terms of the "*strong-coupling*" theory in the limits of the two different vibrational exciton coupling mechanisms involving the cyclic dimer hydrogen bonds, that is, "*side-to-side*" (SS) and "*tail-to-head*" (TH). (a) The SS coupling mechanism. (b) The TH coupling mechanism. (I) The "*minus*" band. (II) The "*plus*" band (III) Superposition of the I and II spectra, each taken with its appropriate individual statistical weight parameter, F^- and F^+. In both mechanism cases, the same coupling parameter value system was used for calculations: $b_H = 1.4$, $C_0 = 1.5$, $C_1 = -0.2$, $F^+ = 1.0$, $F^- = 0.2$, $\Omega_{O\cdots O} = 100\,\text{cm}^{-1}$. The transition frequencies are in the $\omega_{O\cdots O}$ vibrational quantum units, and the transition frequencies are expressed with respect to the gravity center of the hypothetical spectrum of a monomeric hydrogen bond in the cyclic hydrogen bond dimer. Transition intensities are in arbitrary units.

For the *2-furanacrylic acid* crystal spectra, the statistical weight parameter ratio, $P_A(T) : P_B(T)$, for the SS and TH mechanisms were estimated as equal to 0.35 : 0.65 in the case of the room temperature spectrum reconstitution. For the low-temperature spectrum case, this parameter ratio value is equal to 0.55 : 0.45.

In Figures 14 and 15, we present the theoretical ν_{O-H} and ν_{O-D} band contours calculated in terms of the two individual mechanisms of the vibrational exciton interactions involving the dimer hydrogen bonds, SS and TH.

In Figures 16 and 17, the evolution of the ν_{O-H} and ν_{O-D} band contour shapes accompanying the variation in the relative contribution of the SS and TH coupling mechanisms in generation of a dimeric spectra is shown. Similar band

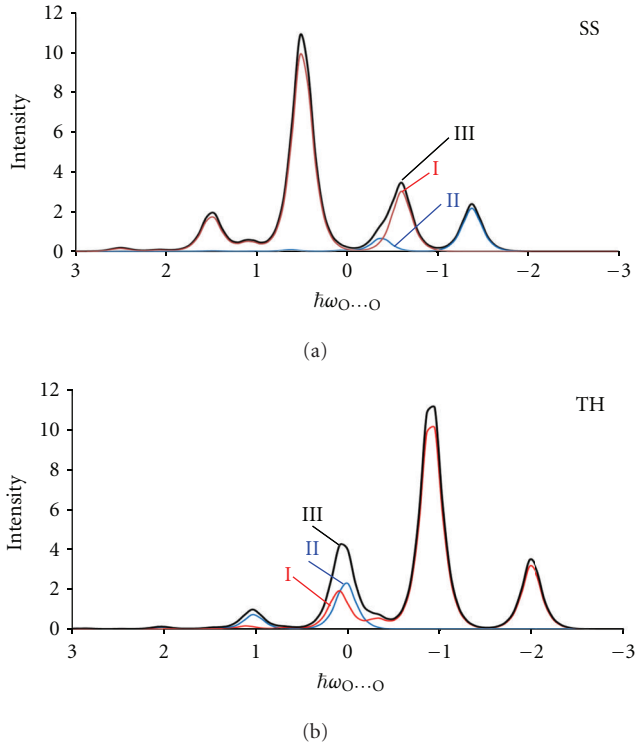

FIGURE 15: The theoretically derived ν_{O-D} band contours calculated in terms of the "*strong-coupling*" theory in the limits of the two different vibrational exciton coupling mechanisms involving the cyclic dimer hydrogen bonds, that is, "*side-to-side*" (SS) and "*tail-to-head*" (TH). (a) The SS coupling mechanism. (b) The TH coupling mechanism. (I) The "*minus*" band. (II) The "*plus*" band. (III) Superposition of the spectra I and II, each taken with its appropriate individual statistical weight parameter, F^- and F^+. In both mechanism cases, the same coupling parameter value system was used for calculations: $b_H = 0.7$, $C_0 = 0.7$, $C_1 = -0.2$, $F^+ = 1.0$, $F^- = 0.2$, $\Omega_{O\cdots O} = 100\,\text{cm}^{-1}$. The transition frequencies are in the $\omega_{O\cdots O}$ vibrational quantum units, and the transition frequencies are expressed with respect to the gravity center of the hypothetical spectrum of a monomeric hydrogen bond in the cyclic deuterium bond dimer. Transition intensities are in arbitrary units.

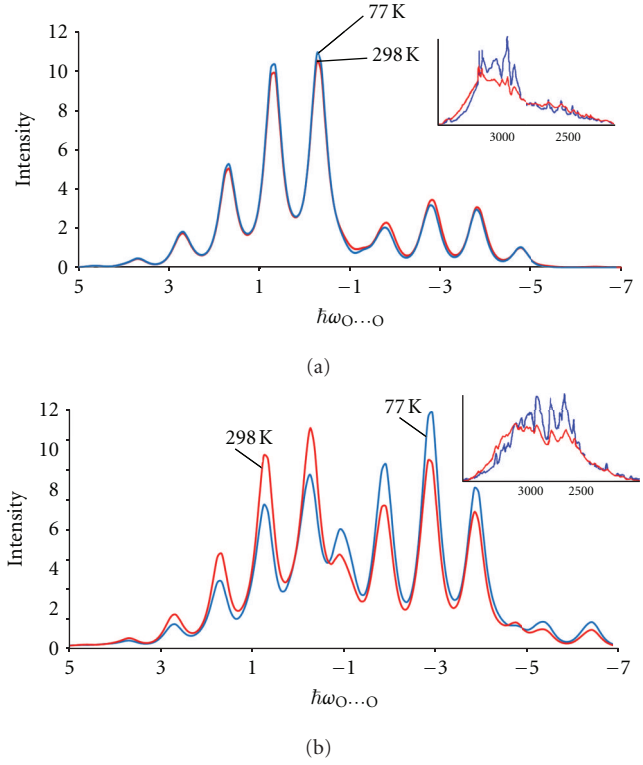

FIGURE 16: Temperature-induced evolution of the ν_{O-H} band contour shapes accompanying the variation in the contribution rate of the two different exciton coupling mechanisms, that is, "*side-to-side*" (SS) and "*tail-to-head*" (TH). Numerical reproduction of the temperature effect in the spectra of hydrogen-bonded (a) *2-furanacetic acid* crystal (b) *2-furanacrylic acid* crystal. The relative contribution ratio of the SS and TH mechanisms in the ν_{O-H} band generation is, for *2-furanacetic acid* crystal: 0.95 : 0.05 at 293 K and 0.95 : 0.05 at 77 K and for *2-furanacrylic acid* crystal: 0.65 : 0.35 at 293 K and 0.40 : 0.60 at 77 K. The experimental spectra are shown in inset.

shape evolution accompanies temperature changes during the spectral experiments.

From the comparison of the corresponding calculated and experimental spectra, it results that the intensity distribution patterns and the temperature effects in the spectra of the two different crystalline systems have been at least semiquantitatively reproduced via the model calculations.

10. Spectra of *2-Furanacetic* and *2-Furanacrylic Acid* Crystals

On comparing the IR spectra of the hydrogen bond for the two crystalline systems, essential differences analyzed crystalline spectra othe ν_{O-H} and ν_{O-D} bands. In the case of *2-furanacetic acid* spectra, the fine structure pattern of each band, ν_{O-H} and ν_{O-D}, is relatively simple. Each band consists of a low number of well-separated spectral lines. In the spectra of *2-furanacrylic acid*, each considered band is composed of a noticeably larger number of lines (ca. 2 times larger). It seems to prove a more complex mechanism of the spectra generation in the case of *2-furanacrylic acid* in relation to the mechanism governing the spectra generation of *2-furanacetic acid*.

The analyzed crystalline spectra of *2-furanacetic acid* seem to fully belong to the case A. On the other hand, the crystalline spectra of *2-furanacrylic acid* seem to satisfy the demands of the case B. The analyzed difference in the spectral properties of *arylacetic acid* dimers and the *arylacrylic acid* dimers most probably results from the influences exerted on to the hydrogen bond dimers, present in the $(COOH)_2$ cycles, by the aromatic rings. The direct contact between the furan rings with carboxyl groups (*arylcarboxylic*, *furanacrylic*, and *thiopheneacrylic acids*) most likely influences the electric charge density in the $(COOH)_2$ cycles. This in turn strengthens the vibronic mechanism of the electronic current generation in the hydrogen bond cycles [45]. Separation of the carboxyl groups from aromatic rings by *methylene*

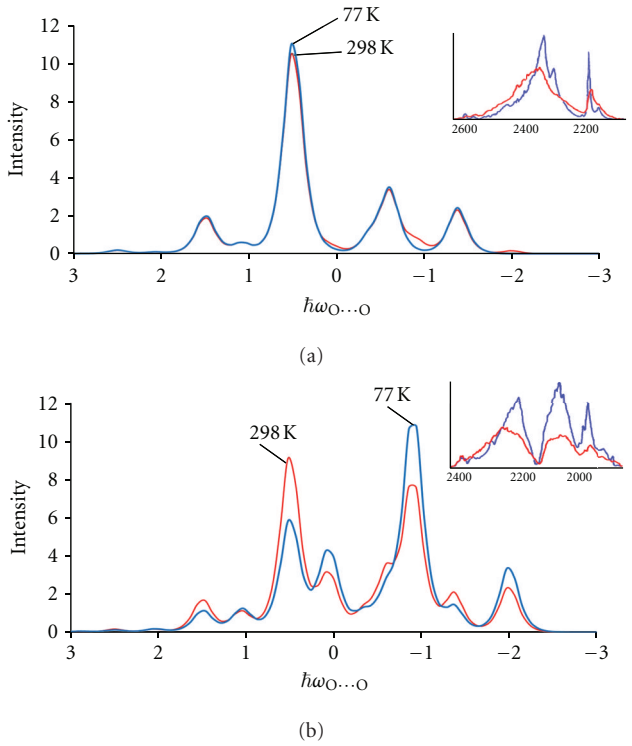

FIGURE 17: Temperature-induced evolution of the ν_{O-D} band-contour shapes accompanying the variation in the contribution rate of the two different exciton coupling mechanisms, that is, "*side-to-side*" (SS) and "*tail-to-head*" (TH). Numerical reproduction of the temperature effect in the spectra of deuterium-bonded: (a) *2-furanacetic acid* crystal (b) *2-furanacrylic acid* crystal.The relative contribution ratio of the SS and TH mechanism in the ν_{O-D} band generation is, for *2-furanacetic acid* crystal: 0.95 : 0.05 at 293 K and 0.95 : 0.05 at 77 K and for *2-furanacrylic acid* crystal: 0.65 : 0.35 at 293 K and 0.40 : 0.60 at 77 K. The experimental spectra are shown in inset.

groups (*arylacetic acids*, *furanacetic acids*, and *thiopheneacetic acids*) effectively weakens the vibronic coupling mechanism. Therefore, these latter systems belong to the A case.

The analyzed spectral properties of the two different crystalline systems, *2-furanacetic acid* and *2-furanacrylic acid*, are in a good agreement with the described above vibrational exciton interaction mechanisms of the spectra generation for cyclic hydrogen bond dimer. This remains in a close relation to the electronic properties of the two carboxylic acid molecules. For *2-furanacetic acid* dimers, the exciton interactions involving the dimer hydrogen bonds of a SS-type is only weakly temperature dependent. In the case of *2-furanacrylic acid* dimers, due to their electronic structure, the interhydrogen bond exciton coupling mechanism changes its character along with the changes in temperature. At very low temperatures, the TH-type interactions, transferred in the $(COOH)_2$ cycles via electrons are dominating. When temperature increases, this mechanism becomes less privileged as being annihilated by the hydrogen-bond atom thermal vibrational motions. It is replaced by the other mechanism depending of the SS-type interactions. Each individual mechanism generates its own spectrum characterized by its unique intensity distribution pattern. Therefore, the ν_{O-H} and ν_{O-D} bands in the spectra of *2-furanacrylic acid* crystals exhibit more complex fine structure patterns, since they are superposition of two different spectra, where each component spectrum is of a different origin. Each component spectrum contributing to the ν_{O-H} and ν_{O-D} band formation, with its statistical weight parameter depended of temperature, corresponds with another exciton interaction mechanism in the cyclic hydrogen bond dimers in the lattice.

Spectra of *2-thiopheneacrylic acid* crystals [50] exhibit qualitatively fairly similar properties as the spectra of *2-furanacrylic acid* crystals. Their ν_{O-H} and ν_{O-D} bands also demonstrate complex and dense fine structure patterns. They also show very similar temperature effects when compared with the corresponding spectra of *2-furanacrylic acid* crystals.

In turn, the spectra of *2-thiopheneacetic acid* crystals [50] exhibit qualitatively very similar properties as the spectra of *2-furanacetic acid* crystals. Their ν_{O-H} and ν_{O-D} bands also exhibit relatively simple fine structure patterns. They also demonstrate fairly similar temperature effects when compared with the corresponding spectra of *2-furanacetic acid* crystals.

From the comparison of the spectra of the two different groups of carboxylic acid crystals, it results that the electronic structure of the associating molecules is the main factor determining the crystal spectral properties in IR, differentiating the spectral properties of the two groups of hydrogen-bonded systems. Namely, the temperature effects registered in IR spectra of the hydrogen bond in carboxylic acid crystals remain in a close connection with the electronic spectra of the associating molecules forming cyclic hydrogen-bonded dimers in the lattices.

11. The Problem of the Vibrational Selection Breaking in IR Spectra of Centrosymmetric Hydrogen Bond Dimers

The mechanism proposed in this paper for understanding the sources of temperature effects in the IR spectra of cyclic centrosymmetric hydrogen bond dimers explains the generation of the lower-frequency ν_{O-H} and ν_{O-D} band branches of extremely high intensities in IR spectra of carboxylic acid crystals. However, at this stage, the relation with the formerly published vibronic mechanism of the vibrational rule selection breaking in the IR spectra of centrosymmetric hydrogen bond dimers [35] ought to be discussed since both mechanisms can generate and also explain qualitatively fairly similar spectral effects.

The vibronic mechanism was originally elaborated in the past for the understanding of the fine structure patterns of the published earlier IR spectra of the cyclic, centrosymmetric N–H$\cdots$S bond dimers formed by 2-thiopyridone and 2-mercaptobenzothiazole molecules as well as extremely nonregular H/D isotopic effects in the spectra [37, 39, 51]. The isotopic effects were expressed by the unusually narrow ν_{N-D} bands in correspondence to the very wide ν_{N-H} bands characterized by complex fine structure patterns. In terms of the vibronic model, these effects were

explained by the disappearance of the intensity of the lower-frequency branch of the ν_{N-D} bands attributed to the N–D bond totally symmetric stretching vibrations in the dimers, due to the weakening of the forbidden transition promotion mechanism [35]. In the case of the ν_{N-H} bands, the promotion mechanism was effective enough generating the forbidden transition spectral branch of noticeably high intensity. Nevertheless, this branch appeared to be less intense when compared with the allowed transition, higher-frequency branch of the ν_{N-H} band. The vibronic model ascribed these effects to the difference in the proton and deuteron vibration anharmonicity and to the extremely high polarizability of the N–H$\cdots$S hydrogen bonds in 2-thiopyridone and 2-mercaptobenzothiazole dimers. These factors were considered as responsible for the magnitude of the vibrational selection rule breaking effects in the dimeric IR spectra [35].

The IR spectra of carboxylic acid crystals with cyclic dimers in their lattices considerably differ by the analogous H/D isotopic effects from the spectra of the N–H$\cdots$S bonded dimers [22–27, 37, 39]. In the case of carboxylic acid crystals practically no impact of the isotopic substitution onto the relative intensity of the lower-frequency band branch intensities of the ν_{O-H} and ν_{O-D} bands in relation to the corresponding higher-frequency band branch intensities. can be noticed. Also the incidentally observed very high intensities of the forbidden transition bands distinguish these IR spectra of carboxylic acid crystals. This proves that the spectra generation mechanism for the carboxylic acid dimers in the crystals essentially differs from the vibronic selection rule breaking mechanism [35].

The following question arises in the scope of our latest estimations: should the vibronic mechanism be definitively rejected as inadequate in the description of the IR spectral properties of centrosymmetric hydrogen bond dimers, especially carboxylic acid dimers in the solid state?

From our hitherto studies of IR spectra of hydrogen-bonded molecular crystals, it results that the two different mechanisms forming the band structures act parallel, each with its individual statistical weight, depending of the electronic properties of the molecular systems forming the dimers. In the case of cyclic dimeric N–H$\cdots$S bonded molecular systems, the vibronic mechanism appeared to be relatively very sufficient, leading to the appearance of intense forbidden transition ν_{N-H} band branches. On the other hand, the ν_{N-D} bands are extremely narrow as practically devoid of the forbidden band branch [37, 39]. The vibronic mechanism is also effective in the generation of IR spectra of crystals with infinite open chains of hydrogen bonded molecules, for example, N-methylthioacetamide [42] or N-phenylacrylamide [52] crystals. Also the H/D isotopic effects in their spectra are fairly similar to the analogous isotopic effects in the corresponding spectra of the N–H$\cdots$S bonded cyclic dimers. In these chain structures, centrosymmetric hydrogen bond dimeric systems are composed of hydrogen bonds, where each moiety belongs to another chain of associated molecules penetrating a unit cell. Most probably, the chain structure of the molecular associates, which excludes the possibility of the induction to circulating electric currents in such dimers, as well as the polarization properties of these hydrogen bonds, is responsible for the existence of the vibronic mechanism [35] in the pure form, influencing the band contour formation.

For the carboxylic acid dimer spectra, the mechanism proposed in this work is dominant regardless of the electronic structure of the substituent atomic groups linked to the carboxyl groups in the molecules. On the basis of the "*state-of-art*" in the spectral studies of the hydrogen bond systems in molecular crystals, the H/D isotopic effects in the spectra seem to be the main criterion for distinguishing these two individual mechanisms. However, this problem demands further intensive studies in the future.

12. Conclusions

In this paper, we report experimental and theoretical study of IR spectra of *2-furanacetic* acid and of *2-furanacrylic acid* crystals measured at 293 K and 77 K in the ν_{O-H} and ν_{O-D} band frequency ranges. The corresponding spectra of the two individual systems strongly differ. Indeed, in the case of *2-furanacetic acid* spectra, the fine structure pattern of each band, ν_{O-H} and ν_{O-D}, is relatively simple. Each band consists of a low number of well-separated spectral lines. In the spectra of *2-furanacrylic acid,* each considered band is composed of a noticeably larger number of lines. In addition, the temperature effect characterizing the bands is not the same for the two compounds. The results presented in this paper for *2-furanacetic acid* and *2-furanacrylic acid* allow for the following observations and conclusions.

(1) The crystal IR spectral properties remain in a close relation with the electronic structure of the two different molecular systems. The vibronic coupling mechanism involving the hydrogen bond protons and the electrons on the π-electronic systems in the molecules determines the way in which the vibrational exciton coupling between the hydrogen bonds in the carboxylic acid dimers occurs.

(2) The analyzed spectral properties of the two different crystalline systems, *2-furanacetic acid* and 2-furanacrylic acid, are in a good agreement with the vibrational exciton interaction mechanisms of the spectra generation for cyclic hydrogen bond dimer.

(3) For *2-furanacetic acid* dimers, the exciton interactions involving the dimer hydrogen bonds of the SS type are only weakly temperature dependent. A weak "through-space" coupling in *2-furanacetic acid* dimers of a van der Waals type is responsible for the SS-type coupling.

(4) In the case of *2-furanacrylic acid* dimers, due to their electronic molecular structure, the interhydrogen bond exciton coupling mechanism strongly changes its character along with the changes in temperature. Strong coupling in *2-furanacrylic acid* dimers prefers a TH-type Davydov coupling widespread by the π-electrons. At very low temperatures, the TH-type interactions, transferred in the $(COOH)_2$ cycles via

electrons are dominating. This mechanism becomes less privileged at higher temperature as annihilated by the hydrogen-bond atom thermal vibrational motions.

(5) Each individual mechanism, that is, the TH and SS, generates its own spectrum characterized by its unique individual intensity distribution pattern. As we can see, the ν_{O-H} and ν_{O-D} bands in the spectra of *2-furanacrylic acid* crystals exhibit more complex fine structure patterns, since they are superposition of two different spectra, where each component spectrum is of a different origin. Each component spectrum contributing to the ν_{O-H} and ν_{O-D} bands formation, with its temperature-dependent statistical weight, corresponds with the different exciton interaction mechanism, TH or SS, acting in the cyclic hydrogen bond dimers in the lattice. This explains the observed difference in the temperature-induced evolution of the compared spectra.

References

[1] C. Pimentel and A. L. McClellan, *The Hydrogen Bond*, W. H. Freeman and Co, San Francisco, Calif, USA, 1960.

[2] P. Schuster, G. Zundel, and C. Sandorfy, *The Hydrogen Bond*, vol. 1–3, North-Holland, Amsterdam, The Netherlands, 1976.

[3] G. L. Hofacker, Y. Marechal, and M. A. Ratner, "The dynamical aspects of hydrogen bonds," in *In The Hydrogen Bond, Recent Developments in Theory and Experiment*, W. P. Schuster, G. Zundel, and C. Sandorfy, Eds., vol. 1, p. 295, North-Holland, Amsterdam, The Netherlands, 1976.

[4] P. Schuster and W. Mikenda, *Hydrogen Bond Research, Monatshefte fûr Chemie, Chemical Monthly*, vol. 130, Springer, New York, NY, USA, 8th edition, 1999.

[5] D. Hadzi, Ed., *Theoretical Treatments of Hydrogen Bonding*, Wiley, New York, NY, USA, 1997.

[6] A. Witkowski, "Infrared spectra of the hydrogen-bonded carboxylic acids," *The Journal of Chemical Physics*, vol. 47, no. 9, pp. 3679–3680, 1967.

[7] Y. Marechal and A. Witkowski, "Infrared spectra of H-bonded systems," *The Journal of Chemical Physics*, vol. 48, no. 8, pp. 3697–3705, 1968.

[8] S. F. Fischer, G. L. Hofacker, and M. A. Ratner, "Spectral behavior of hydrogen-bonded systems: quasiparticle model," *The Journal of Chemical Physics*, vol. 52, no. 4, pp. 1934–1947, 1970.

[9] O. Henri-Rousseau and P. Blaise, "The infrared spectral density of weak hydrogen bonds within the linear response theory," *Advances in Chemical Physics*, vol. 103, pp. 1–137, 1998.

[10] O. Henri-Rousseau and P. Blaise, "The V_{X-H} line shapes of centrosymmetric cyclic dimers involving weak hydrogen bonds," *Advances in Chemical Physics*, vol. 139, pp. 245–496, 2008.

[11] M. J. Wójcik, "Theoretical interpretation of infrared spectra of the Cl–H stretching vibration in the gaseous (Ch3)2O· · · HCl complex," *International Journal of Quantum Chemistry*, vol. 29, no. 4, pp. 855–865, 1986.

[12] J. L. Leviel and Y. Marechal, "Infrared spectra of H-bonded systems: anharmonicity of the H-bond vibrations in cyclic dimers," *The Journal of Chemical Physics*, vol. 54, no. 3, pp. 1104–1107, 1971.

[13] J. Bournay and Y. Maréchal, "Dynamics of protons in hydrogen-bonded systems: propynoic and acrylic acid dimers," *The Journal of Chemical Physics*, vol. 55, no. 3, pp. 1230–1235, 1971.

[14] P. Excoffon and Y. Marechal, "Infrared spectra of H-bonded systems: saturated carboxylic acid dimers," *Spectrochimica Acta A*, vol. 28, no. 2, pp. 269–283, 1972.

[15] M. J. Wójcik, "Theory of the infrared spectra of the hydrogen bond in molecular crystals," *International Journal of Quantum Chemistry*, vol. 10, no. 4, pp. 747–760, 1976.

[16] H.T. Flakus and A. Bańczyk, "Abnormal distribution of protons and deuterons between the hydrogen bonds in cyclic centrosymmetric dimers in partially deuterated samples," *Journal of Molecular Structure*, vol. 476, no. 1–3, pp. 57–68, 1999.

[17] H. T. Flakus, "Vibronic model for H/D isotopic self-organization effects in centrosymmetric dimers of hydrogen bonds," *Journal of Molecular Structure*, vol. 646, no. 1–3, pp. 15–23, 2003.

[18] H. T. Flakus and A. Michta, "Investigations of interhydrogen bond dynamical coupling effects in the polarized IR spectra of acetanilide crystals," *Journal of Physical Chemistry A*, vol. 114, no. 4, pp. 1688–1698, 2010.

[19] R. W. G. Wyckoff, *Crystal Structures*, vol. 5, Wiley, New York, NY, USA, 1972.

[20] Z. Berkovitch-Yellin and L. Leiserowitz, "Atom-atom potential analysis of the packing characteristics of carboxylic acids. A study based on experimental electron density distributions," *Journal of the American Chemical Society*, vol. 104, no. 15, pp. 4052–4064, 1982.

[21] E. B. Wilson, J. C. Decius, and P. C. Cross, *Molecular Vibrations; The Theory of Infrared and Raman Vibrational Spectra*, McGraw- Hill, New York, NY, USA, 1955.

[22] H. T. Flakus and A. Miros, "Infrared spectra of the hydrogen bonded glutaric acid crystals: polarization and temperature effects," *Journal of Molecular Structure*, vol. 484, no. 1–3, pp. 103–115, 1999.

[23] H. T. Flakus and M. Chelmecki, "Infrared spectra of the hydrogen bond in benzoic acid crystals: temperature and polarization effects," *Spectrochimica Acta A*, vol. 58, no. 1, pp. 179–196, 2002.

[24] H. T. Flakus and M. Jabłońska, "Study of hydrogen bond polarized IR spectra of cinnamic acid crystals," *Journal of Molecular Structure*, vol. 707, no. 1–3, pp. 97–108, 2004.

[25] H. T. Flakus and M. Chełmecki, "Polarization IR spectra of the hydrogen bond in phenylacetic acid crystals: H/D isotopic effects-temperature and polarization effects," *Spectrochimica Acta Part A*, vol. 58, no. 9, pp. 1867–1880, 2002.

[26] H. T. Flakus and M. Chełmecki, "Polarization IR spectra of hydrogen bonded 1-naphthoic acid and 2-naphthoic acid crystals: electronic effects in the spectra," *Journal of Molecular Structure*, vol. 659, no. 1–3, pp. 103–117, 2003.

[27] H. T. Flakus and M. Chełmecki, "Polarization IR spectra of the hydrogen bond in 1-naphthylacetic and 2-naphthylacetic acid crystals: H/D isotopic effects. Temperature and polarization effects," *Journal of Molecular Structure*, vol. 705, no. 1–3, pp. 81–89, 2004.

[28] S. E. Filippakis and G. M. J. Schmidt, "Topochemistry. Part XVI. The crystal structure of trans-β-2-furylacrylic acid," *Journal of the Chemical Society B*, pp. 229–232, 1967.

[29] M. Danish, S. Ali, M. Mazhar, A. Badshah, and E. R. T. Tieking, "Crystal structure of 3-(2-Furyl)acrylic Acid, $C_7H_6O_3$," *Zeitschrift für Kristallographie*, vol. 210, no. 9, p. 703, 1995.

[30] H. T. Flakus and A. Tyl, "Polarized IR spectra of the hydrogen bond in acetic acid crystals," *Chemical Physics*, vol. 336, no. 1, pp. 36–50, 2007.

[31] H. T. Flakus and B. Stachowska, "A systematic study of polarized IR spectra of the hydrogen bond in formic acid crystals," *Chemical Physics*, vol. 330, no. 1-2, pp. 231–244, 2006.

[32] A. Tyl, E. Chełmecka, M. Jabłońska et al., "X-ray analysis at 150 K, synthesis and theoretical calculations of 1-naphthaleneacrylic acid," *Structural Chemistry*, vol. 23, no. 2, pp. 325–323, 2012.

[33] H. T. Flakus, M. Jabłońska, and P.G. Jones, "Study of polarized IR spectra of the hydrogen bond system in crystals of styrylacetic acid," *Spectrochimica Acta A*, vol. 65, no. 2, pp. 481–489, 2006.

[34] G. Fisher, *Vibronic Coupling*, Acadamic Press, London, UK, 1984.

[35] H. T. Flakus, "On the vibrational transition selection rules for the centrosymmetric hydrogen-bonded dimeric systems," *Journal of Molecular Structure C*, vol. 187, pp. 35–53, 1989.

[36] H. T. Flakus, A. Pyzik, A. Michta, and J. Kusz, "'Reversal' exciton coupling effect in the IR spectra of the hydrogen bond cyclic dimers; polarized IR spectra of 3-hydroxy-4-methyl-2(3H)-thiazolethione crystals," *Vibrational Spectroscopy*, vol. 44, no. 1, pp. 108–120, 2007.

[37] H. T. Flakus and A. Tyl, "Strong vibrational exciton coupling effects in polarized IR spectra of the hydrogen bond in 2-thiopyridone crystals," *Vibrational Spectroscopy*, vol. 47, no. 2, pp. 129–138, 2008.

[38] H. T. Flakus, A. Tyl, and A. Maślankiewicz, "Electron-induced phase transition in hydrogen-bonded solid-state 2-pyridone," *Journal of Physical Chemistry A*, vol. 115, no. 6, pp. 1027–1039, 2011.

[39] H. T. Flakus, A. Miros, and P. G. Jones, "Influence of molecular electronic properties on the IR spectra of dimeric hydrogen bond systems: polarized spectra of 2-hydroxybenzothiazole and 2-mercaptobenzothiazole crystals," *Journal of Molecular Structure*, vol. 604, no. 1, pp. 29–44, 2002.

[40] H. T. Flakus and A. Machelska, "Polarization IR spectra of hydrogen bonded pyrazole crystals: self-organization effects in proton and deuteron mixture systems. Long-range H/D isotopic effects," *Spectrochimica Acta Part A*, vol. 58, no. 314, pp. 553–566, 2002.

[41] H. T. Flakus, A. Tyl, and P. G. Jones, "'Self-organization' processes in proton and deuteron mixtures in open-chain hydrogen bond systems: Polarization IR spectra of 4-mercaptopyridine crystals," *Spectrochimica Acta A*, vol. 58, no. 2, pp. 299–310, 2002.

[42] H. T. Flakus, W. Śmiszek-Lindert, and K. Stadnicka, "Strong vibronic coupling effects in polarized IR spectra of the hydrogen bond in N-methylthioacetamide crystals," *Chemical Physics*, vol. 335, no. 2-3, pp. 221–232, 2007.

[43] C. A. Davydov, *Teorya Molekularnykh Ekscitonov*, Nauka, Moscow, Russia, 1968.

[44] R. L. Hochstrasser, *Molecular Aspects of Symmetry*, W. A. Benjamin Inc., New York, NY, USA, 1966.

[45] L. A. Nafie, "Adiabatic molecular properties beyond the Born-Oppenheimer approximation. Complete adiabatic wave functions and vibrationally induced electronic current density," *The Journal of Chemical Physics*, vol. 79, no. 10, pp. 4950–4957, 1983.

[46] H.T. Flakus, "The effect of strong coupling between vibrations in hydrogen bonds on the polarized spectra of the mercaptobenzothiazole crystal: an "anomalous" isotopic effect," *Chemical Physics*, vol. 62, no. 1-2, pp. 103–114, 1981.

[47] P. Blaise, M. J. Wojcik, and O. Henri-Rousseau, "Theoretical Interpretation of the Lineshape of the Gaseous Acetic Acid Dimer.," *Journal of Chemical Physics*, vol. 122, Article ID 064306, 2005.

[48] N. Rekik, H. Ghalla, H. T. Flakus, M. Jablońska, P. Blaise, and B. Oujia, "Polarized infrared spectra of the H(D) bond in 2-thiophenic acid crystals: a spectroscopic and computational study," *ChemPhysChem*, vol. 10, no. 17, pp. 3021–3033, 2009.

[49] R. Najeh, G. Houcine, H. T. Flakus, M. Jablonska, and O. Brahim, "Experimental and theoretical study of the polarized infrared spectra of the hydrogen bond in 3-thiophenic acid crystal," *Journal of Computational Chemistry*, vol. 31, no. 3, pp. 463–475, 2010.

[50] H. T. Flakus, N. Rekik, and A. Jarczyk, "Polarized IR spectra of the hydrogen bond in 2-thiopheneacetic acid and 2-thiopheneacrylic acid crystals: H/D isotopic and temperature effects," *The Journal of Physical Chemistry A*, vol. 116, no. 9, pp. 2117–2130, 2012.

[51] L. J. Bellamy and P. E. Rogasch, "Proton transfer in hydrogen bonded systems," *Proceedings of the Royal Society A*, vol. 257, pp. 98–108, 1960.

[52] H. T. Flakus, A. Michta, M. Nowak, and J. Kusz, "Effects of dynamical couplings in IR spectra of the hydrogen bond in N-phenylacrylamide crystals," *Journal of Physical Chemistry A*, vol. 115, no. 17, pp. 4202–4213, 2011.

Hindawi Publishing Corporation
Journal of Atomic, Molecular, and Optical Physics
Volume 2012, Article ID 985490, 17 pages
doi:10.1155/2012/985490

Review Article

Theoretical Studies of Dynamic Interactions in Excited States of Hydrogen-Bonded Systems

Marek J. Wójcik, Marek Boczar, and Łukasz Boda

Faculty of Chemistry, Jagiellonian University, Ingardena 3, Kraków 30-060, Poland

Correspondence should be addressed to Marek J. Wójcik, wojcik@chemia.uj.edu.pl

Received 1 March 2012; Accepted 19 May 2012

Academic Editor: Paul Blaise

Copyright © 2012 Marek J. Wójcik et al. This is an open access article distributed under the Creative Commons Attribution License, which permits unrestricted use, distribution, and reproduction in any medium, provided the original work is properly cited.

Theoretical model for vibrational interactions in the hydrogen-bonded benzoic acid dimer is presented. The model takes into account anharmonic-type couplings between the high-frequency O–H and the low-frequency O$\cdots$O stretching vibrations in two hydrogen bonds, resonance interactions between two hydrogen bonds in the dimer, and Fermi resonance between the O–H stretching fundamental and the first overtone of the O–H in-plane bending vibrations. The model is used for theoretical simulation of the O–H stretching IR absorption bands of benzoic acid dimers in the gas phase in the first excited singlet state. *Ab initio* CIS and CIS(D)/CIS/6-311++G(d,p) calculations have been carried out in the $\tilde{A}$ state of tropolone. The grids of potential energy surfaces along the coordinates of the tunneling vibration and the low-frequency coupled vibration have been calculated. Two-dimensional model potentials have been fitted to the calculated potential energy surfaces. The tunneling splittings for vibrationally excited states have been calculated and compared with the available experimental data. The model potential energy surfaces give good estimation of the tunneling splittings in the vibrationally ground and excited states of tropolone, and explain monotonic decrease in tunneling splittings with the excitation of low-frequency out-of-plane modes and increase of the tunneling splittings with the excitation of low-frequency planar modes.

1. Introduction

There is recently a considerable interest in studies of hydrogen-bonded carboxylic acid dimers. The main reason comes from the fact that they constitute good models to study systems with two interacting intermolecular hydrogen bonds. Of special interest is the process of double proton tunneling along hydrogen bonds in both the ground and excited electronic states.

Electronic spectroscopy of hydrogen-bonded dimers has recently received considerable attention due to significant development and the widespread use of supersonic free jet techniques. Many investigators still use classical spectroscopic techniques, such as the vibrational spectroscopy, to study hydrogen-bonded complexes in their ground electronic states.

It is well known that vibrational spectra provide physical information on the dynamics of hydrogen bonds. The most prominent spectral changes resulting from H bond formation occur in the IR spectra, especially in the region of the X–H stretching bands (ν_s): decrease in the frequency of the ν_s stretching mode, increase of its intensity, broadening of the bands and appearance of a complex fine structure. These spectacular features of the infrared absorption band of the ν_s mode have been a subject of several theoretical studies [1–11].

An anharmonic-type coupling between the high-frequency X–H stretching and the low-frequency X$\cdots$Y hydrogen bond stretching vibration, described in a quantum mechanical way by Maréchal and Witkowski [1] is an important mechanism responsible for the unique structure of ν_s bands of hydrogen-bonded systems. Another important mechanism influencing the fine structure of ν_s band is Fermi resonance. Theoretical quantum mechanical model treating this mechanism was proposed by Witkowski and Wójcik [3]

for a single hydrogen bond and by Wójcik [4] for hydrogen-bonded dimers.

Benzoic acid is the simplest aromatic carboxylic acid and is also one of the most important acids in chemistry. The electronic spectra of benzoic acid have been a subject of extensive studies for a long time. Ito et al. [12] investigated the effect of dimerization on the UV absorption spectrum. Baba and Kitamura [13] examined the emission properties of the monomer and the dimer in glass solution. Baum and McClure, in series of papers, examined the absorption and emission spectra of benzoic acid dimers in single crystals of benzene [14, 15] as well as in hydrocarbon glasses [16, 17]. Later, Poeltl and McVey have reported for the first time the laser induced fluorescence excitation spectrum [18] and next the fluorescence emission spectra [19] of jet-cooled benzoic acid dimers. Tomioka et al. [20] studied the correlation between the frequencies of intermolecular hydrogen bond vibrations between the fluorescence excitation and dispersed fluorescence spectra and concluded that potentials for such vibrations are affected very little upon electronic excitation. Significant discovery was made by Remmers and et al. [21]. On the basis of their high resolution ultraviolet rotationally resolved excitation spectrum of benzoic acid dimer, they have demonstrated convincingly that the linear and planar (C_{2h} symmetry) ground state geometry of the dimer is slightly in-plane bent (C_s symmetry) upon electronic excitation. Recently Nandi and Chakraborty [22] have reinvestigated the laser-induced dispersed fluorescence spectra and analyzed vibronic mode mixing in benzoic acid dimer with aid of DFT calculations. Among jet spectroscopic techniques there is increasing use of double resonance methods, which allow measure, for example, IR absorption of electronically excited species.

In recent years, infrared spectra of the O–H stretch region of benzoic acid dimer have been studied in both the ground and excited electronic state by Florio and et al. [23] using the FDIR (fluorescence-dip infrared) IR-UV double resonance method in supersonic jet. The authors have also computed theoretical IR spectrum of benzoic acid dimer using anharmonic constants [23, 24]. Benzoic acid has been also studied in the ground state by traditional spectroscopic techniques. Infrared spectra of hydrogen-bonded benzoic acid crystals have been recorded and interpreted theoretically by Flakus et al. [25–29] and more recently by Boczar et al. [30] The present work constitutes a development of this study and is also a continuation of our recent spectroscopic and theoretical studies of vibrational spectra of hydrogen-bonded 1-methylthymine [31], acetic acid [32], and salicylic acid [33]. Theoretical studies on different hydrogen-bonded chemical and biochemical systems in excited electronic states have been performed in recent years [34–37].

The motion of protons in hydrogen bonds causes great number of interesting physical effects. Quantum effects, such as the proton tunneling phenomenon, and strong interactions with vibrating surrounding atoms in hydrogen bonds are of special interest. The importance of proton tunneling in chemical and biological systems is well known, for example, for the DNA base pairing, as discussed by Löwdin [38]. The phenomenon of potential barrier penetration plays an important role in many branches of physics: quantum field theory, fission of atomic nuclei, scanning tunneling microscopy, and solid state physics [39]. In recent decade appeared several theoretical studies of proton tunneling in different systems [40–49].

Theoretical studies of proton tunneling require the knowledge of multidimensional potential energy surfaces which are difficult to obtain from *ab initio* calculations, especially for electronically excited states. Tropolone with its intramolecular hydrogen bond is a model substance for studying tunneling process in the ground as well as in the excited electronic state [50–59]. The geometry of tropolone is presented in Figure 4. Multidimensional proton tunneling in tropolone has been theoretically studied by Vener et al. [56] using adiabatic separation of variables. Smedarchina et al. [57] used instanton approach to account for tunneling splittings. Takada and Nakamura [58] studied model potentials. On the base of *ab initio* calculations they proposed model potential energy surfaces (PES) for electronically ground $\tilde{X}$ state of tropolone and employed it to analyze dynamics of proton tunneling. They were however unable to perform similar calculations for the excited $\tilde{A}$ state. In this paper we report results of high accuracy *ab initio* calculations of the potential energy surface in the excited $\tilde{A}$ state of tropolone. We fit two-dimensional analytical model potentials to these surfaces and by solving the two-dimensional vibrational problems, we interpret observed splittings and their dependence on vibrational excitations in the laser fluorescence excitation spectra of jet-cooled tropolone [53, 54]. This work constitutes improvement of previous approach of Wójcik et al. [59] to multidimensional proton tunneling in the excited state of tropolone.

This review presents results published in [60, 61]. In Section 2 we present theoretical interpretation of vibrational interactions in hydrogen bonds in benzoic acid dimer in the first excited electronic state and interpret its experimental FDIR spectrum recorded by Florio et al. [23]. The theoretical model describing these interactions is proposed and used to simulate the fine structure of the O–H stretching IR absorption band in the S_1 electronic state. In addition quantum mechanical *ab initio* calculations have been made in order to obtain the excited state structure of benzoic acid dimer and its vibrational frequencies. In Section 3 we present the results of quantum chemical calculations for the $\tilde{A}$ state of tropolone. We discuss two-dimensional potential models of the tunneling and interpret experimentally observed tunneling splittings [53, 54]. Concluding remarks are given at the end of each section.

2. Theoretical Interpretation of Vibrational Interactions in Hydrogen Bonds in Benzoic Acid Dimer in the First Excited Singlet State S_1

2.1. Quantum Chemical Calculations. All calculations have been carried out using the Gaussian 03 package [62]. The vertical singlet state energies were obtained by the *ab initio* single excitation configuration-interaction calculations at

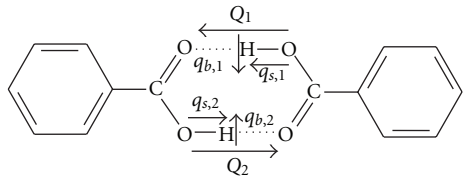

FIGURE 1: Oscillatory motions in the hydrogen bonds in the benzoic acid dimer considered in the models.

the CIS [63] and CIS(D) [64, 65] levels with the 6-311++G(d,p) basis set. The calculations were performed for the five lowest singlet excited states of benzoic acid dimer starting from the C_{2h} ground state geometry optimized at B3LYP/6-311++G(d,p) level. The RHF/6-311++G(d,p) population analysis was also performed for the ground state geometry in order to examine the orbitals involved in proper electronic excitations.

In the first excited singlet state (S_1) the geometry of benzoic acid dimer was optimized and the vibrational frequencies were computed at the CIS/6-311++G(d,p) level. To ensure reliable frequencies of low-frequency vibrational modes (with very small force constants), especially intermolecular, in the present calculations we used the tight convergence criteria.

2.2. Theoretical Model. We make the following physical assumptions in the model of the ν_s IR bandshapes of the benzoic acid dimer in the gas phase in its electronic ground S_0 and the first excited S_1 state. This model will be use for quantitative calculations of the spectra.

(1) In our model the basic physical mechanism responsible for the energy and intensity distributions within the IR O–H stretching absorption band is an anharmonic-type coupling between the high-frequency O–H stretching vibration and the low-frequency hydrogen bond O$\cdots$O stretching vibration (ν_σ) in each hydrogen bond. Since the ν_s oscillatory motion is at least an order of magnitude faster than the oscillatory motion ν_σ, the vibrational wavefunction for these modes is represented in crude adiabatic approximation. This approximation is true only for weak and medium strong hydrogen bonds. The high-frequency ν_s vibration determines potential for the low-frequency ν_σ vibration in each hydrogen bond. The ν_s and ν_σ vibrations are assumed to be harmonic.

(2) When ν_s vibration is excited, there is shift of equilibrium position of the potential energy for ν_σ vibration (linear distortion). We do not consider change of force constant after excitation.

(3) In the ground electronic state (S_0) the benzoic acid dimer has C_{2h} symmetry, therefore in the case of two equivalent intermolecular hydrogen bonds, present in the dimer, a nonadiabatic resonance interaction (Davydov coupling) is considered in the degenerate excited vibrational state of the ν_s vibrations. This effect is a vibrational analogue of the vibronic coupling, such as the pseudo-Jahn-Teller effect, occurring in the electronic spectra of symmetric dimers [64]. From the experimental data it has been concluded that in the first excited electronic state benzoic acid dimer is in-plane bent as an effect of localised electronic excitation on one moiety of the dimer [14, 18, 19, 21].

(4) In our model we also consider Fermi resonance between the O–H stretching fundamental and the first overtone of the O–H in-plane bending (ν_b) in each hydrogen bond in the dimer.

2.2.1. Vibrational Hamiltonians for The Dimer. Let us consider a planar cyclic dimer of benzoic acid, presented in Figure 1. In the ground electronic state it has C_{2h} symmetry with two hydrogen bonds, linking two moieties of the dimer, related by the symmetry operator $\hat{C}_2$ corresponding to two-fold symmetry axis. Theoretical model of such dimer with Fermi resonance, presented below, has been developed by Wójcik [4].

We denote by $q_{s,i}$, $q_{b,i}$, and Q_i ($i = 1, 2$) the coordinates of the O–H stretching, O–H in-plane bending, and O$\cdots$O hydrogen bond stretching vibrations in the first or second hydrogen bond (Figure 1). The corresponding frequencies are denoted by ω_s, ω_b, Ω.

The vibrational Hamiltonian $\hat{H}$ of the dimer has the form:

$$\hat{H} = \hat{T}(Q_1) + \hat{T}(Q_2) + \hat{h}_{s,1} + \hat{h}_{s,2} + \hat{h}_{b,1} + \hat{h}_{b,2} + V_{\mathrm{ah},1} + V_{\mathrm{ah},2} + V_{\mathrm{res}}, \tag{1}$$

where $\hat{T}(Q_i)$ are the kinetic energy operators of the low-frequency O$\cdots$O vibrations; $\hat{h}_{s,i} = \hat{T}(q_{s,i}) + U(q_{s,i}, Q_i)$ the vibrational Hamiltonians of the high frequency O–H stretching vibrations; $\hat{h}_{b,i} = \hat{T}(q_{b,i}) + U(q_{b,i})$ vibrational Hamiltonians of the high-frequency O–H in-plane bending vibrations; $V_{\mathrm{ah},i}$ anharmonic coupling terms between the O–H stretching and O–H in-plane bending vibrations; $V_{\mathrm{res}}(q_{s,1}, q_{s,2})$ is a resonance coupling between two equivalent hydrogen bonds. Udenotes the potential energy.

The total vibrational wavefunction $\Psi^+_{j'}$ describing the first excited state of the ν_s vibration takes a four-component form:

$$\Psi^+_m = \alpha_1\varphi^+_{s,1}\varphi_{b,1}\varphi_{s,2}\varphi_{b,2} + \beta_1\varphi_{s,1}\varphi^+_{b,1}\varphi_{s,2}\varphi_{b,2} + \alpha_2\varphi_{s,1}\varphi_{b,1}\varphi^+_{s,2}\varphi_{b,2} + \beta_2\varphi_{s,1}\varphi_{b,1}\varphi_{s,2}\varphi^+_{b,2}, \tag{2}$$

where $\varphi_{s,i}(q_{s,i}, Q_i)$ are the eigenfunctions of the Hamiltonians $\hat{h}_{s,i}$; $\varphi_{b,i}(q_{b,i})$ the eigenfunctions of the Hamiltonians $\hat{h}_{b,i}$; and $\alpha_i(Q), \beta_i(Q)$ are the wavefunctions of the hydrogen bond vibrations ν_σ, not yet determined.

To determine these wavefunctions and the total vibrational energy we use the variational principle [66]:

$$\delta\left\langle \Psi^+_m \middle| \hat{H} \middle| \Psi^+_m \right\rangle = E_m \delta\langle \Psi^+_m \mid \Psi^+_m \rangle \tag{3}$$

applied to the Schrödinger equation with the Hamiltonian (1) and the wavefunction (2). With the crude adiabatic approximation assumed for the ν_s and ν_σ vibrations ($[\hat{T}(Q_i), \chi_{s,i}] = 0$), the effective Hamiltonian $\hat{\mathbf{H}}^{\text{eff}}$ for the low-frequency vibrations ν_σ takes the four-dimensional matrix form:

$$\hat{\mathbf{H}}^{\text{eff}}\& = \begin{bmatrix} \hat{T}(Q_1) + \hat{T}(Q_2) + \varepsilon^{+}_{s,1}(Q_1) + \varepsilon_{s,2}(Q_2) + \varepsilon_{b,1} + \varepsilon_{b,2}, V^{\text{ah}}_{\text{int}}, V^{\text{res}}_{\text{int}}, 0 \\ V^{\text{ah}}_{\text{int}}, \hat{T}(Q_1) + \hat{T}(Q_2) + \varepsilon_{s,1}(Q_1) + \varepsilon_{s,2}(Q_2) + \varepsilon^{+}_{b,1} + \varepsilon_{b,2}, 0, 0 \\ V^{\text{res}}_{\text{int}}, 0, \hat{T}(Q_1) + \hat{T}(Q_2) + \varepsilon_{s,1}(Q_1) + \varepsilon^{+}_{s,2}(Q_2) + \varepsilon_{b,1} + \varepsilon_{b,2}, V^{\text{ah}}_{\text{int}} \\ 0, 0, V^{\text{ah}}_{\text{int}}, \hat{T}(Q_1) + \hat{T}(Q_2) + \varepsilon_{s,1}(Q_1) + \varepsilon_{s,2}(Q_2) + \varepsilon_{b,1} + \varepsilon^{+}_{b,2} \end{bmatrix}, \tag{4}$$

where $\varepsilon_{s,i}(Q_i)$ are the eigenvalues of the Hamiltonians $\hat{h}_{s,i}$, $\varepsilon_{b,i}$ the eigenvalues of the Hamiltonians $\hat{h}_{b,i}$, $V^{\text{ah}}_{\text{int}}$ the matrix element of the anharmonic coupling between excited states of ν_s and ν_b, and $V^{\text{res}}_{\text{int}}$ is the matrix element of resonance interaction (vibrational analogue of the exchange integral). They are defined as:

$$\begin{aligned} V^{\text{ah}}_{\text{int}} &= \left\langle \varphi^{+}_{s,1}\varphi_{b,1}\varphi_{s,2}\varphi_{b,2} \,|\, V_{\text{ah},1} \,|\, \varphi_{s,1}\varphi^{+}_{b,1}\varphi_{s,2}\varphi_{b,2} \right\rangle_{q_s,q_b} \\ &= \left\langle \varphi_{s,1}\varphi_{b,1}\varphi^{+}_{s,2}\varphi_{b,2} \,|\, V_{\text{ah},2} \,|\, \varphi_{s,1}\varphi_{b,1}\varphi_{s,2}\varphi^{+}_{b,2} \right\rangle_{q_s,q_b}, \\ V^{\text{res}}_{\text{int}} &= \left\langle \varphi^{+}_{s,1}\varphi_{b,1}\varphi_{s,2}\varphi_{b,2} | V_{\text{res}} | \varphi_{s,1}\varphi_{b,1}\varphi^{+}_{s,2}\varphi_{b,2} \right\rangle_{q_s,q_b}. \end{aligned} \tag{5}$$

The energies $\varepsilon_{s,i}(Q_i)$ of the high-frequency O–H stretching vibrations in individual hydrogen bonds determine effective potential for the low-frequency hydrogen bond vibrations. We assume that these potentials are harmonic with the same force constant in the ground and excited states of the O–H stretching vibrations:

$$\varepsilon_{s,i} = \frac{1}{2}KQ_i^2, \qquad \varepsilon^{+}_{s,i} = R + LQ_i + \frac{1}{2}KQ_i^2, \tag{6}$$

where R is the vertical excitation energy, L the linear distortion parameter, and K is the force constant.

Introducing dimensionless quantities:

$$\begin{aligned} q_i &= Q_i\left(\frac{M\Omega}{\hbar}\right)^{1/2}, \qquad p_i = \frac{P_i}{(\hbar M\Omega)^{1/2}}, \\ b &= \frac{L}{(\hbar M\Omega^3)^{1/2}}, \\ r &= \frac{R}{\hbar\Omega}, \qquad r' = \frac{R'}{\hbar\Omega}, \\ V^{\text{ah}} &= \frac{V^{\text{ah}}_{\text{int}}}{\hbar\Omega}, \qquad V^{\text{res}} = \frac{V^{\text{res}}_{\text{int}}}{\hbar\Omega}, \end{aligned} \tag{7}$$

where Ω is the angular frequency and M the reduced mass for the ν_σ vibration we can rewrite the Hamiltonian (4) in the following form:

$$\begin{aligned} \hat{\mathbf{h}}^{\text{eff}} &= \frac{\hat{\mathbf{H}}^{\text{eff}}}{\hbar\Omega} \\ &= \begin{bmatrix} \frac{1}{2}\sum_{i=1}^{2}(p_i^2 + q_i^2) + bq_1 + r, V^{\text{ah}}, V^{\text{res}}, 0 \\ V^{\text{ah}}, \frac{1}{2}\sum_{i=1}^{2}(p_i^2 + q_i^2) + r', 0, 0 \\ V^{\text{res}}, 0, \frac{1}{2}\sum_{i=1}^{2}(p_i^2 + q_i^2) + bq_2 + r, V^{\text{ah}} \\ 0, 0, V^{\text{ah}}, \frac{1}{2}\sum_{i=1}^{2}(p_i^2 + q_i^2) + r' \end{bmatrix}. \end{aligned} \tag{8}$$

Dimensionless parameters r and r' describe vertical excitation energies to the first excited state of the ν_s vibration and to the first overtone of the ν_b vibration. For exact Fermi resonance $r = r'$.

The four-dimensional matrix Hamiltonian (8) can be reduced to the two-dimensional Hamiltonians $\hat{\mathbf{h}}^{+}$ and $\hat{\mathbf{h}}^{-}$ using the symmetry operator $\hat{C}_2$. The method of reduction was devised by Fulton and Gouterman [67]. The Hamiltonians $\hat{\mathbf{h}}^{+}$ and $\hat{\mathbf{h}}^{-}$ are given by the formula:

$$\hat{\mathbf{h}}^{\pm} = \begin{bmatrix} \frac{1}{2}\sum_{i=1}^{2}(p_i^2 + q_i^2) + bq_1 + r + V^{\text{res}}\hat{C}_2, V^{\text{ah}} \\ V^{\text{ah}}, \frac{1}{2}\sum_{i=1}^{2}(p_i^2 + q_i^2) + r' \end{bmatrix}. \tag{9}$$

Eigenfunctions of this Hamitonians have the spinor form:

$$\begin{bmatrix} \alpha^{(m)}_{\pm} \\ \beta^{(m)}_{\pm} \end{bmatrix}. \tag{10}$$

In the first excited singlet state benzoic acid dimer is in-plane bent [14, 19, 21]. Such symmetry lowering (from C_{2h} to C_s) causes that degeneracy is removed and Davydov coupling significantly decreases. Also two hydrogen bonds are no longer equivalent, thus the model parameters (linear distortion b, vertical excitation energies r and r', and matrix elements describing Fermi resonance $V^{\text{ah}}_{\text{int}}$ must be different for two hydrogen bonds. Since benzoic acid dimer is no longer centrosymmetric in the S_1 state, the effective matrix Hamiltonian (8) cannot be reduced in this case to

Table 1: Calculated wavelengths of electronic transitions to the three lowest allowed [1] (π, π^*) states of benzoic acid dimer.

Electronic state	Experiment [16, 18]	CIS/6-311++G(d,p)	CIS(D)/6-311++G(d,p)
S_1 (B_u)	280 nm (35724 cm^{-1})	214 nm	248 nm
S_2 (B_u)	230 nm	211 nm	204 nm
S_3 (A_u)	190 nm	178 nm	182 nm

two-dimensional Hamiltonians by the Fulton-Gouterman method and takes the following form:

$$\hat{\mathbf{h}}^{\text{eff}}_{(S_1)} = \begin{bmatrix} \frac{1}{2}\sum_{i=1}^{2}(p_i^2+q_i^2) + bq_1 + r_1, V_1^{\text{ah}}, V^{\text{res}}, 0 \\ V_1^{\text{ah}}, \frac{1}{2}\sum_{i=1}^{2}(p_i^2+q_i^2) + r_1', 0, 0 \\ V^{\text{res}}, 0, \frac{1}{2}\sum_{i=1}^{2}(p_i^2+q_i^2) + bq_2 + r_2, V_2^{\text{ah}} \\ 0, 0, V_2^{\text{ah}}, \frac{1}{2}\sum_{i=1}^{2}(p_i^2+q_i^2) + r_2' \end{bmatrix}. \quad (11)$$

Compared with (8), the model parameters in the Hamiltonian (10) have indices 1 or 2 to describe two hydrogen bonds, which are no longer equivalent in the excited electronic state of the benzoic acid dimer.

2.2.2. Intensities. IR intensities of the transitions from the ground state to the excited state of the O–H stretching vibrations are given by the formula:

$$I_{nm} = \left| \left\langle \Psi_n \left| \hat{\vec{\mu}} \right| \Psi_m^+ \right\rangle \right|^2 \exp\left[-\frac{E_n}{kT} \right], \quad (12)$$

where Ψ_n is the nth wavefunction of the ground vibrational state of the ν_s and ν_b vibrations, Ψ_m^+ is the mth wavefunction of the excited vibrational state, $\vec{\mu}$ is the dipole moment of the dimer, and E_n is the vibrational energy of the ground vibrational state of the ν_s and ν_b vibrations.

The wavefunctions Ψ_m^+ are given by (2) and the wavefunctions Ψ_n, in the adiabatic approximation, have the form:

$$\Psi_n = \alpha_0^{(n)} \varphi_{s,1} \varphi_{b,1} \varphi_{s,2} \varphi_{b,2}. \quad (13)$$

Neglecting dependence of the dipole moment $\vec{\mu}$ on the coordinates Q of the low-frequency hydrogen bond vibration, we obtain the intensity given as a combination of the Franck-Condon integrals between the wavefunctions $\alpha_0^{(n)}$ and the symmetrical low-frequency eigenfunctions $\alpha_\pm^{(m)}$, $\beta_\pm^{(m)}$ of the Hamiltonians (9):

$$I_{nm}^{IR(S_0)} = |M_{0s}| \left| \left\langle \alpha_0^{(n)} \left| 1 \pm \hat{C}_2 \right| \alpha_\pm^{(m)} \right\rangle + \delta \left\langle \alpha_0^{(n)} \left| 1 \pm \hat{C}_2 \right| \beta_\pm^{(m)} \right\rangle \right|^2 \exp\left[-\frac{E_n}{kT} \right], \quad (14)$$

where:

$$M_{0s} = \left\langle \varphi_{s,1}\varphi_{b,1}\varphi_{s,2}\varphi_{b,2} \left| \hat{\vec{\mu}} \right| \varphi_{s,1}^+ \varphi_{b,1}\varphi_{s,2}\varphi_{b,2} \right\rangle_{q_s, q_b} = \text{const}, \quad (15)$$

and δ^2 is the ratio of the intensities of the bending overtone to the fundamental stretching bands.

In the S_1 state of the dimer, due to nonequivalence of the two hydrogen bonds, the formula for intensities of IR transitions takes the form:

$$I_{nm}^{IR(S_1)} \sim \left| \left\langle \alpha_0^{(n)} \mid \alpha_1^{(m)} \right\rangle + \delta \left\langle \alpha_0^{(n)} \mid \beta_1^{(m)} \right\rangle + \left\langle \alpha_0^{(n)} \mid \alpha_2^{(m)} \right\rangle + \delta \left\langle \alpha_0^{(n)} \mid \beta_2^{(m)} \right\rangle \right|^2 \exp\left[-\frac{E_n}{kT} \right]. \quad (16)$$

To obtain this formula we used spinor eigenfunctions of the Hamiltonian (11):

$$\begin{bmatrix} \alpha_1^{(m)} \\ \beta_1^{(m)} \\ \alpha_2^{(m)} \\ \beta_2^{(m)} \end{bmatrix}. \quad (17)$$

For simplicity we assumed in the formula (16) that transition moments (15) are the same for both hydrogen bonds in the dimer in the S_1 state.

2.3. Results and Discussion. The UV absorption spectrum of benzoic acid consists of three bands: A (190 nm), B (230 nm), and C (280 nm) [16, 18], which result from single photon transitions to three lowest electronic states. All three bands are associated with the $\pi^* \leftarrow \pi$ transitions and there is general agreement that the C band is an effect of transition analogous to the $^1B_{2u} \leftarrow ^1A_{1g}$ transition in benzene. Table 1 presents the calculated excitation energies for benzoic acid dimer for the first three allowed excited states obtained by the CIS and CIS(D) methods, which are compared with the experimental data. The comparison was made on the basis of the analysis of orbitals involved in electronic excitations, calculated oscillator strengths, and symmetry of the states.

Figure 2 presents the geometry of benzoic acid dimer in excited electronic state optimized at the CIS/6-311++G(d,p) and numbering the atoms. Calculated bond lengths and bond angles are summarized in Table 2. The calculated values confirm the experimental predictions that electronic excitation leads to the shortening of one of the hydrogen bonds, whereas the other is lengthened. Also one can observe the asymmetry in calculated corresponding geometrical parameters within the aromatic rings.

The predicted dipole moment of benzoic acid dimer in the S_1 state is 0.55 D with 0.54 D component along axis of the dimer and 0.12 D component perpendicular to the axis of the dimer. The calculated rotational constants for the electronically excited dimer are A = 1949.2 MHz, B = 124.6 MHz, and C = 117.1 MHz.

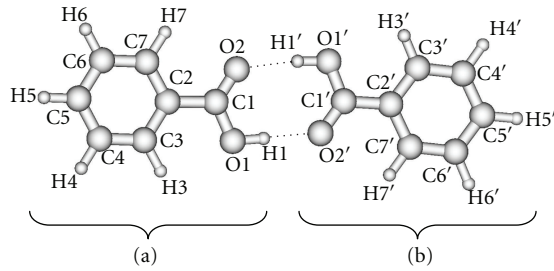

Figure 2: Geometry of the benzoic acid dimer in S_1 state, optimized at the CIS/6-311++G(d,p) level with numbering of atoms and labelling of the monomer units (a and b).

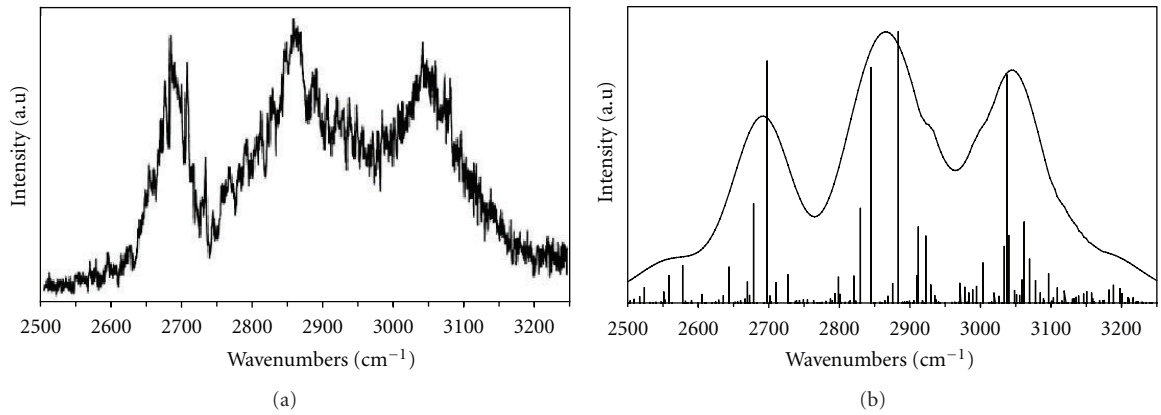

Figure 3: Comparison between (a) the experimental [23] and (b) theoretical (Dirac δ functions and solid line) O–H stretching IR absorption bands for benzoic acid dimer in the S_1 state.

In Table 3 we present the calculated vibrational frequencies of benzoic acid dimer in the S_1 state. This table contains also symmetry and description of the normal modes. All frequencies have been uniformly scaled by a factor of 0.9 as recommended to compensate for the neglect of mechanical anharmonicity and lack of electron correlation in the CIS method [68]. We used the MOLDEN program [69] to visualize the amplitudes of the normal modes.

The experimental FDIR (fluorescence-dip infrared) spectra of benzoic acid dimers in the excited state, taken from [23], are presented in Figure 3(a) for the O–H stretch region. Both bands exhibit fine structures. The ν_s bands are composed of three main branches, which suggest presence of Fermi resonances. To reproduce the fine structure of experimental O–H stretching absorption bands of benzoic acid dimer, we used theoretical model presented in Section 2.2.1. The model describes complex interplay of three different vibrational couplings in a network of hydrogen bonds in benzoic acid dimer—an anharmonic coupling between the high-frequency O–H stretching and the low-frequency intermolecular O$\cdots$O stretching modes, resonance (Davydov) interaction between two intermolecular hydrogen bonds in a cyclic system, and Fermi resonance between the O–H stretching and the overtone of the O–H in-plane bending vibrations. For the dimers in the S_1 state lowering of their symmetry upon electronic excitation was taken into account.

The experimental frequencies of the O$\cdots$O hydrogen bonds stretching modes, observed in the jet-dispersed fluorescence and laser induced fluorescence spectra of benzoic acid, have been reported to be 118 cm^{-1} for both the S_0 and S_1 states of the dimer [18, 22]. This frequency was taken into account in our model calculations.

To calculate energies and intensities of transitions between the ground and first excited vibrational states of the O–H stretching vibrations, we solved the Schrödinger equations for both states. In the ground state the energies and eigenfunctions are the solutions of equations for harmonic oscillator. In the excited state they are solutions of the Schrödinger equation with the Hamiltonian (11) for S_1. The energies and eigenfunctions in the excited vibrational O–H state were calculated variationally by approximating two components of the spinor (10) in the ground electronic state or four components of the spinor (17) in the excited electronic state by finite linear combinations of fourfold products of harmonic oscillator wavefunctions. We assumed the temperature 10 K as close to typical temperature of cold environment of free-jet expansion.

We have fitted the calculated spectra to the position of the peak with maximum intensity. In calculations of the S_1 IR spectra we took the frequencies 3367 and 3473 cm^{-1} from *ab initio* CIS calculations for two O–H groups forming hydrogen bonds. We also assumed exact Fermi resonances ($r_1 = r_1'$, $r_2 = r_2'$).

In order to determine optimum parameters we performed series of calculations of the ν_s stretching bands to minimize the square root deviation between experimental and

Table 2: Optimized geometry of the S_1 excited-state benzoic acid dimer by the CIS/6-311++G(d,p) method.

Bond lengths (Å)		Angles (deg)	
O1· · · O2′	2.739	O1–H1· · · O2′	176.7
O2· · · O1′	2.800	O1′–H1′ · · · O2	175.3
O1–H1	0.963	C1–O1–H1	110.8
O1′–H1′	0.958	C1′–O1′–H1′	110.5
O2′ · · · H1	1.776	C1–O2· · · H1′	129.8
O2· · · H1′	1.844	C1′–O2′ · · · H1	131.1
C1–O1	1.304	O1–C1–O2	123.2
C1′–O1′	1.315	O1′–C1′–O2′	122.6
C1=O2	1.200	O1–C1–C2	114.2
C1′=O2′	1.213	O1′–C1′–C2′	114.6
C1–C2	1.489	O2–C1–C2	122.6
C1′–C2′	1.447	O2′–C1′–C2′	122.8
C2–C3	1.389	C1–C2–C3	121.4
C2′–C3′	1.402	C1′–C2′–C3′	123.5
C3–C4	1.384	C2–C3–C4	119.9
C3′–C4′	1.414	C2′–C3′–C4′	120.4
C4–C5	1.386	C3–C4–C5	120.0
C4′–C5′	1.417	C3′–C4′–C5′	121.9
C5–C6	1.387	C4–C5–C6	120.3
C5′–C6′	1.397	C4′–C5′–C6′	118.1
C6–C7	1.383	C5–C6–C7	119.9
C6′–C7′	1.412	C5′–C6′–C7′	120.7
C7–C2	1.390	C6–C7–C2	120.0
C7′–C2′	1.436	C6′–C7′–C2′	121.3
C3–H3	1.073	C7–C2–C3	120.0
C3′–H3′	1.072	C7′–C2′–C3′	117.7
C4–H4	1.075	C7–C2–C1	118.6
C4′–H4′	1.074	C7′–C2′–C1′	118.8
C5–H5	1.076	C2–C3–H3	119.7
C5′–H5′	1.072	C2′–C3′–H3′	120.1
C6–H6	1.075	C3–C4–H4	119.9
C6′–H6′	1.074	C3′–C4′–H4′	118.7
C7–H7	1.073	C4–C5–H5	119.9
C7′–H7′	1.073	C4′–C5′–H5′	120.6
		C5–C6–H6	120.2
		C5′–C6′–H6′	120.6
		C6–C7–H7	120.9
		C6′–C7′–H7′	120.3

theoretical spectra. All parameters were determined with the accuracy of 0.01.

Theoretical spectrum of benzoic acid in the S_1 state is shown and compared with the experimental spectrum in Figure 3. The optimized parameters are listed in Table 4. The theoretical spectra are shown as the Dirac delta functions and as bandshapes calculated with Gaussian functions of the optimal half width.

The reproduction of the experimental band is good. Presented results of model calculation correctly reproduce main features of the experimental spectrum. Discrepancies

Table 3: Calculated vibrational frequencies for S_1 state of benzoic acid dimer at the CIS/6-311++G(d,p) level (ν, stretching; δ, in-plane bending; γ, out-of-plane bending; τ, torsion).

No.	Sym.	Freq. ν (cm^{-1})	Approximate description
1	A″	16	"Butterfly" monomers twisting
2	A″	30	Oop. monomers twisting
3	A′	45	Ip. monomers twisting ("cogwheel")
4	A″	52	Oop. monomers rocking
5	A″	71	τ(COOH)
6	A″	80	τ(COOH)
7	A′	87	Ip monomers rocking (H-bond shearing)
8	A′	96	H-Bonds stretching
9	A″	103	τ(COOH)
10	A″	172	γ(–COOH) (A)
11	A′	214	δ(–COOH) (B)
12	A″	215	γ(–COOH) (B)
13	A′	249	δ(–COOH) (A)
14	A″	306	Oop. ring deform. (B)
15	A′	307	Ip. ring deform. (B)
16	A″	327	Oop. asym. rings deform.
17	A′	380	Ip. ring deform. (A)
18	A′	402	Ip. ring deform. (B)
19	A″	409	Oop. ring deform. (A)
20	A″	437	Oop. ring deform. (A)
21	A′	497	δ(C–COOH) (A)
22	A′	525	δ(C–COOH) (B)
23	A′	592	δ(COOH) sciss. + ip. ring deform. (B)
24	A′	606	Ip. ring deform. (A)
25	A″	624	γ(CH) (B)
26	A′	646	δ(COOH) sciss. + ip. ring deform. (A)
27	A″	673	Oop. ring deform. (A)
28	A″	700	γ(COOH) + γ(CH) (B)
29	A″	718	γ(CH) (A)
30	A′	740	δ(COOH) sciss. + ring breath. (B)
31	A″	746	γ(OH) + γ(CH) (B)
32	A″	755	γ(OH) + γ(CH) (B)
33	A′	777	δ(COOH) sciss. + ring breath. (A)
34	A″	780	γ(C–COOH) + γ(OH) + γ(CH) (B)
35	A″	816	γ(C–COOH) + γ(OH) + γ(CH) (A)
36	A″	836	γ(CC) + γ(CH) (B)
37	A″	860	γ(CC) + γ(CH) (A)
38	A″	877	γ(OH) (A)
39	A″	901	γ(OH) (B)
40	A′	903	$\nu(CC)_{ring}$ (B)
41	A′	944	Ring breath. (B)
42	A′	965	$\nu(CC)_{ring}$ (B)
43	A″	965	γ(CH)
44	A′	976	Ring breath. (A)
45	A′	1003	Ring breath. (A)

Table 3: Continued.

No.	Sym.	Freq. ν (cm^{-1})	Approximate description
46	A″	1004	γ_A(CH) (A)
47	A″	1009	γ_A(CH) (A)
48	A′	1021	$\nu(CC)_{ring}$ (B)
49	A′	1050	$\nu(CC)_{ring}$ (A)
50	A′	1089	$\nu(CC)_{ring} + \delta$(CH) (A)
51	A′	1099	$\delta(CC)_{ring} + \delta$(CH) (B)
52	A′	1111	$\nu(CC)_{ring} + \delta$(CH) (A)
53	A′	1133	δ(CH) (B)
54	A′	1155	δ(CH) (A)
55	A′	1201	$\nu(CC)_{ring} + \delta$(CH) (A)
56	A′	1205	$\nu(CC)_{ring} + \delta$(CH) (B)
57	A′	1254	δ(OH) (B)
58	A′	1282	δ(OH) (A)
59	A′	1309	δ(CH) (B)
60	A′	1312	δ(CH) (A)
61	A′	1385	δ(CH) (B)
62	A′	1392	δ(CH) (A+B)
63	A′	1417	δ(CH) (A+B)
64	A′	1437	$\nu(CC)_{ring} + \delta$(CH) (A)
65	A′	1445	$\nu(CC)_{ring} + \delta$(CH) (B)
66	A′	1485	$\nu(CC)_{ring} + \delta$(CH) (A)
67	A′	1533	$\nu(CC)_{ring} + \delta$(CH) (B)
68	A′	1586	$\nu(CC)_{ring}$ (B)
69	A′	1587	$\nu(CC)_{ring}$ (A)
70	A′	1609	$\nu(CC)_{ring}$ (A)
71	A′	1653	ν(C=O) (B)
72	A′	1723	ν(C=O) (A)
73	A′	2990	ν(CH) (A)
74	A′	3004	ν(CH) (A)
75	A′	3013	ν(CH) (A)
76	A′	3015	ν(CH) (B)
77	A′	3020	ν(CH) (B)
78	A′	3034	ν(CH) (A)
79	A′	3038	ν(CH) (A)
80	A′	3039	ν(CH) (B)
81	A′	3047	ν(CH) (B)
82	A′	3051	ν(CH) (B)
83	A′	3367	ν(OH) (A)
84	A′	3473	ν(OH) (B)

The calculated frequencies were uniformly scaled by a factor of 0.9. (A) and (B) label the molecule of the dimer, which is necessary for proper mode description.

between theory and experiment are related to assumptions of the present model. Our model assumes that low-frequency O· · · O motion is harmonic and does not consider electrical anharmonicity. Further improvements of the model should improve agreement between theoretical and experimental bands.

Table 4: Optimized parameters (the frequencies of the O–H stretching vibrations for S_1 state were taken at 3367 and 3473 cm^{-1}).

	S_1-state
Ω (exp.)	118 cm^{-1}
b_1	0.89
b_2	0.82
V^{res}	−0.09
V_1^{ah}	0.66
V_2^{ah}	0.72
δ^2 (fixed)	0.01
Half-width	60 cm^{-1}

2.4. Conclusions. We developed a theoretical model for an isolated hydrogen-bonded dimer of benzoic acid, in the excited electronic state, describing vibrational couplings between high- and low-frequency stretching modes in the hydrogen bonds, resonance interactions between two hydrogen bonds, and Fermi resonances between the fundamental O–H stretching and the overtone of the O–H in plane bending vibrations. This model was successfully used for reproduction of experimental spectrum in the excited electronic state of benzoic acid dimer. The experimental frequencies assigned to intermolecular O· · · O hydrogen bond stretching vibrations by *ab initio* calculations were used in our model calculations. The calculated bandshapes and fine structures are in good agreement with the experimental ones. Our results show that considered mechanisms are the most important for hydrogen dynamics in hydrogen-bonded dimers. Infrared spectroscopy is the leading method for studying hydrogen bond properties. Quantitative theory of the IR spectra of hydrogen-bonded dimer, presented in this paper, allows for systematic study of the relation between the properties of the hydrogen bonds in the ground and excited electronic states, which is a problem of major scientific interest.

3. Theoretical Simulation of Proton Tunneling in the Excited Electronic State of Tropolone

3.1. Quantum Chemical Calculations. We performed *ab initio* CIS calculations of the Ã state of tropolone using the GAUSSIAN 03 program package [62]. The geometry was optimized and the vibrational frequencies were calculated by the *ab initio* single-excitation configuration interaction [70] (CIS) with the 6-311++G(d,p). Optimized geometries are summarized in Table 5. Previous calculations of Wójcik et al. [59] performed at the CIS/6-31++G(d,p) gave slightly nonplanar geometry (in the 6-31G(d,p) basis it was planar). Our calculations confirm nonplanar structure. Increased basis set diminishes the C=O bond length by 0.007 Å. The O· · · O distance becomes larger by 0.002 Å and the O–H distance is shorter by 0.002 Å.

The calculated frequencies of the normal modes of the tropolone molecule are summarized in Table 6. The modes used in model calculations are pictured in Figure 5. All

Table 5: Optimized geometries of the tropolone molecule in the Ã state by the CIS method.

Bond lengths	CIS/6-31++G(d,p) [59] (Å)	CIS/6-311++G(d,p) (Å)	Bond angles	CIS/6-31++G(d,p) [59] (°)	CIS/6-311++G(d,p) (°)	Dihedral angles	CIS/6-311++G(d,p) (°)
O1· · · O2	2.534	2.536	O1–H1· · ·O2	—	115.6	C1–C2–C3–C4	−2.2
O1–H1	0.954	0.952	C1–O1–H1	108.4	108.3	C2–C3–C4–C5	8.8
C2=O2	1.218	1.211	O2–O1–H1	44.5	44.5	C3–C4–C5–C6	−0.1
C1–O1	1.320	1.320	C1–C2–O2	113.3	113.5	C4–C5–C6–C7	−10.0
C1–C2	1.512	1.510	C1–C2–C3	125.3	125.3	C5–C6–C7–C1	4.6
C2–C3	1.432	1.435	C2–C3–C4	128.3	128.5	C6–C7–C1–C2	8.6
C3–C4	1.398	1.395	C3–C4–C5	129.7	129.9	C7–C1–C2–C3	−9.8
C4–C5	1.387	1.386	C4–C5–C6	129.4	129.4	O1–C1–C2–O2	−5.9
C5–C6	1.425	1.424	C5–C6–C7	128.3	128.4		
C6–C7	1.387	1.385	C6–C7–C1	128.8	129.0		
C7–C1	1.388	1.388	C7–C1–C2	128.7	128.8		
C3–H3	1.074	1.074	C2–C3–H3	—	113.0		
C4–H4	1.076	1.076	C3–C4–H4	—	115.0		
C5–H5	1.076	1.076	C4–C5–H5	—	115.7		
C6–H6	1.075	1.074	C5–C6–H6	—	115.7		
C7–H7	1.076	1.076	C6–C7–H7	—	117.0		

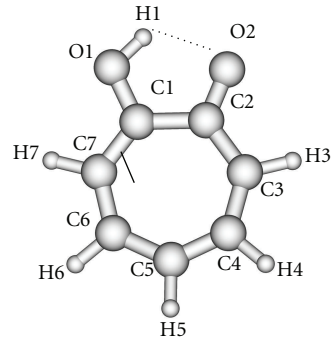

Figure 4: Geometry of the tropolone in the Ã state optimized by the CIS/6-311++G(d,p), with numbering of atoms.

frequencies have been scaled by a factor of 0.9 as recommended to compensate for the neglect of electron correlation [68]. The lowest-frequency ν_{39} mode strikingly changes its frequency from 109 cm^{-1} in the ground $\tilde{X}$ state to 39 cm^{-1} in the excited Ã state [54]. These experimental frequencies are reproduced by calculations of Takada and Nakamura [58] and the present one (105 cm^{-1} and 29 cm^{-1}, resp.). This frequency is especially important for the interpretation of the long sequence of the tunneling energy splittings suppressed by the excitation of this mode [53, 54].

To obtain two-dimensional potential energy surfaces for the high-frequency tunneling mode and one of selected low-frequency modes, nearly planar modes ν_{33} and ν_{34} and out-of-plane modes ν_{38} and ν_{39} we performed *ab initio* calculations of the normal modes of tropolone in the Ã state in high precision format. We applied the keyword "HPModes" in GAUSSIAN in order to obtain the high precision format (to five digits) for vibrational frequency eigenvectors in the frequency output in addition to the normal three-digit output. In the next step, beginning from the optimized equilibrium geometry of the tropolone molecule in the Ã state, the series of geometries were generated. We varied the amplitudes of atomic movements for a given vibrational mode, independently for each of two coupling modes, high frequency O–H stretching tunneling mode and one of the low-frequency modes. For each geometry mass-weighed normal coordinates have been calculated for the tunneling mode and for the low-frequency mode. The amplitudes of atomic movements were varied in the range comprising structures where distances between hydrogen atom and two oxygen atoms are equal. Such points correspond to the barrier in the double well potential surface and the corresponding structures are planar. The number of generated structures for four low-frequency modes coupled with the tunneling mode varied between 620–670 including points corresponding the barrier. For each point the single point energy was calculated at the CIS/6-311++G(d,p) level in the Ã state of tropolone. In this way the one half (including barrier) of double well

Table 6: Computed vibrational frequencies for the tropolone molecule in the $\tilde{A}$ state by the CIS method.

No.	Sym.	CIS/6-31++G(d,p)[59] Freq. (cm^{-1})	CIS/6-311++G(d,p) Freq. (cm^{-1})
1	A	3591	3594
2	A	3041	3021
3	A	3035	3015
4	A	3021	3001
5	A	3015	2994
6	A	3003	2983
7	A	1615	1611
8	A	1548	1538
9	A	1517	1506
10	A	1478	1470
11	A	1431	1423
12	A	1395	1391
13	A	1353	1347
14	A	1281	1273
15	A	1231	1227
16	A	1183	1178
17	A	1145	1139
18	A	1059	1033
19	A	945	998
20	A	899	938
21	A	842	910
22	A	899	894
23	A	842	832
24	A	827	821
25	A	760	752
26	A	703	701
27	A	675	673
28	A	631	617
29	A	616	606
30	A	575	564
31	A	516	515
32	A	477	466
33	A	417	414
34	A	350	348
35	A	347	344
36	A	317	314
37	A	259	262
38	A	132	130
39	A	37	29

potential surface was obtained for each pair of coupled modes. The second half was obtained using the symmetry of the potential.

3.2. Model Calculations. On the basis of the *ab initio* calculations we constructed two-dimensional model PES's for the proton tunneling mode ν_1 coupled to low-frequency modes of tropolone which largely affect the tunneling. These are nearly planar hydrogen-bond streching modes ν_{33} and ν_{34} and the lowest-frequency out-of-plane modes ν_{38} and ν_{39}. They are shown in Figure 5 and their calculated and experimental vibrational frequencies are compared in Table 7.

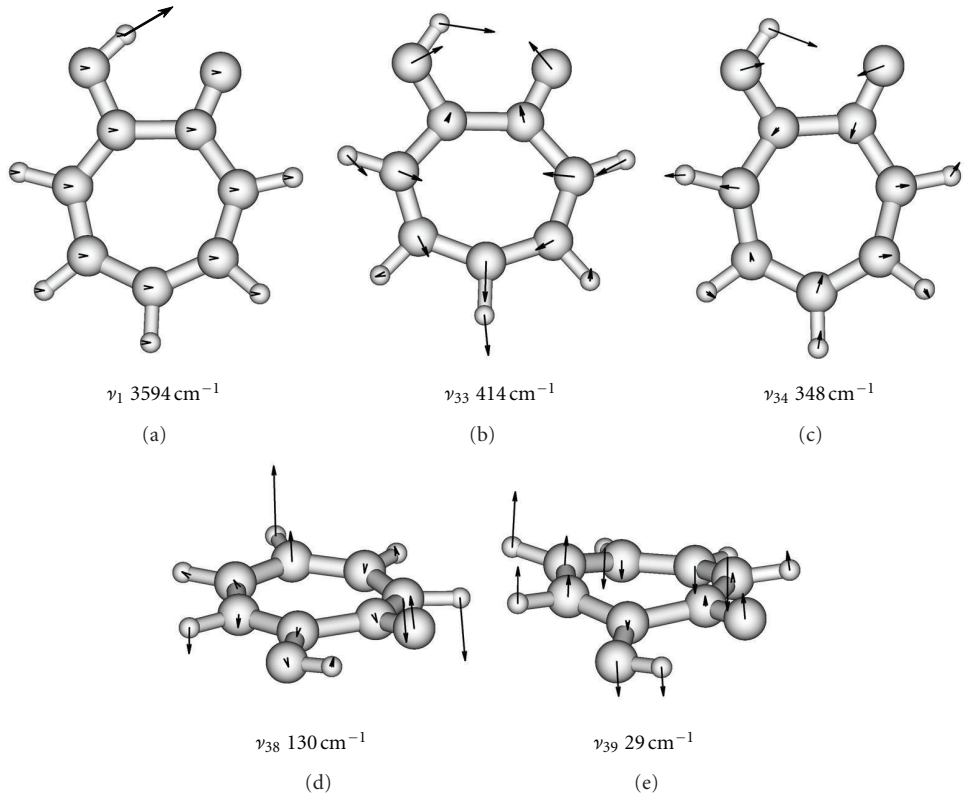

Figure 5: Selected modes of tropolone molecule in the $\tilde{A}$ state calculated by the CIS/6-311++G(d,p) method.

Table 7: Vibrational fundamentals in the $\tilde{A}$ state of tropolone.

Mode	CIS/6-311++G(d,p) (cm^{-1})	Exp. [54] (cm^{-1})
33	414	414
34	348	296
38	130	171
39	29	39

The two-dimensional model potentials used to simulate vibrational couplings are [58]

(a) the symmetric mode coupling potential (SMC) describing couplings of the proton tunneling mode ν_1 with the nearly planar modes ν_{33} and ν_{34}:

$$V_{\mathrm{SMC}} = \frac{1}{8x_0}(x-x_0)^2(x+x_0)^2 + \frac{1}{2}\frac{\omega_y}{\omega_x}\left[y+\alpha(x^2-x_0^2)\right]^2 \tag{18}$$

and

(b) the squeezed double well potential (SQZ) describing couplings of the proton tunneling mode ν_1 with the out-of-plane modes ν_{38} and ν_{39}:

$$V_{\mathrm{SMC}} = \frac{1}{8x_0}(x-x_0)^2(x+x_0)^2 + \frac{1}{2x_0^2}\left[\frac{\omega_z}{\omega_x} - \frac{\gamma(x^2-x_0^2)}{(\omega_z/\omega_x)}\right]^2 z^2, \tag{19}$$

where x (proton tunneling) and y and z (low frequency modes) denote the coordinates of the modes ω_x, ω_y, and ω_z are the angular frequencies $2x_0$, the distance between the two minima, α and γ the coupling strengths. In the formulas (18) and (19), the potentials are expressed in the units of the quantum $\hbar\omega_x$ and the coordinates x, y, and z are dimensionless

$$x = \tilde{x}\sqrt{\frac{m_x\omega_x}{\hbar}}, \quad y = \tilde{y}\sqrt{\frac{m_y\omega_y}{\hbar}}, \quad z = \tilde{z}\sqrt{\frac{m_z\omega_z}{\hbar}}. \tag{20}$$

where $\tilde{x}$, $\tilde{y}$, and $\tilde{z}$ denote the dimensional coordinates and m_x, m_y, and m_z are the effective masses. The model potentials (18) and (19) have been fitted to the grids of

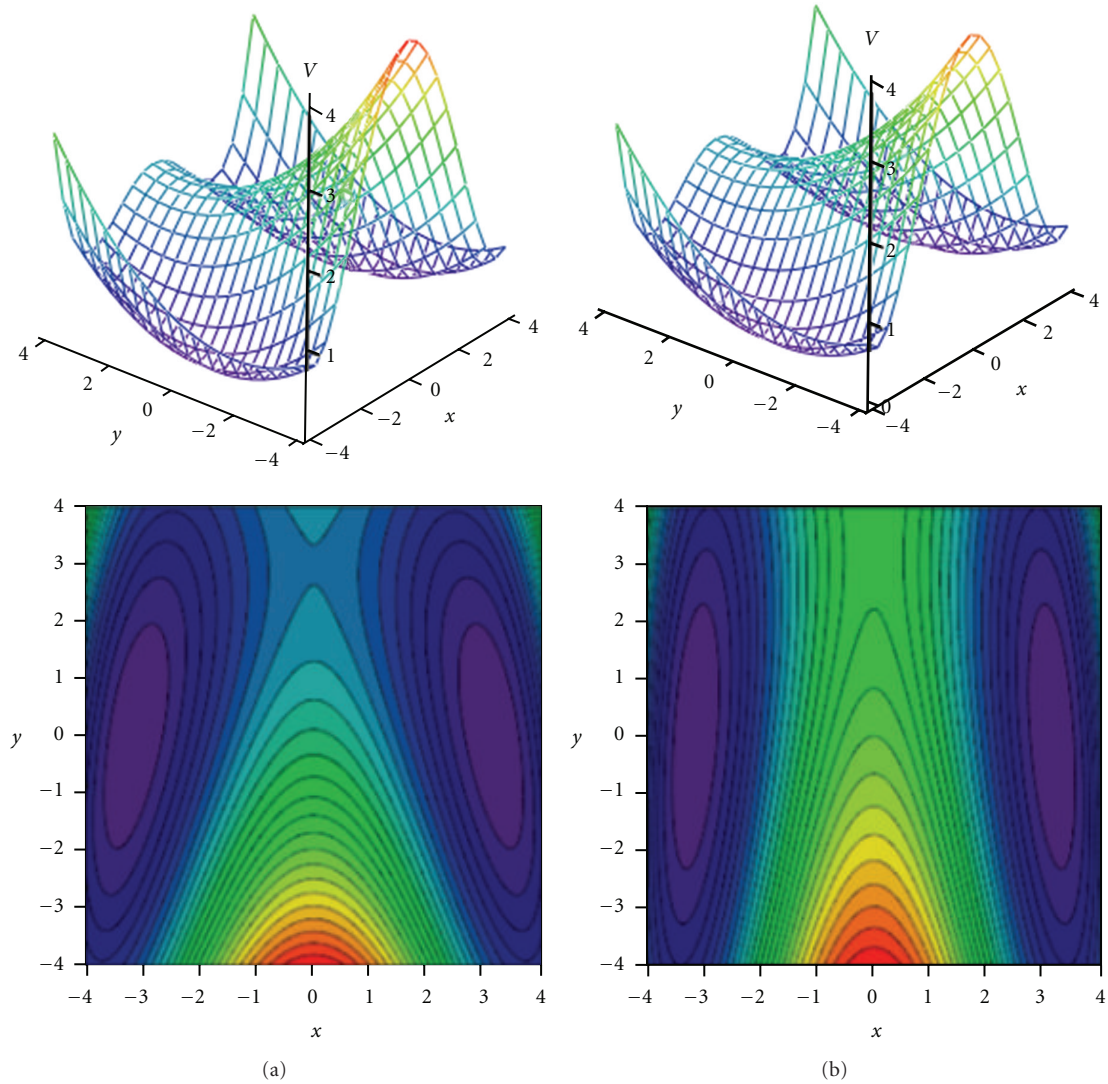

Figure 6: Surface plots and contour maps of the two-dimensional SMC potentials obtained from the *ab initio* CIS calculations for: (a) coupling of ν_1 and ν_{33} modes, (b) coupling of ν_1 and ν_{34} modes.

energy single points obtained from the *ab initio* calculations for each pair: high-frequency tunneling mode and low-frequency mode. The obtained potentials are shown as a surface plots and as a contour plots in Figures 6 and 7. The energy is expressed in the units of the quantum of the high-frequency tunneling mode ν_1. The optimal values of parameters x_0, α, γ, for the model potentials have been found through the nonlinear least-squares method with the Levenberg-Marquardt algorithm [71, 72]. These parameters have been used in subsequent calculations of the energy splittings and they are listed in Table 8. The parameter α describing coupling between the O–H stretching mode ν_1 and the mode ν_{33} or ν_{34} represents an analogue of a linear distortion parameter b_2 used for theoretical reproduction of the O–H infrared bandshape of tropolone [70]. Infrared spectra of tropolone in the excited electronic state $\tilde{A}$ are yet unknown, but the value of the parameter $b_2 = 0.4$, describing the coupling between the ν_1 and ν_{34} modes and used to reproduce IR bandshape of tropolone in the ground electronic state $\tilde{X}$ [73], is consistent with the value of the parameter $\alpha = 0.323$ presently used to reproduce the dependence of the tunneling splittings on excitations of the ν_{34} mode. Both different spectroscopic facts have the same origin, the anharmonic-type coupling in the potential energy between the two O–H and O$\cdots$O vibrations.

Table 8: Parameters of the two-dimensional model potentials given by (18) and (19).

Mode	X_0	α	γ
33	3.15	0.301	
34	3.15	0.323	
38	3.15		0.006640
39	3.15		0.000911

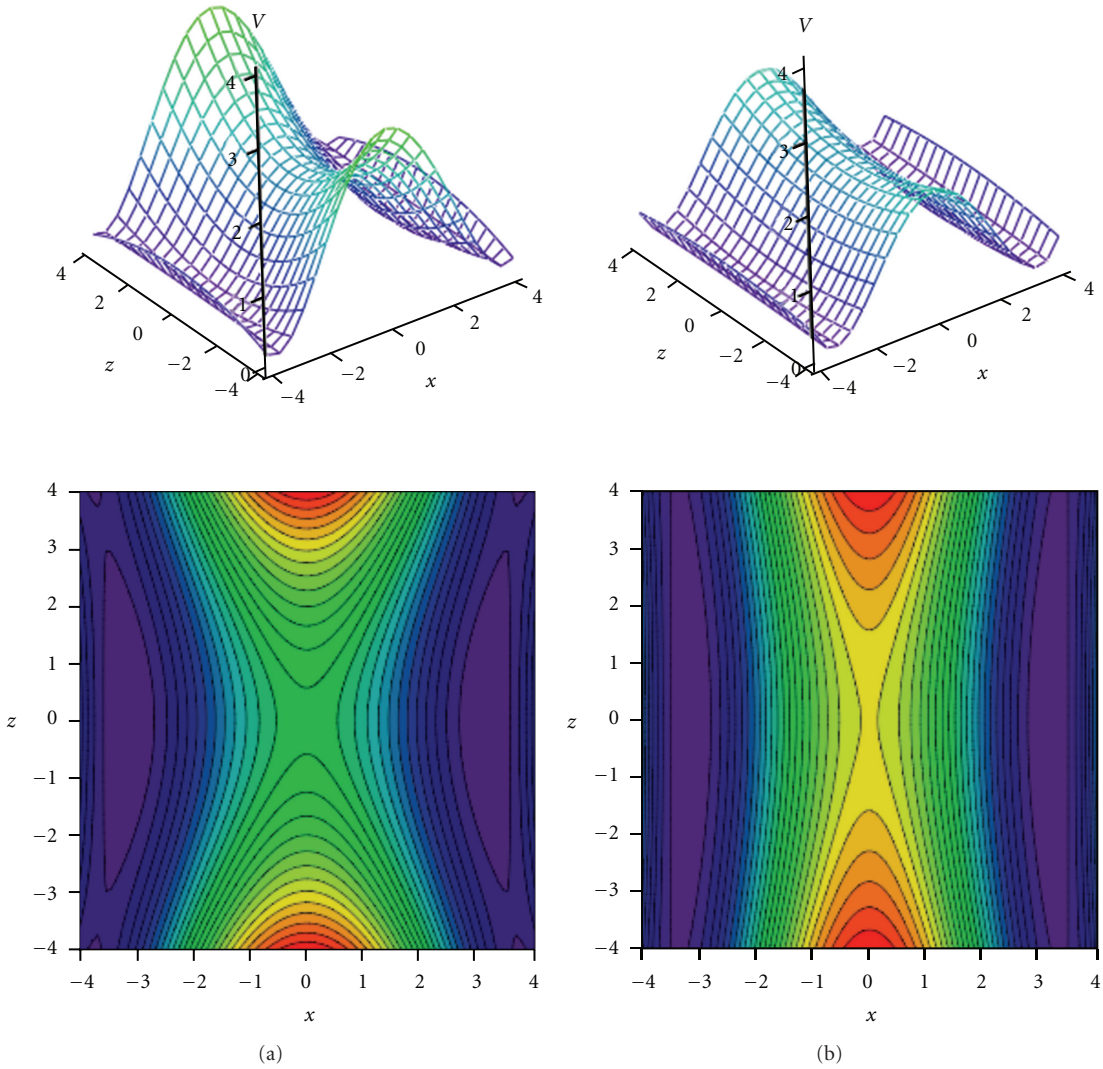

Figure 7: Surface plots and contour maps of the two-dimensional SQZ potentials obtained from the *ab initio* CIS calculations for: (a) coupling of ν_1 and ν_{38} modes, (b) coupling of ν_1 and ν_{39} modes.

Tunneling energy splittings have been calculated variationally by the DVR method [74, 75]. The results are presented in Table 9. Comparison between calculated and experimental splittings shows that two-dimensional model potentials fitted to the grids of energies calculated by the CIS/6-311++G(d,p) method very well reproduce experimentally observed tunneling splittings and their dependence on vibrational excitations in tropolone. The calculated potential energy surfaces quantitatively explain increase of the tunneling splittings with excitations of the nearly planar ν_{33} and ν_{34} modes and decrease of the splittings with excitation of the out-of-plane ν_{38} and ν_{39} modes. Especially striking is long sequence of monotonic decrease of the energy splittings accompanying excitations of the out-of-plane ν_{39} mode quantitatively reproduced by our calculations. Our calculations predict monotonic increase of tunneling splitting with vibrational excitations for the nearly planar ν_{34} mode. The experimental results show an oscillatory behavior of the energy splitting as a function of the vibrational quantum number for this mode. Our model cannot explain such behavior. According to Takada and Nakamura [58], the energy splitting oscillates with respect to quantum number in the case of antisymmetric mode coupling potential in so-called *mixed tunneling* region which can be an explanation of the observed effect.

Present approach constitutes improvement of the previous work [59] which used the same model potentials, given by (18) and (19); however the method to obtain parameters was different. The coupling parameters α and γ were obtained from approximate formulas taking into account only two structures in the $\tilde{A}$ state, stable structure and saddle point structure (transition state). Parameters obtained in such way were different, especially values of γ were by one order of magnitude lower than values obtained in this work. Previous model calculations reproduced quantitatively experimental tunneling energy splitting in the vibrationally ground state of tropolone but only qualitatively changes of

Table 9: Energy splittings calculated for the two-dimensional model potentials for the Ã state of tropolone.

Band	CIS/6-31++G** (cm^{-1}) [59]	CIS/6-311++G** (cm^{-1})	Exp. [53, 54] (cm^{-1})
33^0	22.9	20.3	20
33^1	25.1	30.2	33
33^2	27.4	41.2	
33^3	29.7	53.2	
34^0	20.7	20.0	20
34^1	24.7	28.0	31
34^2	28.8	36.7	29
34^3	33.2	46.1	
38^0	24.5	24.4	20
38^1	24.0	18.2	
38^2	23.5	9.4	5
38^3	23.0	5.5	
39^0	24.7	22.9	20
39^1	24.5	20.1	
39^2	24.3	16.8	8
39^3	24.1	12.9	
39^4	23.9	10.5	6
39^5	23.7	7.9	
39^6	23.5	5.3	5
39^7	23.3	3.5	
39^8	23.1	1.6	2

the tunneling splittings with excitations of low-frequency modes.

Previously there have been other attempts to interpret tunneling splittings in the Ã state of tropolone, by Vener et al. [56] and Smedarchina et al. [57] Vener et al. used an adiabatic description in a model three-dimensional potential based on the *ab initio* CIS/6-31G calculations. Their approach was not successful in describing the dynamics of the excited state. Smedarchina et al. employed an instanton method combined with the PES obtained by the *ab initio* CIS/6-31G** calculations. They were able to obtain satisfactory agreement between theory and experiment for linearly coupled modes, however they had to adjust the adiabatic barrier height. Our present results do not require such adjustment and present pure quantum mechanical approach to the problem of tunneling splittings in the excited state of tropolone. Burns et al. have also provided detailed quantum mechanical computations for the vibrations and potential energy surface properties of tropolone in its lowest pi*-pi electronic excited state [76].

In this approach we do not deal with the other low-frequency modes. The modes we took are typical ones to explain the effects of vibrational excitation on tunneling. The other modes are either higher-frequency modes or not hydrogen-bond stretching modes (e.g., ν_{35}, ν_{36}, ν_{37}). The model potentials used in this paper are not adequate to describe the influence of these modes on proton tunneling.

3.3. Conclusions. The proton tunneling dynamics of tropolone in the excited Ã state have been studied by performing the high accuracy quantum mechanical calculations of the potential energy surfaces and fitting them by two-dimensional model potentials. The tunneling energy splittings for different vibrationally excited states of low-frequency modes have been calculated and compared with the available experimental data. The experimentally observed promotion of the tunneling by the excitation of the planar ν_{33} and ν_{34} modes and suppression by the excitation of the out-of-plane ν_{38} and ν_{39} modes have been reproduced quantitatively by our calculations. They reproduce the long sequence of monotonic decrease of the tunneling splittings accompanying excitations of the out-of-plane ν_{39} mode.

Acknowledgments

Figures 1–3 and Tables 1–4 are reprinted with permission from M. Boczar, Ł. Boda and M.J. Wójcik, J. Chem. Phys. **127**, 084307 (2007). Copyright 2007, American Institute of Physics. Figures 4–7 and Tables 5–9 are reprinted with permission from M.J. Wójcik, Ł. Boda and M. Boczar, J. Chem. Phys. **130**, 164306 (2009). Copyright 2009, American Institute of Physics.

References

[1] Y. Maréchal and A. Witkowski, "Infrared spectra of H-bonded systems," *The Journal of Chemical Physics*, vol. 48, no. 8, pp.

3697–3705, 1968.

[2] M. J. Wójcik, "Theory of the infrared spectra of the hydrogen bond in molecular crystals," *International Journal of Quantum Chemistry*, vol. 10, pp. 747–760, 1976.

[3] A. Witkowski and M. Wójcik, "Infrared spectra of hydrogen bond a general theoretical model," *Chemical Physics*, vol. 1, pp. 9–16, 1973.

[4] M. J. Wójcik, "Fermi resonance in dimers : a model study," *Molecular Physics*, vol. 36, pp. 1757–1767, 1978.

[5] O. Henri-Rousseau and D. Chamma, "IR spectral density of weak H-bonded complexes involving damped Fermi resonances. I. Quantum theory," *Chemical Physics*, vol. 229, no. 1, pp. 37–50, 1998.

[6] A. M. Yaremko, H. Ratajczak, J. Baran, A. J. Barnes, E. V. Mozdor, and B. Silvi, "Theory of profiles of hydrogen bond stretching vibrations: Fermi-Davydov resonances in hydrogen-bonded crystals," *Chemical Physics*, vol. 306, no. 1–3, pp. 57–70, 2004.

[7] N. Rösch and M. A. Ratner, "Model for the effects of a condensed phase on the infrared spectra of hydrogen-bonded systems," *The Journal of Chemical Physics*, vol. 61, no. 8, pp. 3344–3351, 1974.

[8] S. Bratos, "Profiles of hydrogen stretching ir bands of molecules with hydrogen bonds: a stochastic theory. I. Weak and medium strength hydrogen bonds," *The Journal of Chemical Physics*, vol. 63, no. 8, pp. 3499–3509, 1975.

[9] G. N. Robertson and J. Yarwood, "Vibrational relaxation of hydrogen-bonded species in solution. I. Theory," *Chemical Physics*, vol. 32, no. 2, pp. 267–282, 1978.

[10] O. Henri-Rousseau and P. Blaise, "The infrared spectral density of weak hydrogen bonds within the linear response theory," *Advances in Chemical Physics*, vol. 103, p. 1, 1998.

[11] P. Blaise, M. J. Wójcik, and O. Henri-Rousseau, "Theoretical interpretation of the line shape of the gaseous acetic acid cyclic dimer," *The Journal of Chemical Physics*, vol. 122, no. 6, Article ID 064306, pp. 1–12, 2005.

[12] M. Ito, H. Tsukioka, and S. Imanishi, "Effect of temperature on ultraviolet absorption spectra of benzoic acids and its relation to hydrogen bonding," *Journal of the American Chemical Society*, vol. 82, no. 7, pp. 1559–1564, 1960.

[13] H. Baba and M. Kitamura, "Molecular association and emission spectra of benzoic acid," *Journal of Molecular Spectroscopy*, vol. 41, no. 2, pp. 302–309, 1972.

[14] J. C. Baum and D. S. McClure, "The ultraviolet transitions of benzoic acid. 4. High-resolution spectral studies of hydrogen bonding in the excited states of the benzoic acid dimer," *Journal of the American Chemical Society*, vol. 102, no. 2, pp. 720–727, 1980.

[15] J. C. Baum and D. S. McClure, "The ultraviolet transitions of benzoic acid. 2. Hydrogen bonding in the ground and excited states," *Journal of the American Chemical Society*, vol. 101, no. 9, pp. 2340–2343, 1979.

[16] J. C. Baum and D. S. McClure, "The ultraviolet transitions of benzoic acid. 1. Interpretation of the singlet absorption spectrum," *Journal of the American Chemical Society*, vol. 101, no. 9, pp. 2335–2339, 1979.

[17] J. C. Baum, "The ultraviolet transitions of benzoic acid. 3. Effects of hydrogen bonding on the emission properties," *Journal of the American Chemical Society*, vol. 102, no. 2, pp. 716–719, 1980.

[18] D. E. Poeltl and J. K. McVey, "Laser induced fluorescence excitation spectrum of jet-cooled benzoic acid dimers," *The Journal of Chemical Physics*, vol. 78, no. 7, pp. 4349–4355, 1983.

[19] D. E. Poeltl and J. K. McVey, "Excited-state dynamics of hydrogen-bonded dimers of benzoic acid," *The Journal of Chemical Physics*, vol. 80, no. 5, pp. 1801–1811, 1984.

[20] Y. Tomioka, H. Abe, N. Mikami, and M. Ito, "Electronic spectra of benzoic acid in a supersonic free jet," *Journal of Physical Chemistry*, vol. 88, no. 11, pp. 2263–2270, 1984.

[21] K. Remmers, W. L. Meerts, and I. Ozier, "Proton tunneling in the benzoic acid dimer studied by high resolution ultraviolet spectroscopy," *The Journal of Chemical Physics*, vol. 112, no. 24, pp. 10890–10894, 2000.

[22] C. K. Nandi and T. Chakraborty, "Hydrogen bond-induced vibronic mode mixing in benzoic acid dimer: a laser-induced fluorescence study," *The Journal of Chemical Physics*, vol. 120, no. 18, pp. 8521–8527, 2004.

[23] G. M. Florio, E. L. Sibert, and T. S. Zwier, "Fluorescence-dip IR spectra of jet-cooled benzoic acid dimer in its ground and first excited singlet states," *Faraday Discussions*, vol. 118, pp. 315–330, 2001.

[24] G. M. Florio, T. S. Zwier, E. M. Myshakin, K. D. Jordan, and E. L. Sibert III, "Theoretical modeling of the OH stretch infrared spectrum of carboxylic acid dimers based on first-principles anharmonic couplings," *The Journal of Chemical Physics*, vol. 118, no. 4, pp. 1735–1746, 2003.

[25] H. T. Flakus and M. Chelmecki, "Infrared spectra of the hydrogen bond in benzoic acid crystals: temperature and polarization effects," *Spectrochimica Acta*, vol. 58, no. 1, pp. 179–196, 2002.

[26] H. T. Flakus, "A new approach to the problem of the hydrogen bond spectra of the adipic acid crystal: the polarization and temperature effects," *Journal of Molecular Structure*, vol. 285, no. 3, pp. 281–292, 1993.

[27] H. R. Flakus and A. Bryk, "Strong-coupling mechanism for interpretation of the IR spectra of the hydrogen bonded imidazole crystal," *Journal of Molecular Structure*, vol. 372, no. 2-3, pp. 215–227, 1995.

[28] H. T. Flakus and A. Bryk, "An extended "strong-coupling" model of the IR spectral properties of molecular crystals with four H-bonds in a unit cell: the imidazole-type crystals," *Journal of Molecular Structure*, vol. 372, no. 2-3, pp. 229–240, 1995.

[29] H. T. Flakus and A. Miros, "Infrared spectra of the hydrogen bonded glutaric acid crystals: polarization and temperature effects," *Journal of Molecular Structure*, vol. 484, no. 1–3, pp. 103–115, 1999.

[30] M. Boczar, K. Szczeponek, M. J. Wójcik, and C. Paluszkiewicz, "Theoretical modeling of infrared spectra of benzoic acid and its deuterated derivative," *Journal of Molecular Structure*, vol. 700, no. 1–3, pp. 39–48, 2004.

[31] M. Boczar, Ł. Boda, and M. J. Wójcik, "Theoretical model of infrared spectra of hydrogen bonds in molecular crystals and its application to interpretation of infrared spectra of 1-methylthymine," *The Journal of Chemical Physics*, vol. 125, no. 8, Article ID 084709, 2006.

[32] P. Blaise, M. J. Wójcik, and O. Henri-Rousseau, "Theoretical interpretation of the line shape of the gaseous acetic acid cyclic dimer," *The Journal of Chemical Physics*, vol. 122, no. 6, Article ID 064306, pp. 1–12, 2005.

[33] M. Boczar, Ł. Boda, and M. J. Wójcik, "Theoretical model for a tetrad of hydrogen bonds and its application to interpretation of infrared spectra of salicylic acid," *The Journal of Chemical Physics*, vol. 124, no. 8, Article ID 084306, 2006.

[34] G.-J. Zhao, J.-Y. Liu, L.-C. Zhou, and K.-L. Han, "Site-selective photoinduced electron transfer from alcoholic solvents to the

chromophore facilitated by hydrogen bonding: a new fluorescence quenching mechanism," *Journal of Physical Chemistry B*, vol. 111, no. 30, pp. 8940–8945, 2007.

[35] G.-J. Zhao and K.-L. Han, "Early time hydrogen-bonding dynamics of photoexcited coumarin 102 in hydrogen-donating solvents: theoretical study," *Journal of Physical Chemistry A*, vol. 111, no. 13, pp. 2469–2474, 2007.

[36] G.-J. Zhao and K.-L. Han, "Site-specific solvation of the photoexcited protochlorophyllide *a* in methanol: formation of the hydrogen-bonded intermediate state induced by hydrogen-bond strengthening," *Biophysical Journal*, vol. 94, p. 38, 2008.

[37] G.-J. Zhao and K.-L. Han, "Effects of hydrogen bonding on tuning photochemistry: concerted hydrogen-bond strengthening and weakening," *ChemPhysChem*, vol. 9, no. 13, pp. 1842–1846, 2008.

[38] P.-O. Löwdin, "Proton tunneling in DNA and its biological implications," *Reviews of Modern Physics*, vol. 35, pp. 724–732, 1963.

[39] H. Nakamura, "Theoretical studies of chemical dynamics: overview of some fundamental mechanisms," *Annual Review of Physical Chemistry*, vol. 48, no. 1, pp. 299–328, 1997.

[40] V. A. Benderskii, I. S. Irgibaeva, E. V. Vetoshkin, and H. P. Trommsdorff, "Tunneling splittings in vibrational spectra of non-rigid molecules. VIII. Six-dimensional tunneling dynamics of hydrogen peroxide and its isotopomers," *Chemical Physics*, vol. 262, no. 2-3, pp. 369–391, 2000.

[41] V. A. Benderskii, E. V. Vetoshkin, I. S. Irgibaeva, and H. P. Trommsdorff, "Tunneling splittings in vibrational spectra of non-rigid molecules: IX. Malonaldehyde and its isotopomers as a test case for fully coupled multidimensional tunneling dynamics," *Chemical Physics*, vol. 262, no. 2-3, pp. 393–422, 2000.

[42] M. V. Pak and S. Hammes-Schiffer, "Electron-proton correlation for hydrogen tunneling systems," *Physical Review Letters*, vol. 92, no. 10, p. 103002, 2004.

[43] C. S. Tautermann, A. F. Voegele, and K. R. Liedl, "The ground-state tunneling splitting of various carboxylic acid dimers," *The Journal of Chemical Physics*, vol. 120, no. 2, pp. 631–637, 2004.

[44] C. S. Tautermann, M. J. Loferer, A. F. Voegele, and K. R. Liedl, "Double hydrogen tunneling revisited: the breakdown of experimental tunneling criteria," *The Journal of Chemical Physics*, vol. 120, no. 24, pp. 11650–11657, 2004.

[45] G. V. Mil'nikov, K. Yagi, T. Taketsugu, H. Nakamura, and K. Hirao, "Simple and accurate method to evaluate tunneling splitting in polyatomic molecules," *The Journal of Chemical Physics*, vol. 120, no. 11, pp. 5036–5045, 2004.

[46] K. Yagi, G. V. Mil'nikov, T. Taketsugu, K. Hirao, and H. Nakamura, "Effect of out-of-plane vibration on the hydrogen atom transfer reaction in malonaldehyde," *Chemical Physics Letters*, vol. 397, no. 4–6, pp. 435–440, 2004.

[47] G. V. Mil'nikov and H. Nakamura, "Instanton theory for the tunneling splitting of low vibrationally excited states," *The Journal of Chemical Physics*, vol. 122, no. 12, p. 124311, 2005.

[48] G. V. Mil'nikov, T. Ishida, and H. Nakamura, "Tunneling splitting of energy levels and rotational constants in the vinyl radical C_2H_3," *Journal of Physical Chemistry A*, vol. 110, no. 16, pp. 5430–5435, 2006.

[49] G. V. Mil'nikov and H. Nakamura, "Tunneling splitting and decay of metastable states in polyatomic molecules: invariant instanton theory," *Physical Chemistry Chemical Physics*, vol. 10, pp. 1374–1393, 2008.

[50] A. C. P. Alves and J. M. Hollas, "The near ultra-violet absorption spectrum of tropolone vapour," *Molecular Physics*, vol. 25, pp. 1305–1314, 1973.

[51] R. L. Redington and T. E. Redington, "Tropolone monomer. Vibrational spectrum and proton tunneling," *Journal of Molecular Spectroscopy*, vol. 78, no. 2, pp. 229–247, 1979.

[52] Y. Tomioka, M. Ito, and N. Mikami, "Electronic spectra of tropolone in a supersonic free jet. Proton tunneling in the S_1 state," *Journal of Physical Chemistry*, vol. 87, no. 22, pp. 4401–4405, 1983.

[53] R. L. Redington, Y. Chen, G. J. Scherer, and R. W. Field, "Laser fluorescence excitation spectrum of jet-cooled tropolone: the $\tilde{A}^1B_2$-X~ $^1A_1$ system," *The Journal of Chemical Physics*, vol. 88, no. 2, pp. 627–633, 1988.

[54] H. Sekiya, Y. Nagashima, and Y. Nishimura, "Electronic spectra of jet-cooled tropolone. Effect of the vibrational excitation on the proton tunneling dynamics," *The Journal of Chemical Physics*, vol. 92, no. 10, pp. 5761–5769, 1990.

[55] K. Nishi, H. Sekiya, H. Kawakami, A. Mori, and Y. Nishimura, "Coupling of internal rotation of methyl group with proton transfer in the S_1 state of 5-methyltropolone," *The Journal of Chemical Physics*, vol. 109, no. 5, pp. 1589–1592, 1998.

[56] M. V. Vener, S. Scheiner, and N. D. Sokolov, "Theoretical study of hydrogen bonding and proton transfer in the ground and lowest excited singlet states of tropolone," *The Journal of Chemical Physics*, vol. 101, no. 11, pp. 9755–9765, 1994.

[57] Z. Smedarchina, W. Siebrand, and M. Z. Zgierski, "Mode-specific hydrogen tunneling in tropolone: an instanton approach," *The Journal of Chemical Physics*, vol. 104, no. 4, pp. 1203–1212, 1996.

[58] S. Takada and H. Nakamura, "Effects of vibrational excitation on multidimensional tunneling: general study and proton tunneling in tropolone," *The Journal of Chemical Physics*, vol. 102, no. 10, pp. 3977–3992, 1995.

[59] M. J. Wójcik, H. Nakamura, S. Iwata, and W. Tatara, "Theoretical study of multidimensional proton tunneling in the excited state of tropolone," *The Journal of Chemical Physics*, vol. 112, no. 14, pp. 6322–6328, 2000.

[60] M. Boczar, Ł. Boda, and M. J. Wójcik, "Theoretical modeling of the O-H stretching IR bands of hydrogen-bonded dimers of benzoic acid in S_0 and S_1 electronic states," *The Journal of Chemical Physics*, vol. 127, no. 8, Article ID 084307, 2007.

[61] M. J. Wójcik, Ł. Boda, and M. Boczar, "Theoretical study of proton tunneling in the excited state of tropolone," *The Journal of Chemical Physics*, vol. 130, no. 16, Article ID 164306, 2009.

[62] M. J. Frisch, G. W. Trucks, H. B. Schlegel et al., *GAUSSIAN 03, Revision D.01*, Gaussian, Wallingford, Conn, USA, 2004.

[63] J. B. Foresman, M. Head-Gordon, J. A. Pople, and M. J. Frisch, "Toward a systematic molecular orbital theory for excited states," *Journal of Physical Chemistry*, vol. 96, no. 1, pp. 135–149, 1992.

[64] M. Head-Gordon, R. J. Rico, M. Oumi, and T. J. Lee, "A doubles correction to electronic excited states from configuration interaction in the space of single substitutions," *Chemical Physics Letters*, vol. 219, pp. 21–29, 1994.

[65] M. Head-Gordon, D. Maurice, and M. Oumi, "A perturbative correction to restricted open shell configuration interaction with single substitutions for excited states of radicals," *Chemical Physics Letters*, vol. 246, no. 1-2, pp. 114–121, 1995.

[66] C. H. Longuet-Higgins, in *Advances in Spectroscopy*, H. W. Thompson, Ed., vol. 2, p. 429, Wiley-Interscience, New York, NY, USA, 1961.

[67] R. L. Fulton and M. Gouterman, "Vibronic coupling. I. Mathematical treatment for two electronic states," *The Journal of Chemical Physics*, vol. 35, no. 3, pp. 1059–1071, 1961.

[68] W. J. Hehre, L. Radom, P. V. R. Schleyer, and J. A. Pople, *Ab*

Initio Molecular Orbital Theory, Wiley, New York, NY, USA, 1986.

[69] G. Schaftenaar, "MOLDEN: a portable electron density program," *QCPE Bulletin*, vol. 619, p. 12, 1992.

[70] J. B. Foresman, M. Head-Gordon, J. A. Pople, and M. J. Frisch, "Toward a systematic molecular orbital theory for excited states," *Journal of Physical Chemistry*, vol. 96, no. 1, pp. 135–149, 1992.

[71] K. Levenberg, "A method for the solution of certain problems in least squares," *Quarterly of Applied Mathematics*, vol. 2, pp. 164–168, 1944.

[72] D. Marquardt, "An algorithm for least-squares estimation of nonlinear parameters," *Journal on Applied Mathematics*, vol. 11, pp. 431–441, 1963.

[73] M. J. Wójcik, M. Boczar, and M. Stoma, "Spectroscopic and theoretical study of vibrational spectra of hydrogen-bonded tropolone," *International Journal of Quantum Chemistry*, vol. 73, no. 3, pp. 275–282, 1999.

[74] J. C. Light, I. P. Hamilton, and J. V. Lill, "Generalized discrete variable approximation in quantum mechanics [a)]," *The Journal of Chemical Physics*, vol. 82, pp. 1400–1409, 1985.

[75] M. Whitnell and J. C. Light, "Efficient pointwise representations for vibrational wave functions: eigenfunctions of H3(+)," *The Journal of Chemical Physics*, vol. 90, p. 1774, 1989.

[76] L. A. Burns, D. Murdock, and P. H. Vaccaro, "An exploration of electronic structure and nuclear dynamics in tropolone: II. the $\tilde{A}\ ^1B_2$ $(\pi\pi)$ excited state," *The Journal of Chemical Physics*, vol. 130, no. 14, Article ID 144304, 2009.

Hindawi Publishing Corporation
Journal of Atomic, Molecular, and Optical Physics
Volume 2012, Article ID 754879, 8 pages
doi:10.1155/2012/754879

Research Article

Theoretical Investigation of the Cooperativity in $CH_3CHO.2H_2O$, $CH_2FCHO.2H_2O$, and $CH_3CFO.2H_2O$ Systems

Asit K. Chandra[1] and Thérèse Zeegers-Huyskens[2]

[1] *Department of Chemistry, North Eastern Hill University, Shillong 793022, India*
[2] *Department of Chemistry, University of Leuven, 200F Celestijnenlaan, Heverlee 3001, Belgium*

Correspondence should be addressed to Thérèse Zeegers-Huyskens, therese.zeegers@chem.kuleuven.be

Received 29 February 2012; Accepted 30 April 2012

Academic Editor: Joanna Sadlej

Copyright © 2012 A. K. Chandra and T. Zeegers-Huyskens. This is an open access article distributed under the Creative Commons Attribution License, which permits unrestricted use, distribution, and reproduction in any medium, provided the original work is properly cited.

The hydrogen bond interaction between CH_3CHO, CH_2FCHO, and CH_3CFO and two water molecules is investigated at the B3LYP/6-311++G(d,p) level. The results are compared with the complexes involving the same carbonyl derivatives and one water molecule. The calculations involve the optimization of the structure, the harmonic vibrational frequencies, and relevant NBO (natural bond orbital) parameters such as the NBO charges, the occupation of antibonding orbitals, and intra- and intermolecular hyperconjugation energies. Two stable cyclic structures are predicted. The two structures are stabilized by C=O$\cdots$HO hydrogen bond. The A structures are further stabilized by CH$\cdots$O bond involving the CH_3 (CH_2F) group. This bond results in an elongation of the CH bond and red shift of the ν(CH) vibration. The B structures are stabilized by CH$\cdots$O interaction involving the aldehydic CH bond. The formation of this bond results in a marked contraction of the CH bond and blue shift of the ν(CH) vibration indicating the predominance of the lone pair effect in determining the CH distances. The total interaction energies range from -12.40 to -13.50 kcal mol^{-1}. The cooperative energies calculated at the trimer geometry are comprised between -2.30 and -2.60 kcal mol^{-1}.

1. Introduction

Cooperative interactions involving three or more molecules are an important component of intermolecular interactions, particularly those involving hydrogen bonds. The cooperativity of hydrogen bonds plays an important role in controlling and regulating the processes in living materials. This has been recognized since a long time and quantitative aspects of cooperativity have been discussed [1–7]. Cooperativity can be positive or negative. It has been shown that a first hydrogen bond involving a given site of a molecule weakens the reactivity of the neighboring sites of the same nature whereas it enhances the electron donor power of the adjacent sites of opposite nature [4]. Cooperativity between water molecules is particularly important, because in liquid water at room temperature, the great majority of the molecules are hydrogen-bonded to each other, the concentration of "free" OH groups being very low [8]. For this reason, extensive theoretical calculations have been carried out on the cooperativity in water [9–13]. In recent works, the interaction between proton acceptors (or donors) and two (or more) water molecules has been discussed [14–21].

In a recent work [22], the complexes between acetaldehyde and some of its monofluorinated derivatives and one water molecule have been investigated by theoretical methods. It was shown in this work that water acts as a proton donor toward the C=O bond forming C=O$\cdots$HO hydrogen bonds but that water can also act as a proton acceptor forming weak CH$\cdots$O hydrogen bonds. It seemed to us interesting to investigate the interaction between some of these carbonyl derivatives (CH_3CHO, CH_2FCHO, and CH_3CFO) and two water molecules in order to discuss the effect of cooperativity in these hydrogen-bonded systems. To the best of our knowledge, no experimental data are available for these systems.

This paper is arranged as follows. The first step of our study deals with the structure of the complexes. In the second section, the intramolecular distances, some

vibrational frequencies and the results of a natural bond orbital (NBO) analysis are discussed. A special attention is paid to the NBO charges, occupation of antibonding orbitals, and hyperconjugation energies. In the last section, the cooperative energies are discussed.

2. Computational Methods

Calulations of the properties of CH_3CHO, CH_2FCHO, and CH_3CFO, complexed with two water molecules were carried out using the density functional B3LYP method [23] and the Gaussian suite of programs [24]. The basis set 6-311++G(d, p) was invoked. The second-order Møller-Plesset MP2/aug-cc-PVTZ method was also used to calculate some of the structures or binding energies. The computed interaction energies were corrected for the basis superposition error (BSSE) [25].

The cooperativity in a molecular trimer containing A, B, and C molecules is given by the three-body term ΔE_{coop} which can be defined as the difference between the total interaction energy $E_{\text{int}}(\text{ABC})$ and the sum of the pairwise or two-body interaction energies $E_2(\text{AB})$, E_2 (BC), E_2 (AC).

$$\Delta E_{\text{coop}} = E_{\text{int}}(\text{ABC}) - E_2(\text{AB}) - E_2(\text{BC}) - E_2(\text{AC}). \quad (1)$$

Here, the E_2 values correspond to the two-body contributions at the trimer geometry [26–28] calculated with the same basis set.

The harmonic vibrational frequencies were calculated to characterize the stationary points. No scaling factor was used. The charges on individual atoms, orbital occupancies, and hyperconjugation energies were obtained by an NBO analysis [29].

3. Results and Discussion

3.1. Structure of the Complexes between CH_3CHO, CH_2FCHO, and CH_3CFO with Two Water Molecules. Figure 1 illustrates the structure of the 1-2 complexes between CH_3CHO, CH_2CHO, and CH_3CFO with two water molecules calculated with the B3LYP functional. The distances calculated with the MP2 method are somewhat shorter. The structure of the complexes with one water molecule taken from a previous work [22] is shown for the comparison. As shown in this work, the 1-1 complexes are characterized by two stable structures. In both A and B structures, the molecules are held together by a C=O$\cdots$HO hydrogen bond. The A complexes are cyclic and stabilized by a weak $C_4H_5\cdots O$ interaction and they are slightly more stable than the B complexes. These structures have been established by considering the intermolecular $H_5\cdots O$ distances and some NBO parameters such as the weak intermolecular charge transfer from the O atom of water to the $\sigma^*(C_4H_5)$ orbital. In none of the 1-1 complexes *the C_1H_3 bond was involved in the formation of a cyclic structure.* Let us notice that CH_3CFO is also able to form a cyclic complex with two water molecules, one of the OH bonds of the water dimer being bonded to the F atom. This complex will not be considered here.

In none of the 1-2 complexes the second water molecule is bonded to the second electron pair of the carbonyl O atom. This structure is anticooperative, both electron donor sites having the same nature [4]. As shown in Figure 1, the intermolecular C=O$\cdots$HO distances are shortened with respect to their values in the 1-1 complexes by amounts ranging from 0.081 to 0.109 Å. Further, the $O_9\ldots H_{11}$ distances ranging from 1.840 to 1.866 Å are shorter than in the water dimer (1.933 Å). The most spectacular indication of a positive cooperativity is the shortening of the $H_5\cdots O$ distances by 0.212 Å in CH_3CHO (A1-2), 0.585 Å in CH_2FCHO (A1-2), and 0.194 Å in CH_3CFO (A1-2). The short $H_3\cdots O$ distances of 2.319 Å in CH_3CHO (B1-2), and 2.255 Å in CH_2FCHO(B1-2) also indicates that the trimer is stabilized by a $C_1H_3\cdots O$ interaction. This will be further confirmed by the NBO data. Therefore, the hydrogen bond pattern appears to be different in the B(1-1) and B(1-2) complexes. We note also an increase in the angles, the $C_4H_5\cdots O$ bond becoming almost linear in both A(1-2) complexes involving CH_3CHO and CH_3CFO and increasing by 40–50° in the other structures. The OH$\cdots$O angles decrease by 10 to 17° from its value in the water dimer (175°).

3.2. Geometrical and NBO Properties of the Complexes. Tables 1, 2, and 3 list some relevant geometrical properties of the complexes, namely the C_1H_3, C_4H_5, C=O, and HO distances in the isolated monomers, in the 1-1 and in the 1-2 complexes with water. The corresponding vibrational frequencies are indicated as well. Tables 1, 2, and 3 also indicate important NBO parameters, namely, the occupation of $\sigma^*(C_1H_3)$ or $\sigma^*(C_4H_5)$ antibonding orbitals, the NBO charges along with some intra- or intermolecular hyperconjugative interactions.

Inspection of the results of Tables 1, 2, and 3 shows that the elongation of the C=O bonds and the decrease of the ν(C=O) vibrational frequencies are larger for the 1-2 than for the 1-1 complexes. Both parameters are linearly related [30] and suggest a reinforcement of the C=O$\cdots$HO interaction in the 1-2 complexes. These data will no more be discussed hereafter, the main scope of this section being the discussion of the properties of the CH bonds.

Let us at first discuss the properties of the C_1H_3 bond in the CH_3CHO and CH_2FCHO complexes. As discussed in [22], the contraction of the C_1H_3 bond and the increase of the corresponding vibrational $\nu(C_1H_3)$ frequencies in the A(1-1) and B(1-1) complexes results from the classical lone pair effect [31–40]. The C_1H_3 distances, the $\sigma^*(C_1H_3)$ occupation and the intramolecular $LPO_2 \rightarrow \sigma^*(C_1H_3)$ hyperconjugation energies are almost identical in the A(1-1) and A(1-2) complexes. The intramolecular hyperconjugation energies decrease by 1.42 kcal mol^{-1} (CH_3CHO(1-2) and by 1.61 kcal mol^{-1} (CH_2FCHO(1-2) from the isolated molecules. As discussed in the first section, the short intermolecular $H_3\cdots O$ distances suggest that the C_1H_3 bond is involved in the formation of the cyclic structure in the two B(1-2) complexes. This is in full agreement with the relatively large intermolecular charge transfer from the O_{12} atom of water to the $\sigma^*(C_1H_3)$ orbital (2.70 and

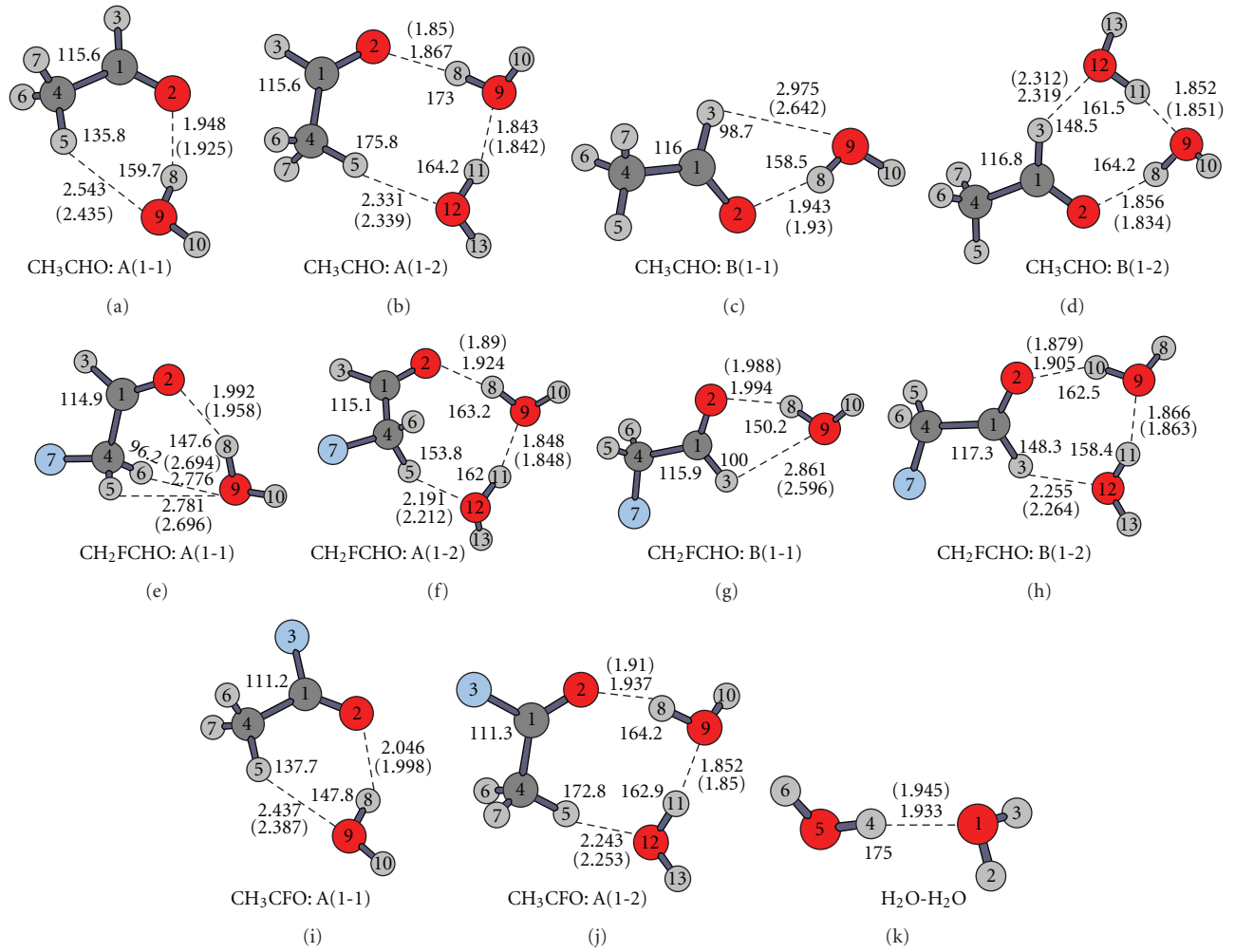

Figure 1: A and B structures of CH_3CHO, CH_2FCHO, and CH_3CFO complexed with one and two water molecules calculated at B3LYP/6-311++G(d,p) level. The distances calculated with the MP2/aug-cc-PVTZ method are indicated in parentheses.

3.40 kcal mol^{-1}). Despite this charge transfer, the $\sigma^*(C_1H_3)$ occupation decreases. This can be explained by the large variation of the $LPO_2\sigma^*(C_1H_3)$ hyperconjugation which decreases by 4.8 kcal mol^{-1} in both B(1-2) complexes. This illustrates *the predominance of the lone pair effect in determining the* C_1H_3 *distances.* These distances are linearly related to the σ^* (C_1H_3) occupation as follows:

$$r(C_1H_3)(\text{Å}) = 0.448\ \sigma^*(C_1H_3)(\text{e}) + 1.0801 \quad (r = 0.961). \tag{2}$$

The small increase of the s-character of the $C_1(H_3)$ atom in the B(1-2) complexes does not influence the C_1H_3 distances to a great extent.

Parallel to the decrease of the C_1H_3 distances, the large blue shift of the ν (C_1H_3) vibration must be noticed (93 cm^{-1} and 61 cm^{-1}). Let us notice that the blue shift of 93 cm^{-1} in the CH_3CHO (B1-2) system is one of the largest ones predicted in CH$\cdots$O hydrogen bonds involving neutral molecules [41–48]. In the present cases, the cooperativity results in an increase of the blue shift. This increase has also been found for other systems. For $H_2C{=}O$ complexed with one and two water molecules, the blue shifts of the ν^s(CH) vibration are 45 and 66 cm^{-1}, respectively, [17]. For CH_3Cl complexed with one and two water molecules, the blue shifts are 13 and 25 cm^{-1}, respectively [19]. Further, the increase of the polarity of the C_1H_3 bond in the B(1-2) complexes is also worth noticing, the positive charge on the proton being about 0.06e larger than in the isolated molecules.

In a next step, we will discuss the properties of the C_4H_5 bond in the three carbonyl complexes. As shown in our previous study [22], the C_4H_5 bonds in the CH_3 or CH_2F groups are weakly sensitive to the formation of a hydrogen bond with the O atom of water. In the acetone$\cdot 1H_2O$ complex as, for example, the two CH bonds which do not participate in the interaction show a greater sensitivity to hydrogen bond formation than the CH bond involved in the interaction. This was rather unexpected and was explained by the orbital interaction between the bonding σ (CH) orbital and the antibonding σ^*(C=O) and π^*(C=O) orbitals [22]. For the 1-2 complexes considered here, the value of this interaction remains almost constant. For the C_4H_5 bond of CH_3CHO, the value of this orbital interaction is equal

Table 1: Properties of the isolated CH_3CHO and H_2O molecules, A and B complexed with 1 and 2 water molecules (distances in Å, σ^* occupation in e, hyperconjugation energies in kcal mol^{-1}, and frequencies in cm^{-1}).

	Isolated CH_3CHO	A(1-1)	A(1-2)	B(1-1)	B(1-2)
$r(C_1H_3)$	1.1122	1.1094	1.1094	1.1082	1.1054
$\nu(C_1H_3)$	2871	2905	2906	2923	2964
$\sigma^*(C_1H_3)$	0.071	0.064	0.063	0.062	0.057
$\%sC_1(H_3)$	30.0	30.0	29.7	30.0	31.7
$q(C_1)$	0.442	0.463	0.474	0.457	0.451
$q(H_3)$	0.092	0.103	0.103	0.116	0.153
$r(C_4H_5)$	1.0898	1.0897	1.0910	1.0896	1.0898
$\nu(C_4H_5)$	3136	3142	3125	3139	3136
$\sigma^*(C_4H_5)$	0.0066	0.0071	0.0122	0.0064	0.0065
$\%sC_4(H_5)$	25.4	26.2	27.05	25.46	25.48
$q(C_4)$	−0.679	−0.689	−0.699	−0.679	−0.680
$q(H_5)$	0.222	0.245	0.262	0.224	0.222
$r(C_1 = O_2)$	1.206	1.212	1.214	1.212	1.218
$\nu(C_1 = O_2)$	1808	1789	1783	1788	1764
$LPO_2 \rightarrow \sigma^*(C_1H_3)$	23.64	22.43	22.22	20.71	18.84
$LPO_{12} \rightarrow \sigma^*(C_1H_3)$	—	—	—	—	2.70
$LPO_2 \rightarrow \sigma^*(O_9H_8)$	—	7.11	9.93	7.35	9.34
$LPO_9(O_{12}) \rightarrow \sigma^*(C_4H_5)$	—	0.46	2.95	—	—
	Isolated H_2O	A(1-1)	A(1-2)	B(1-1)	B(1-2)
$r(OH)$	0.9620	0.9711	0.9755[a]	0.9711	0.9777[a]
			0.9760[b]		0.9764[b]
$\nu(H_2O)$	3926,3820	3894,3681	3889,3629[c]	3894,3680	3888,3579[c]
			3890,3579[d]		3890,3603[d]
$\Sigma q(H_2O)$	—	−0.017	+0.009[e]	−0.019	−0.004[e]
			−0.017[f]		−0.017[f]

[a]O_9H_8 bond. [b]$O_{12}H_{11}$ bond. $r(OH\cdots)$ in the water dimer is 0.9700 Å. [c]$\nu(H_8O_9H_{10})$ [d]$\nu(H_{11}O_{12}H_{13})$, [e]Σq on $(H_8O_9H_{10})$ [f]Σq on $(H_{11}O_{12}H_{13})$.

to 0.81 kcal mol^{-1} in the isolated molecule, 0.71 kcal mol^{-1} in the A(1-2) complex, and 0.86 kcal mol^{-1} in the B(1-2) complex. In contrast with the A(1-1) complexes, there is a significant elongation of the C_4H_5 bond in the A(1-2) complexes equal to 0.0012 Å in CH_3CHO, 0.0022 Å in CH_2FCHO and 0.0024 Å in CH_3CFO. The corresponding red shifts of the $\nu(C_4H_5)$ vibration are 11, 20 (average value of the ν^{as} and ν^{s} vibrations), and 22 cm^{-1}. It may be interesting to note that the C_4H_5 bond contracts by 0.006 Å when we consider the A(1-1) complex with the $C_4H_5\cdots O$ bond at the trimer geometry and this is mainly due to the increase in % *s*-character of $C_4(H_5)$ by almost 1.3%. In fact, at the optimized geometry considered here, the cooperativity markedly enhances the $LPO_{12} \rightarrow \sigma^*(C_4H_5)$ charge transfer, resulting in an elongation of the C_4H_5 bond. Indeed, in CH_3CHO, this charge transfer is equal to 0.46 kcal mol^{-1} in the A(1-1) complex and 2.95 kcal mol^{-1} in the A(1-2) complex. This increase is larger in the CH_2FCHO system, being 0.10 kcal mol^{-1} in the A(1-1) complex and 4.56 kcal mol^{-1} in the A(1-2) complex. In agreement with this charge transfer, the $\sigma^*(C_4H_5)$ occupation increases by amounts ranging from 0.0025e (CH_2FCHO), and 0.0070e (CH_3CFO) with respect to the A(1-1) complexes.

In these cases also, the hybridization of the $C_4(H_5)$ atom slightly increases by ca 1.5% when the C_4H_5 bond is involved in the A(1-2) interaction, and this increase does not influence the C_4H_5 distances to a great extent.

The C_4H_5 distances are linearly correlated to the $\sigma^*(C_4H_5)$ occupation as follows:

$$r(C_4H_5)(\text{Å}) = 0.371\sigma^*(C_4H_5)(\text{e}) + 1.0886. \quad (r = 0.973). \tag{3}$$

It should be noticed that in all the systems the C4H5 distances where the $C_4(H_5)$ atom has an sp^3 hybridization are smaller than the C_1H_3 distances when the $C_1(H_3)$ atom has hybridization between $sp^{2.1}$ and $sp^{2.3}$. This in contrast with the usual trend for the CH distances: $C(sp^3)$–H > $C(sp^2)$–H. Let us notice that the intercept of (2) (1.0801) is smaller than the intercept of (3) (1.0886). *This possibly reflects the larger CH distances in C (sp^3)–H than in C (sp^2)–H bonds when the σ^*(CH) occupation tends to zero*.

We may also notice that the increase of linearity of the intermolecular $O_9H_8\cdots O_2$ and $C_4H_5\cdots O_{12}$ bonds may also contribute to the stability of the trimers.

We will now briefly discuss the changes induced in the water molecules. It is known that the OH bond of the water dimer (O_9H_8 bond in the present systems) is a better proton donor and the O atom (O_{12} atom in the present systems) is a better proton acceptor than in the water monomer [9–13].

Table 2: Properties of the isolated CH_2FCHO and H_2O molecules and the A and B complexes between CH_2FCHO and one and two water molecules (distances in Å, σ^* occupation in e, hyperconjugation energies in kcal mol^{-1}, and frequencies in cm^{-1}).

	IsolatedCH_2FCHO	A(1-1)	A(1-2)	B(1-1)	B(1-2)
$r(C_1H_3)$	1.1096	1.1077	1.1077	1.1065	1.1053
$\nu(C_1H_3)$	2914	2938	2938	2958	2975
$\sigma^*(C_1H_3)$	0.068	0.063	0.062	0.060	0.056
$\%sC_1(H_3)$	32.1	31.8	31.7	32.5	33.7
$q(C_1)$	0.408	0.427	0.440	0.421	0.417
$q(H_3)$	0.117	0.125	0.124	0.141	0.177
$r(C_4H_5)$	1.0940	1.0933	1.0962	1.0942	1.0945
$\nu(C_4H_5H_6)$	3096,3045	3106,3058	3077,3024	3094,3044	3090,3041
$\sigma^*(C_4H_5)$	0.0199	0.0196	0.0250	0.0200	0.0200
$\%sC_4(H_5)$	25.74	25.97	27.46	25.70	25.61
$q(C_4)$	−0.011	−0.021	−0.038	−0.011	−0.011
$q(H_5)$	0.190	0.207	0.246	0.193	0.191
$r(C_1 = O_2)$	1.203	1.208	1.210	1.208	1.213
$\nu(C_1 = O_2)$	1816	1798	1793	1797	1773
$LPO_2 \rightarrow \sigma^*(C_1H_3)$	22.94	21.42	21.33	20.83	18.15
$LPO_9 \rightarrow \sigma^*(C_1H_3)$	—	—	—	—	3.4
$LPO_2 \rightarrow \sigma^*(H_8O_9)$	—	5.53	6.94	5.51	9.11
$LPO_9\ (O_{12}) \rightarrow \sigma^*(C_4H_5)$	—	0.10	4.56	—	—
	Isolated H_2O	A(1-1)	A(1-2)	B(1-1)	B(1-2)
$r(OH)$	0.9620	0.9696	0.9724[a]	0.9689	0.9753[a]
			0.9756[b]		0.9746[b]
$\nu(H_2O)$	3926,3820	3896,3725	3893,3676[c]	3898,3720	3889,3594[c]
			3892,3579[d]		3892,3631[d]
$\Sigma q(H_2O)$	—	−0.013	+0.006[e]	−0.019	0.000[e]
			−0.012[f]		−0.014[f]

[a]O_9H_8 bond. [b]$O_{12}H_{11}$ bond. $r(OH\cdots)$ in the water dimer is 0.9700 Å. [c]$\nu(H_8O_9H_{10})$. [d]$\nu(H_{11}O_{12}H_{13})$. [e]Σq on $(H_8O_9H_{10})$[f]Σq on $(H_{11}O_{12}H_{13})$.

Table 3: Properties of isolated CH_3CFO and the 1-1 and 1-2 complexes with H_2O. Distances in Å, σ^* occupation in e, hyperconjugation energies in kcal mol^{-1}, and frequencies in cm^{-1}.

	Isolated CH_3CFO	$CH_3CFO\cdot1H_2O$	$CH_3CFO\cdot2H_2O$
$r(C_4H_5)$	1.0877	1.0881	1.0900
$\nu(C_4H_5)$	3162	3160	3139
$\sigma^*(C_4H_5)$	0.0049	0.0064	0.0122
$\%sC_4(H_5)$	25.4	26.3	27.1
$q(C_4)$	−0.697	−0.707	−0.716
$q(H_5)$	0.231	0.257	0.273
$r(C_1 = O_2)$	1.182	1.188	1.189
$\nu(C_1 = O_2)$	1912	1884	1875
$LPO_{12} \rightarrow \sigma^*(C_4H_5)$	—	0.78	3.56
$LPO_2 \rightarrow \sigma^*(O_9H_8)$	—	4.10	6.67
	Isolated H_2O	$CH_3CFO\cdot1H_2O$	$CH_3CFO\cdot2H_2O$
$r(OH)$	0.9620	0.9677	0.9710[a]
			0.9756[b]
$\nu(H_2O)$	3926,3820	3901,3748	3891,3704[c]
			3890,3600[d]
$\Sigma q(H_2O)$	—	−0.008	+0.009[e]
			−0.014[f]

[a]O_9H_8 bond. [b]$O_{12}H_{11}$ bond. [c]$\nu(H_8O_9H_{10})$. [d]$\nu(H_{11}O_{12}H_{13})$, [e]Σq on $(H_8O_9H_{1O})$. [f]Σq on $(H_{11}O_{12}H_{13})$.

For NBO charges on H and O atoms in the monomer, dimer, and complexes, see S.I.).

As previously mentioned, the intermolecular $O_9 \cdots H_{11}$ distances do not markedly differ in the 1-2 complexes. From this, it can be anticipated that the properties of the water dimer considered as subsystem will not vary on a spectacular way. For all the complexes, the results indicate that the bonds between the two water molecules is stronger than in the water dimer. Further, as indicated in Tables 1, 2, and 3, the C=O$\cdots$HO bond in the 1-2 complexes is stronger than in the 1-1 complexes. This is shown by the larger elongation of the O_9H_8 bond, the larger decrease of the corresponding vibrational frequencies, and the larger $LPO_2 \rightarrow \sigma^*(O_9H_8)$ hyperconjugation.

The elongations of the OH bond are linearly related to frequency shifts of the ν^s(OH) vibration of water as follows:

$$\Delta r(\text{OH})(\text{Å}) = 5.10^{-5}\Delta\nu^s(\text{OH})(\text{cm}^{-1}) + 0.0029 \quad (r = 0.978). \tag{4}$$

This correlation includes all the 1-1 and 1-2 complexes.

Other water properties such as the σ^*(OH) occupation are summarized in S.I. These results indicate a large positive NBO charge of the bonding protons H_8 and H_{11}, a larger negative charge on the O_9 or O_{12} atoms, and a larger $\sigma^*(O_9H_8)$ or $\sigma^*(O_{11}H_{12})$ occupation than in the 1-1 complexes. It should be also noticed that in the 1-1 complexes, the water molecule acts as an electron acceptor, with the charge transfer from the carbonyl derivative to the water molecule ranging from 0.008 to 0.017e. In the 1-2 complexes, the sum of the charge on the $H_8O_9H_{10}$ molecule remains weak (positive or negative), the charge being transferred to the second water molecule which always bears a negative charge.

3.3. Binding Energies. Table 4 reports the total binding energies in the trimer, E(ABC); the binding energies between the AB, BC, and AC molecules at the trimer geometry along with the cooperative energies, ΔE^{coop}, calculated by (1).

The % cooperativity defined as the ratio $\Delta E^{\text{coop}}/E_{\text{ABC}}$ ranges between 18% and 20% and is almost constant for the five systems considered here. This percentage is slightly larger than in the $H_2C{=}O{\cdot}2H_2O$ system (16%) [27] but smaller than in the $NH_2CHO{\cdot}2H_2O$ system (26%) where the C=O$\cdots$HO and CH$\cdots$O bonds are formed [20].

The binding energies between the two water molecules are almost the same for all the systems, between -4.50 and -4.62 kcal mol^{-1}. These results are in line with the small differences in intermolecular distances and the NBO parameters in the two bonded water molecules discussed in the previous section.

The binding energies E_{AB} vary between -4.73 and -3.60 kcal mol^{-1}. They are ordered according to the proton affinities of the O atom of the carbonyl group which vary from 170.1 to 185.3 kcal mol^{-1} (Table 4)

$$-E_{\text{HB}}\left(\text{kcal mol}^{-1}\right) = 0.0786\,\text{PA}\left(\text{kcal mol}^{-1}\right) - 9.83 \quad (r = 0.998). \tag{5}$$

Table 4: B3LYP/6-311++G(d,p) Total Binding Energies (E_{ABC}), E_{AB}, E_{BC}, and E_{CA} binding energies in the trimer geometry and cooperative energies (ΔE_{coop}) for the CH_3CHO, CH_2FCHO, and CH_3CFO complexes with two water molecules (with BSSE-corrections in kcal mol^{-1})[a].

System	E_{ABC}	E_{AB}[b]	E_{AC}	E_{BC}	ΔE_{coop}
$CH_3CHO{\cdot}2H_2O$ (A)	-13.04	-4.64 (183.8)	-1.52	-4.56	-2.32
$CH_3CHO{\cdot}2H_2O$ (B)	-13.48	-4.73 (185.3)	-1.66	-4.50	-2.59
$CH_2FCHO\ 2H_2O$(A)	-13.00	-3.60 (170.1)	-2.31	-4.59	-2.50
$CH_2FCHO{\cdot}2H_2O$ (B)	-12.49	-3.71 (172.4)	-1.72	-4.54	-2.52
$CH_3CFO{\cdot}2H_2O$ (A)	-12.41	-3.60 (171.4)	-1.87	-4.62	-2.32

[a]A = carbonyl derivative, B and C = water. [b]The numbers in parentheses are the Proton Affinities of the O atom of the C=O group (kcal mol^{-1}) taken from [22].

The slope of this correlation is slightly larger than the slope of the correlation calculated for the 1-1 complexes (0.061) [22]. This conclusion must be taken with caution owing to the small range of considered energies. In a broad energy range, the cooperativity effects are usually nonlinear [49].

Let us also notice that the C_4H_5 bonds characterized by deprotonation enthalpies between 357 and 364 kcal mol^{-1} are better proton donors that the C_1H_3 bonds having much larger deprotonation enthalpies, between 382 and 391 kcal mol^{-1}. The binding energies E_{AC} are weak but do not reflect the differences in acidity of the CH bonds. The same remark also holds for the % of cooperativity which is almost constant.

4. Conclusions

The present work deals with a theoretical investigation of the cooperativity in $CH_3CHO{\cdot}2H_2O$, $CH_2FCHO{\cdot}2H_2O$, and $CH_3CFO{\cdot}2H_2O$ systems. The results are compared with the complexes involving one water molecule. The main conclusions of our work are the following ones.

(1) For the three systems, two stable cyclic structures are predicted. Both structures are stabilized by C=O$\cdots$HO interaction. In the A structures, the system is stabilized by a CH$\cdots$O interaction involving the CH_3 (or CH_2F) group. In the B structures, the CH bond of the HC=O group participates to the CH$\cdots$O interaction. The optimized structures indicate shorter intermolecular distances than in the 1-1 complexes or than in the water dimer.

(2) Formation of the A(1-2) complexes results in an elongation of the CH bond of the CH_3 or CH_2F group involved in the CH$\cdots$O interaction, a red shift of the ν(CH) vibration, and an increase in occupation of the σ^*(CH) orbitals. This elongation is negligible in the A(1-1) complexes. In contrast,

formation of the B(1-2) complexes results in a contraction of the aldehydic CH bond and a marked blue shift of the ν(CH) vibration, which are both larger than in the B(1-1) complexes. This effect is explained by a large decrease of the intramolecular LPO $\rightarrow$ σ^*(CH) hyperconjugation energy and illustrates the predominance of the lone pair effect in determining the CH distances.

(3) The elongation of the OH bonds in the water molecules, the red shifts of the ν(OH) vibrations are larger than in the water dimer. The same remark also holds for the variation of the NBO charges on the H and O atoms.

(4) Quantitative correlations between the CH distances and the σ^*(CH) occupations or between the frequency shifts of the ν(OH) stretching vibrations and the elongations of the OH bond of water are presented.

(5) The total binding energies in the ternary systems range between -12.41 and $-13.48\,\text{kcal mol}^{-1}$. The two-body interaction energies are calculated at the trimer geometries. At this geometry, the interaction energies between the carbonyl derivative and the considered water molecules slightly increase with the basicity of the C=O group. The cooperative energies are comprised between -2.32 and $-2.59\,\text{kcal mol}^{-1}$.

Acknowledgments

A. K. Chandara thanks CSIR India for financial assistance through Project no. 01(2494)/11/EMR-II. T. Z. -Huyskens thanks the Department of Chemistry, University of Leuven for computer facilities.

References

[1] H. S. Frank and W.-Y. Wen, "Ion-solvent interaction. Structural aspects of ion-solvent interaction in aqueous solutions: a suggested picture of water structure," *Discussions of the Faraday Society*, vol. 24, pp. 133–140, 1957.

[2] F. Kohler and P. Huyskens, "Some aspects of the structure and interaction potential of hydrogen bonded complexes," *Advances in Molecular Relaxation Processes*, vol. 8, no. 2, pp. 125–154, 1976.

[3] V. Gutman, *Structure and Bonding*, vol. 15, p. 141, 1974.

[4] P. L. Huyskens, "Factors governing the influence of a first hydrogen bond on the formation of a second one by the same molecule or ion," *Journal of the American Chemical Society*, vol. 99, p. 2576, 1993.

[5] A. Karpfen, "Case studies of cooperativity in hydrogen-bonded clusters and polymers in Hydrogen Bonding," in *Hydrogen Bonding : A Theoretical Perspective*, S. Scheiner, Ed., Oxford University Press, New York, NY, USA, 1997.

[6] G. A. Jeffrey, *An Introduction in Hydrogen Bonding*, Oxford University Press, New York, NY, USA, 1997.

[7] T. Zeegers-Huyskens, "Cooperative effects involved in hydrogen bond formation," in *Recent Research Developments in Physical Chemistry*, S. G. Pandai, Ed., vol. 2, 1998.

[8] W. A. P Luck, "How to understand liquids" in Intermolecular Forces: An Introduction to Modern Methods and Results," in *Intermolecular Forces: An Introduction to Modern Methods and Results*, P. L. Huyskens, W. A. P. Luck, and T. Zeegers-Huyskens, Eds., Springer, Berlin, Germany, 1991.

[9] G. Chalasinski and M. M. Szczesniak, "Origins of structure and energetics of van der waals clusters from ab *initio* calculations," *Chemical Reviews*, vol. 94, no. 7, pp. 1723–1765, 1994.

[10] J. E. H. Koehler, W. Saenger, and B. Lesyng, "Cooperative effects in extended hydrogen bonded systems involving O–H groups. Ab *initio* studies of the cyclic S4 water tetramer," *Journal of Computational Chemistry*, vol. 8, no. 8, pp. 1090–1098, 1987.

[11] O. Mó, M. Yanez, and J. Elguero, "Cooperative (nonpairwise) effects in water trimers: an ab *initio* molecular orbital study ," *Journal of Chemical Physics*, vol. 97, p. 6628, 1992.

[12] W. A. P. Luck, D. Klein, and K. Rangsriwatanonon, "Anti-cooperativity of the two water OH groups," *Journal of Molecular Structure*, vol. 416, pp. 287–296, 1997.

[13] K. Hermansson, "Blue-shifting Hydrogen Bonds," *Journal of Physical Chemistry A*, vol. 106, p. 4696, 2002.

[14] M. F. Rode and J. Sadlej, "The $(H_2O)_2CO$ ternary complex: cyclic or linear?" *Chemical Physics Letters*, vol. 342, pp. 220–230, 2001.

[15] T. Kar and S. Scheiner, "Comparison of cooperativity in CH$\cdots$O and OH$\cdots$O hydrogen bonds," *Journal of Physical Chemistry A*, vol. 108, no. 42, pp. 9161–9168, 2004.

[16] Q. Li, X. An, B. Gong, and J. Cheng, "Cooperativity between OH$\cdots$O and CH$\cdots$O hydrogen bonds involving dimethyl sulfoxide-H_2O-H_2O complex," *Journal of Physical Chemistry A*, vol. 111, pp. 10166–10169, 2007.

[17] A. Karpfen and E. S. Kryachko, "Blue-shifted A-H stretching modes and cooperative hydrogen bonding. 1. Complexes of substituted formaldehyde with cyclic hydrogen fluoride and water clusters," *Journal of Physical Chemistry A*, vol. 111, no. 33, pp. 8177–8187, 2007.

[18] T. Kar and S. Scheiner, "Cooperativity of conventional and unconventional hydrogen bonds involving imidazole," *International Journal of Quantum Chemistry*, vol. 106, no. 4, pp. 843–851, 2006.

[19] N. Dozova, L. Krim, M.E. Alikhami, and N. Lacome, "Vibrational spectra and structure of CH_3 Cl$:(H_2O)_2$ and CH_3 Cl$:(D_2O)_2$ complexes. IR matrix isolation and ab *initio* calculations," *Journal of Physical Chemistry A*, vol. 111, no. 40, pp. 10055–10061, 2007.

[20] E. L. Angelina and N. M. Peruchena, "Strength and nature of hydrogen bonding interactions in mono- and di-hydrated formamide complexes," *Journal of Physical Chemistry A*, vol. 115, no. 18, pp. 4701–4710, 2011.

[21] M. Smiechowski, "Theoretical study of the structure, energetics and vibrational frequencies of water-acetone and water-butanone complexes," *Chemical Physics Letters*, vol. 480, no. 4–6, pp. 178–184, 2009.

[22] A. K. Chandra and T. Zeegers-Huyskens, "A theoretical investigation of the interaction between substituted carbonyl derivatives and water: open or cyclic complexes?" *Journal of Computational Chemistry*, vol. 33, no. 11, pp. 1131–1141, 2012.

[23] A. D. Becke, "Density-functional thermochemistry. IV. A new dynamical correlation functional and implications for exact-exchange mixing," *Journal of Chemical Physics*, vol. 104, p. 1040, 1996.

[24] M. J. Frisch, *Gaussian 03, Revision D. 01*, Gaussian, Wallingford, Conn, USA, 2004.

[25] S. F. Boys and F. Bernardi, *Molecular Physics*, vol. 19, p. 553, 1970.

[26] S. S. Xantheas, "On the importance of the fragment relaxation energy terms in the estimation of the basis set superposition error correction to the intermolecular interaction energy," *Journal of Chemical Physics*, vol. 104, p. 8821, 1996.

[27] M. Masella and J. P. Flament, "A theoretical study of five water/ammonia/formaldehyde cyclic trimers: influence of cooperative effects," *Journal of Chemical Physics*, vol. 110, no. 15, pp. 7245–7255, 1999.

[28] M. Weimann, M. Fárník, M. A. Suhm, M. E. Alikhani, and J. Sadlej, "Cooperative and anticooperative mixed trimers of HCl and methanol," *Journal of Molecular Structure*, vol. 790, no. 1–3, pp. 18–26, 2006.

[29] A. E. Reed, L. A. Curtiss, and F. Weinhold, "Intermolecular interactions from a natural bond orbital, donor-acceptor viewpoint," *Chemical Reviews*, vol. 88, no. 6, pp. 899–926, 1988.

[30] ν(C=O) (cm^{-1}) = −407 r(C=O) (Å) +6722(r = 0.9907).

[31] F. Bohlmann, "Die Konfiguration des Matrins," *Angewandte Chemie International Edition*, vol. 69, no. 20, p. 642, 1957.

[32] E. E. Ernstbrunner and J. Hudec, "Bohlmann bands, a reassessment," *Journal of Molecular Structure*, vol. 17, no. 2, pp. 249–256, 1973.

[33] A. Barnes, "Blue-shifting hydrogen bonds- arethey proper or improper?" *Journal of Molecula Structure*, vol. 113, p. 259, 1983.

[34] A. Barnes and T. R. Beech, "The vibrational spectrum of the dimethylether-water complex," *Chemical Physics Letters*, vol. 94, p. 568, 1983.

[35] A. Karpfen and E. S. Kryachko, "On blue shifts of C-H stretching modes of dimethyl ether in hydrogen- and halogen-bonded complexes," *Chemical Physics Letters*, vol. 431, no. 4–6, pp. 428–433, 2006.

[36] B. Nelander, "A matrix isolation study of the water-formaldehyde complex The far-infrared region," *Chemical Physics*, vol. 159, p. 281, 1992.

[37] T. Zeegers-Huyskens, "Vibrational frequencies in hydrogen-bonded and non-hydrogen-bonded CH groups," *Journal of Molecular Structure*, vol. 887, no. 1–3, pp. 2–8, 2008.

[38] A. K. Chandra, S. Parveen, and T. Zeegers-Huyskens, "Anomeric effect in the symmetrical and asymmetrical structure of triethylamine," *Journal of Physical Chemistry*, vol. 115, p. 8884, 2007.

[39] A.Y. Li, "Theoretical study of linear and bifurcated H-bonds in the systems Y$\cdots$H$_2$CZ$_n$," *Journal of Molecular Structure*, vol. 862, p. 31, 2008.

[40] T. Zeegers-Huyskens and E. S. Kryachko, "Methyl formate and its mono and difluoro derivatives: conformational manifolds, basicity, and interaction with HF theoretical investigation," *Journal of Physical Chemistry A*, vol. 115, no. 45, pp. 12586–12601, 2011.

[41] Y. Gu, T. Kar, and S. Scheiner, "Fundamental properties of the CH$\cdots$O interaction: is it atrue hydrogen bond?" *Journal of the American Chemical Society*, vol. 121, no. 40, pp. 9411–9422, 1999.

[42] A. Masunov, J. J. Dannenberg, and R. H. Contreras, "C-H bond-shortening upon hydrogen bond formation: influence of an electric field," *Journal of Physical Chemistry A*, vol. 105, no. 19, pp. 4737–4740, 2001.

[43] K. Hermansson, "Blue-shifting hydrogen bonds," *Journal of Physical Chemistry A*, vol. 106, no. 18, pp. 4695–4702, 2002.

[44] S. N. Delanoye, W. A. Herrebout, and B. J. van der Veken, "Improper or classical hydrogen bonding? A comparative cryosolutions infrared study of the complexes of $HCCIF_2$, $HCCI_2F$, and $HCCI_3$ with dimethyl ether," *Journal of the American Chemical Society*, vol. 124, no. 25, pp. 7490–7498, 2002.

[45] X. Li, L. Liu, and H. B. Schlegel, "On the physical origin of blue-shifted hydrogen bonds," *Journal of the American Chemical Society*, vol. 124, no. 32, pp. 9639–9647, 2002.

[46] I. V. Alabugin, M. Manoharan, S. Peabody, and F. Weinhold, "Electronic basis of improper hydrogen bonding: a subtle balance of hyperconjugation and rehybridization," *Journal of the American Chemical Society*, vol. 125, no. 19, pp. 5973–5987, 2003.

[47] A. Karpfen and E. S. Kryachko, "On the intramolecular origin of the blue shift of a-h stretching frequencies: triatomic hydrides HAX," *Journal of Physical Chemistry A*, vol. 113, no. 17, pp. 5217–5223, 2009.

[48] J. Joseph and E. D. Jemmis, "Red-, blue- or no-shift in hydrogen bonds: an unified explanation," *Journal of the American Chemical Society*, vol. 129, no. 15, pp. 4620–4632, 2007.

[49] T. Zeegers-Huyskens, "Non-linearity of the cooperativity effects in hydrogen bond complexes involving hydrogen halides in solid argon," *Journal of Molecular Structure*, vol. 297, pp. 149–150, 1993.

Hindawi Publishing Corporation
Journal of Atomic, Molecular, and Optical Physics
Volume 2012, Article ID 236793, 11 pages
doi:10.1155/2012/236793

Research Article

Polymorphism, Hydrogen Bond Properties, and Vibrational Structure of 1H-Pyrrolo[3,2-*h*]Quinoline Dimers

Alexandr Gorski,[1] Sylwester Gawinkowski,[1] Roman Luboradzki,[1] Marek Tkacz,[1] Randolph P. Thummel,[2] and Jacek Waluk[1]

[1] *Institute of Physical Chemistry, Polish Academy of Sciences, Kasprzaka 44/52, 01-224 Warsaw, Poland*
[2] *Department of Chemistry, University of Houston, Houston, TX 77204-5003, USA*

Correspondence should be addressed to Jacek Waluk, waluk@ichf.edu.pl

Received 29 February 2012; Accepted 30 May 2012

Academic Editor: Paul Blaise

Copyright © 2012 Alexandr Gorski et al. This is an open access article distributed under the Creative Commons Attribution License, which permits unrestricted use, distribution, and reproduction in any medium, provided the original work is properly cited.

Two forms of cyclic, doubly hydrogen-bonded dimers are discovered for crystalline 1H-pyrrolo[3,2-*h*]quinoline, a bifunctional molecule possessing both hydrogen bond donor and acceptor groups. One of the forms is planar, the other is twisted. Analysis of IR and Raman spectra, combined with DFT calculations, allows one to assign the observed vibrations and to single out vibrational transitions which can serve as markers of hydrogen bond formation and dimer structure. Raman spectra measured for samples submitted to high pressure indicate a transition from the planar towards the twisted structure. Formation of intermolecular hydrogen bonds leads to a large increase of the Raman intensity of the NH stretching band: it can be readily observed for the dimer, but is absent in the monomer spectrum.

1. Introduction

In studies of the intermolecular hydrogen bond (HB), an important class of model compounds consists of molecules which can form both H-bonded dimers and complexes with water or alcohols [1]. Such molecules are usually characterized by the simultaneous presence of HB donor and acceptor groups. Whether the strength of the intermolecular HBs is greater for dimers or complexes depends on the relative positions of the donor and acceptor in the molecular frame. Interestingly, different structures and stoichiometries are often encountered for the same molecule. A well-known example is 7-azaindole (7AI, Figure 1), which forms doubly hydrogen bonded dimers in solution [2], while the X-ray data reveal a tetrameric structure in the crystalline state [3]. Different stoichiometries and structures are possible for the complexes of 7AI with methanol and water: 1 : 1, 1 : 2, and 1 : 3 species have been detected [4–9].

The crystal structure of multiply H-bonded dimers/oligomers seems to be determined by the interplay of H-bonding and longer range intermolecular interactions. For instance, 1-azacarbazole (1AC), a molecule closely related to 7AI, exists in the crystal in the form of planar, doubly hydrogen bonded dimers [10] (Figure 2). While there is no doubt that 1AC also forms dimers in solutions, various possible structures have been discussed [11–14].

1H-pyrrolo[3,2-*h*]quinoline (PQ, Scheme 1) can be considered a counterpart to 7AI with regard to intermolecular HB characteristics. The NH group of PQ (HB-donor) and the pyridine nitrogen (HB-acceptor) are positioned three bonds apart, whereas in 7AI these groups are separated by two bonds. This change results in completely different excited state behaviour of complexes with water or alcohols [15–20]. Rapid photoinduced double proton transfer is observed for PQ in complexes of 1 : 1 stoichiometry. The process occurs on the time scale of single picoseconds and is not stopped by lowering of temperature or by increasing the viscosity of the medium. On the contrary, the reaction is slower and viscosity-dependent in 7AI complexes [21], since it requires a solvent rearrangement around an excited chromophore [22–27]. These different phototautomerization

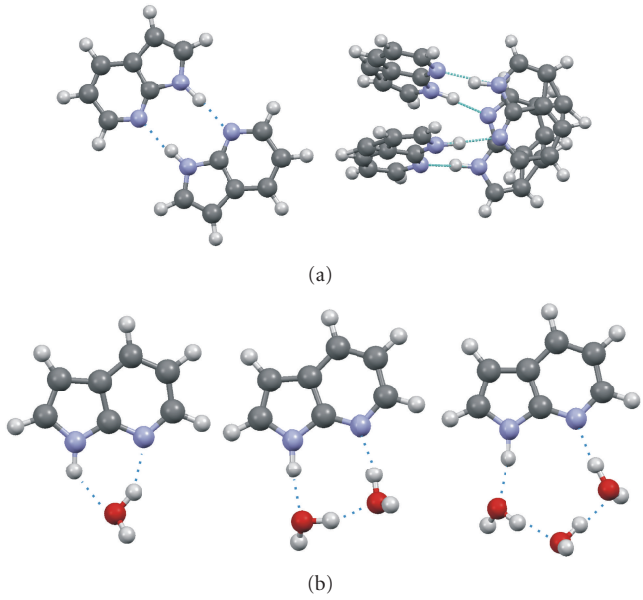

Figure 1: Various motifs of intermolecular HB formed by 7-azaindole. (a) Dimers and tetramers, (b) complexes with water.

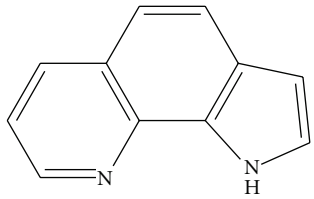

Scheme 1

characteristics reflect different intermolecular HB strengths, imposed by molecular structure.

The HB characteristics, and, in consequence, tautomerization abilities in the dimeric species are expected to become reversed in PQ and 7AI. For the latter, a planar dimeric structure reveals two strong, linear, equivalent HBs. Therefore, it is not quite surprising that photoinduced double proton transfer in 7AI dimers has been observed at temperatures as low as 4 K [28]. In contrast, PQ dimers are predicted by theory to be nonplanar. This has been confirmed by X-ray studies, which reported an angle of 22.6° between the two monomeric units [29]. Our previous work on a similar structure, dipyrido[2,3-*a*:3,2-*i*]carbazole [30] demonstrated that in the crystalline phase this molecule forms cyclic, but strongly nonplanar doubly hydrogen-bonded dimers (Figure 3). No tautomeric fluorescence has been observed for such a dimer, but it could be readily detected when the crystalline sample was exposed to water vapor, prepared on a hydrophilic support, or embedded in a polymer containing hydroxyl groups. A general conclusion from this study was that HB-donor-acceptor molecules which readily form flat dimers should have a weak tendency for the formation of cyclic complexes, and *vice versa*.

In this work, we analyze structure and vibrational spectra of crystalline PQ dimers. Somewhat unexpectedly, our X-ray

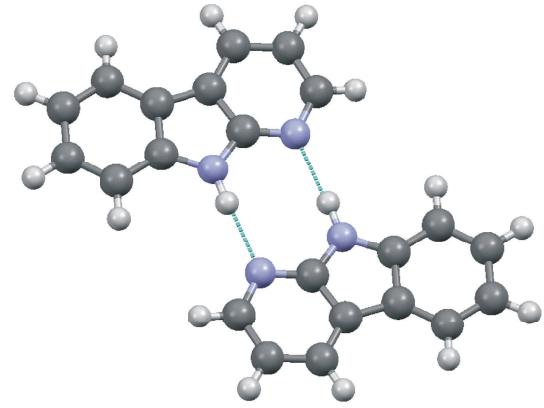

Figure 2: The structure of dimers of 1-azacarbazole in the solid phase.

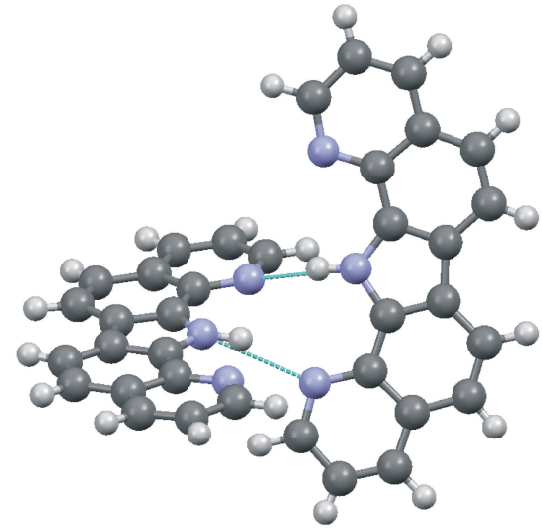

Figure 3: The X-ray structure of dipyrido[2,3-*a*:3,2-*i*]carbazole.

measurements of PQ reveal the existence of planar, doubly hydrogen-bonded dimeric species, and thus a structure very different than the one reported previously [29] (Figure 4). We analyze the experimental and theoretically predicted vibrational patterns, with particular interest regarding the vibrations involved in intermolecular hydrogen bonds. Finally, we show the influence of high pressure upon the HB strength, manifested by spectral shifts observed in the Raman spectra.

2. Experimental and Theoretical Details

Synthesis and purification of PQ have been described before [31].

The IR spectra were recorded on a Nicolet Magna 560 FTIR spectrometer, equipped with MCT/B liquid-nitrogen-cooled detector, with 1 cm^{-1} resolution. For the measurements of infrared spectra, thin polycrystalline PQ films were prepared on KBr or ZnSe windows by quick evaporation from a concentrated solution. The monomer IR

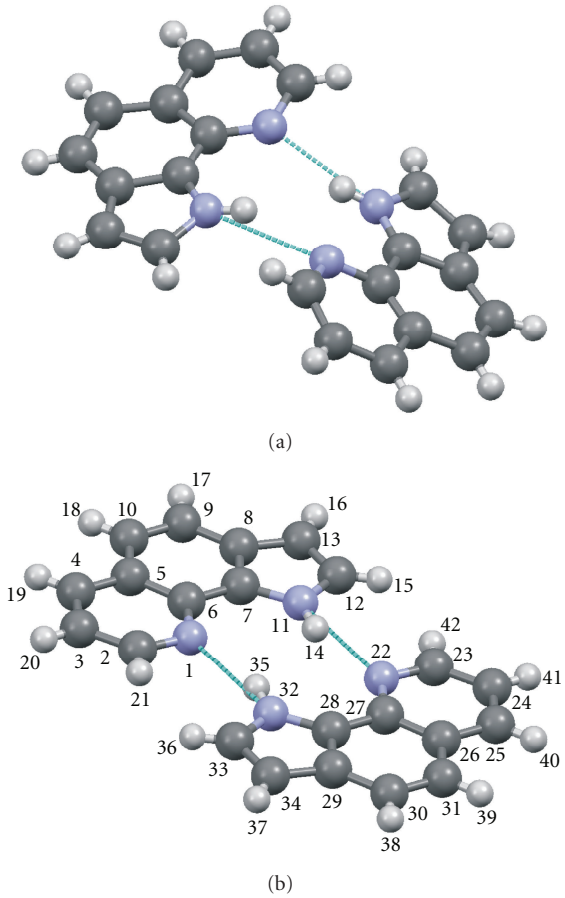

FIGURE 4: (a) X-ray structure of PQ reported in [29]; the geometrical positions of hydrogen atoms were inserted. (b) Our X-ray structure and atom numbering.

spectra have been recorded for PQ isolated in argon matrices using a closed-cycle helium cryostat (CSW-202N, Advanced Research Systems). The compound, contained in a glass tube, was heated to 350 K and codeposited with argon at a ratio of about 1 : 1000 onto a cold (20 K) KBr window mounted in a cryostat with 10^{-6} Torr background pressure. During spectral measurements the matrix temperature was kept at 10 K.

Renishaw inVia microscopic system was used for the measurements of Raman spectra. Ar^+ 514.5 nm (Stellar Pro Modu-Laser, LLC) laser line and a diode laser (HPNIR785) emitting 785 nm line were used as the excitation sources. With a ×100 microscope objective the laser light was focused on a sample, the laser power at the sample being 5 mW or less. The Raman scattered light was collected by the same objective through a cut-off filter to block out Rayleigh scattering. Gratings of 1800 and 1200 grooves/mm were used for 514.5 and 785 nm laser lines, respectively. The resolution was 5 cm^{-1}, with the wavenumber accuracy of 2 cm^{-1}, both calibrated with the Rayleigh line and the 520.6 cm^{-1} line of silicon. The Raman scattered light was recorded by a 1024 × 256 pixel Peltier-cooled RenCam CCD detector.

High pressure experiments have been performed in Takemura type of diamond anvil cell [32]. The diameter of the diamond culet was 600 μm and a gasket made of stainless steel was used with 300 μm centrally drilled hole. Sample powder was loaded into the gasket hole without any pressure transmitting medium. Pressures were measured by recording the fluorescence spectrum of a small ruby chip embedded in the sample and converting the shift of the wavelength of the R_1 line to pressure, according to the scale proposed by Mao [33].

The samples of different polymorphs were prepared by quick crystallization by evaporation from concentrated PQ solutions in dichloromethane, diethyl ether, methanol, cyclohexane, and toluene.

For the X-ray studies, a colorless PQ crystal of approximate dimensions of 0.1 × 0.2 × 0.2 mm^3 was used. Diffraction data were collected at 100 K using a Bruker Kappa CCD diffractometer with graphite monochromated Mo Kα radiation. Structure was solved by direct methods (SHELXS-97) and refined on F^2 by full-matrix least-squares method (SHELXL-97) [34]. Formula is $C_{11}H_8N_2$, monoclinic, space group $P2_1/c$, $a = 9.0104(4)$, $b = 4.7302(1)$, $c = 19.3117(9)$ Å, $\beta = 103.1825(17)^\circ$, $R_1 = 0.0449$ ($I > 2\sigma(I)$), $wR_2 = 0.1144$ for all data.

Unit cell parameters (but not the whole data) were also measured at room temperature, showing no significant differences compared with 100 K data ($a = 9.13$, $b = 4.87$, $c = 19.42$ Å, $\beta = 102.54^\circ$, parameters not refined).

The crystallographic data have been deposited with the Cambridge Crystallographic Data Centre as a supplementary publication no. CCDC 868707. The data can be obtained free of charge at http://www.ccdc.cam.ac.uk or from the Cambridge Crystallographic Data Centre, 12 Union Road, Cambridge CB2 1EZ, UK.

Geometry optimizations were performed using density functional theory (DFT), with B3LYP functional and cc-PVTZ basis set, as implemented in Gaussian 09. This choice of functional/basis set was guided by extensive calculations for the PQ monomer which resulted in reliable assignments of nearly all of the vibrations.

In order to simulate the structure of PQ dimers in the crystalline environment, DFT-based quantum chemical calculations were performed using the CASTEP (Cambridge Serial Total Energy Package) computer code [35] in the framework of the generalized gradient approximation (GGA), as proposed by Perdew et al. [36], in combination with Vanderbilt ultrasoft pseudopotentials [37]. The plane wave basis set was truncated at a kinetic energy of 240 eV. Computations were performed over a range of k-points within the Brillouin zone as generated by the full Monkhorst-Pack scheme [38] with a 2 × 2 × 1 mesh. A further increase of the cutoff energy and the number of k-points resulted in negligibly small changes in structure energies, indicating that the energy values are well converged. Two initial geometries of planar and twisted PQ dimers were taken from the X-ray data. In every case a slab including 16 molecules of PQ was constructed and repeated periodically.

3. Results

3.1. Dimer Structure. Geometry optimization performed for the PQ dimer yields a nonplanar, doubly H-bonded structure. The calculated nonplanar geometry agrees qualitatively with the X-ray data published in 1991 (Figure 4(a)). However, the quantitative differences are quite significant. The calculated twisting angle between the monomeric moieties, 45.6°, is much larger than the experimental one, 22.6°. For the separation of the H-bonded nitrogen atoms, the same value, 2.98 Å, is computed for both pairs, while the reported X-ray distances are very different, 2.92 and 2.99 Å. The calculations yield nearly planar monomeric units in the dimer, whereas the experiment clearly shows distortions. For instance, the experimental NCCN angles are 3.8° and 5.4°, while the calculations yield the same, smaller value of 2.5°. These results suggest that intermolecular interactions in the crystal may affect the dimer structure. We have therefore repeated the X-ray measurements, performing experiments both at 293 K and at lower temperatures. Surprisingly, a different structure than previously reported was obtained (Figure 4(b)), consisting of two doubly H-bonded PQ monomeric units in a planar arrangement. In order to obtain a theoretical model for the planar dimer, we imposed the planarity in the optimization procedure. This resulted in one negative frequency in the optimized structure, the vibration corresponding to mutual twisting of the planar moieties. Computationally, the planar geometry shows the NN distance of 3.12 Å, whereas the experimental value is 3.01 Å.

One can conclude that PQ forms polymorphs in the crystal, which differ in the structure of dimers, especially with regard to parameters usually considered important for the strength of intermolecular hydrogen bond. Therefore it seemed interesting to carry out vibrational spectroscopy studies in order to (i) determine how does the formation of a doubly H-bonded dimer affect the vibrational pattern and (ii) probe the possible differences in the vibrational structure between planar and nonplanar (but both doubly H-bonded) dimers.

3.2. IR Measurements. Figure 5 presents the IR spectra recorded for the monomeric PQ isolated in an Ar matrix and the spectra of polycrystalline PQ, corresponding to the planar dimeric structure, measured on a KBr window. The experimental data are compared with the results of calculations performed for the monomer and for the two forms of the dimer: a fully-optimized non-planar structure and a form with imposed planar geometry.

The spectra of monomeric PQ are very well reproduced by calculations with regard to both band positions and intensities. They will be treated in detail in a separate work, in which the combination of theoretical modelling, IR, Raman, and high resolution fluorescence spectra obtained for supersonic jet-isolated PQ allowed reliable assignments of nearly all of 57 vibrations of monomeric PQ. Here, we focus on the dimer, using the monomer vibrations as a starting point. Figure 5 shows that, while the general pattern of the IR spectrum of dimeric PQ roughly resembles that

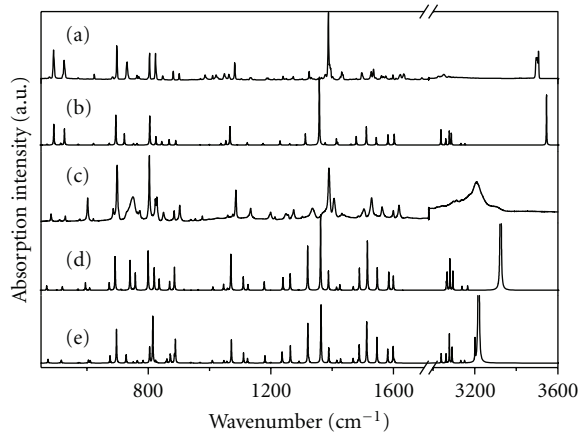

Figure 5: (a) IR spectrum of the monomer in Ar matrix at 15 K; (b) simulated monomer spectrum; (c) dimeric, polycrystalline PQ at 293 K; results of calculations performed for the planar (d) and twisted (e) dimer. The scaling factor of 0.9682 was used in calculations.

of the monomer, significant differences are observed in specific regions. The largest difference is observed for the NH stretching mode. The monomer peak observed around 3500 cm^{-1} (the observed triplet is due to argon site structure) disappears in the crystalline sample, where a broad band is detected, centered at 3210 cm^{-1}. This red shift of almost 300 cm^{-1} is characteristic for the formation of fairly strong NH$\cdots$N intermolecular hydrogen bonds. The calculations predict the shifts of 320 and 220 cm^{-1} for the twisted and planar forms, respectively. As expected, the larger shift is computed for a structure with a shorter N–N distance, and thus a stronger hydrogen bond. The better agreement with experiment for the larger value is somewhat misleading, since the X-ray measurements demonstrated that the sample corresponded to a planar dimer. Further arguments are provided by the analysis of the IR spectrum in the energy region corresponding to out-of-plane vibrations. For the monomeric PQ, calculations yield two modes that contain significant NH out-of-plane contributions. They can be readily identified in the experimental spectrum as the bands at 491 and 527 cm^{-1}. In the IR spectrum of a dimer these bands are still observed, but, in addition, a broad band appears at 743 cm^{-1}, in nice agreement with calculations, which predict for a planar structure a transition at 734 cm^{-1}. For the twisted dimer structure, there no longer exist pure "out-of-plane" modes. The mode which still retains much of that character is predicted to lie at 807 cm^{-1} and to have an intensity twice that of the planar structure. Comparison of the experimental and simulated IR spectra in the region of 650–950 cm^{-1} leaves no doubt that the observed spectrum originates from a planar species. The value of the blue shift of the NH out-of-plane bending mode, which exceeds 200 cm^{-1}, again points to a strong intermolecular HB in dimeric PQ.

There is no single particular vibration in the monomer which could be assigned to a pure NH in-plane bending mode. This is also true for the dimer. The IR transitions

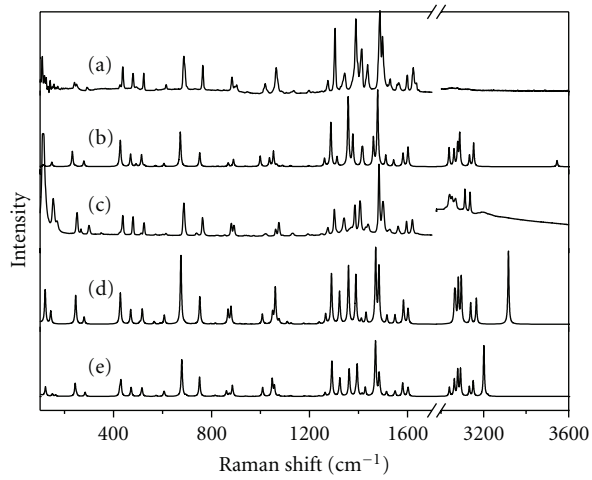

Figure 6: (a) Raman spectrum of the monomer in Ar matrix at 15 K; (b) simulated monomer spectrum; (c) dimeric, polycrystalline PQ, measured at 293 K; results of calculations performed for the planar (d) and twisted (e) dimer. The scaling factor of 0.9682 was used in calculations.

computed for the planar dimer consist of symmetric and antisymmetric combinations of the monomer modes. Only the latter are IR-active. A very similar pattern of IR transitions is obtained for the nonplanar dimer. Figure 5 shows that in the region above 1000 cm^{-1} the predicted IR spectra for both planar and twisted dimer are almost identical.

The analysis of the IR spectra demonstrates that both NH stretching and out-of-plane bending modes are efficient markers for the HB formation. However, only the latter can be used to indicate the planar structure of the H-bonded dimer.

3.3. Raman Spectra. Comparison of Raman spectra simulated and measured for monomeric and dimeric PQ is presented in Figure 6. Contrary to the case of the IR spectra, the calculations now predict differences between monomeric and dimeric species in the region above 1200 cm^{-1}. Below that value, the simulated spectra are very similar for the three species. But even above 1200 cm^{-1}, the Raman spectra computed for planar and twisted dimers resemble each other very strongly, excluding their use for structure determination.

The calculations predict that the Raman activity of the NH stretching mode should be drastically increased, about 15 times, upon HB formation. This increase was confirmed by experiment. No band corresponding to the NH stretch was observed for monomeric PQ, but it could be readily detected at 3200 cm^{-1} for the crystalline sample. Thus, formation of the intermolecularly H-bonded dimer enhances the polarizability to a degree that enables observation of a vibrational feature characteristic of the hydrogen bond.

3.4. Vibrational Assignments. Based on IR and Raman spectra and the results of calculations, we present in Table 1 the tentative assignments for the vibrations of dimeric PQ. The experimental data given in the Table correspond to the planar structure, whereas the calculations are given for both planar and twisted forms. Since the planarity was artificially imposed in the calculations, one might expect that the results in this case are less reliable. Still, as can be seen from Figures 5 and 6, the calculated vibrational patterns are very similar, both for IR and Raman spectra. The largest differences are observed for the NH stretching and out-of-plane bending modes, which were specifically discussed above.

3.5. Obtaining Different Polymorphic Forms. As already mentioned, the crystalline samples of PQ which we have examined by X-ray, IR and Raman techniques corresponded to planar dimers, and thus to a different polymorphic form than observed previously [29]. We have tried to obtain both forms by crystallization from different solvents, and then using Raman spectroscopy as a tool for structure determination. A trial and error approach was adopted, since no information about crystallization details was given in the work reporting the twisted structure [29]. Figure 7 presents the Raman spectra measured for samples crystallized from five different solvents. The spectra are similar, but significant differences can be detected in two regions. A peak of weak intensity appears at 738 cm^{-1} for PQ crystallized from cyclohexane, toluene, and methanol, but not from diethyl ether and dichloromethane. The second region corresponds to two fairly strong peaks observed at 1062 and 1074 cm^{-1}. Their relative intensity patterns (a more intense feature lying at higher energy) are the same for the samples revealing the 738 cm^{-1} transition. For two other samples, which lack the 738 cm^{-1} peak, the intensity ratio changes: now the lower energy peak becomes higher. Such behavior strongly suggests that the PQ samples obtained from cyclohexane, toluene, and methanol correspond to planar dimers, whereas those crystallized from diethyl ether and dichloromethane, to the nonplanar ones. This is confirmed by the results of calculations, which predict exactly such reversal of the relative intensity pattern for the 1062 and 1074 cm^{-1} peaks upon going from a planar to a twisted dimeric form (see Figure 6).

3.6. High-Pressure Experiments. The idea behind spectral measurements for samples submitted to high pressures was to observe pressure-induced changes in the strength, and possibly also of the structure of the intermolecular hydrogen bond. Figure 8 shows the Raman spectra recorded for PQ dimers under normal and elevated pressures. Nearly all peaks observed below 1700 cm^{-1} evolve in a similar way with increasing pressure: the maxima shift to the blue by 5–8 cm^{-1}. Much larger shifts towards higher transition energies are detected for the CH stretching bands, which shift by 30 cm^{-1} or more. A reversal of the relative intensities is observed for the bands at 3114 and 3137 cm^{-1}. All these changes are reversible, as shown by comparison of the spectra recorded for the same sample before and after going through the high pressure cycle.

The effects most relevant to this work are related to changes in the HB strength and structure. Figure 8 shows that the NH stretching band, observed at 3200 cm^{-1}, moves to

Table 1: Comparison of the experimental IR and Raman spectra with the vibrational frequencies calculated for the twisted and planar forms of the PQ dimer.

	Calculated[a]						Observed				
	frequency[e] (cm^{-1})	frequency[f] (cm^{-1})	IR intensity[g] (km/mol)		Raman activity[g] (A^4/amu)		IR[b]		Raman[c]		Assignment[d]
							3362				
ν_1	3218.9	3218.8	2578.38	(1802.54)	28.41	(0)	3180[h]	s			as NH str
ν_2	3201.3	3211.2	48.28	(0.01)	1126.68	(1032.01)			3193[h]	s	s NH str
ν_3	3151.3	3065.3	4.97	(7.27)	49.50	(53.58)					as CH str
ν_4	3151.3	3065.3	0.52	(1.43)	281.36	(272.92)			3137	w	s CH str
ν_5	3133.0	3039.3	0.75	(0.64)	164.25	(237.43)			3112	w	s CH str
ν_6	3133.0	3039.3	5.02	(6.87)	39.47	(22.30)					as CH str
ν_7	3091.4	2996.7	4.88	(0.14)	453.54	(555.04)			3067	w	s CH str
ν_8	3091.4	2996.6	29.73	(36.36)	95.36	(2.32)					as CH str
ν_9	3078.3	2983.2	1.61	(0.01)	501.64	(515.94)			3052	w	s CH str
ν_{10}	3078.2	2983.1	63.42	(60.51)	27.11	(0.05)					as CH str
ν_{11}	3062.4	2970.2	0.17	(17.58)	302.47	(121.90)			3040	w	s CH str
ν_{12}	3062.4	2969.9	19.75	(17.35)	24.36	(125.43)					as CH str
ν_{13}	3059.7	2966.6	2.18	(8.51)	2.32	(113.18)					as CH str
ν_{14}	3059.6	2966.4	0.33	(6.59)	12.54	(140.11)			3019	sh	s CH str
ν_{15}	3039.2	2964.5	4.87	(0.27)	148.24	(30.94)			3000		s CH str
ν_{16}	3039.1	2964.5	15.73	(0.38)	28.75	(42.60)					as CH str
							1660	m			
							1632	m			
ν_{17}	1602.8	1551.4	6.25	(0)	50.40	(53.35)			1620	m	NH s b, CC str cr
ν_{18}	1598.7	1548.4	36.68	(27.79)	10.29	(0)	1615	s			NH as b,CC str cr
ν_{19}	1581.1	1534.2	27.87	(34.95)	13.16	(0.07)	1594	m			(CC, CN) as str pyridine
ν_{20}	1580.3	1533.4	4.33	(0.03)	66.13	(81.74)			1595	m	(CC, CN) s str pyridine
ν_{21}	1549.9	1499.8	0.99	(0.01)	28.48	(30.40)			1562	m	NH, CH s b pyridine
ν_{22}	1545.9	1497.7	57.03	(43.42)	6.11	(0.01)	1560	m			NH, CH as b pyridine
ν_{23}	1515.0	1468.1	4.14	(0)	21.16	(27.48)			1528	w	NH, CH18,20,41,39 s b
ν_{24}	1512.5	1466.6	90.78	(95.24)	5.73	(0)	1524	s			NH, CH18,20,41,39 as b
ν_{25}	1488.0	1441.3	40.20	(42.88)	17.42	(0)	1497	m			NH as b, CC str pyr
ν_{26}	1484.3	1436.4	4.55	(0)	111.20	(172.84)			1500	s	NH s b, CC str pyr
ν_{27}	1469.8	1423.5	1.32	(0)	243.81	(225.53)			1484	vs	CH20 s b, skel def CC
ν_{28}	1468.1	1422.0	9.96	(7.03)	56.54	(0)	1482	w			CH20 as b, skel def CC
ν_{29}	1427.9	1385.4	0.77	(0)	37.40	(32.30)			1440	w	NH, CH20,21,41,42 s b, skel def pyr
ν_{30}	1427.2	1379.4	9.25	(10.49)	6.91	(0)	1435	w			NH, CH20,21,41,42 as b, skel def pyr
ν_{31}	1414.9	1369.1	4.96	(6.27)	0.97	(0)	1428	w			CH17,18,19,20,38,39,40,41 as b, CC str cr
ν_{32}	1414.7	1366.9	0.84	(0)	9.32	(13.32)			1430	m	CH17,18,19,20,38,39,40,41 s b, CC str cr
ν_{33}	1394.6	1345.2	0.04	(0)	152.39	(137.61)			1407	m	NH, CH21,42 s b, CC str pyr
ν_{34}	1388.7	1343.6	33.68	(37.34)	17.26	(0.01)	1403	m			NH, CH21,42 as b, CC str pyr,
ν_{35}	1363.7	1318.7	124.83	(146.01)	22.36	(0)	1386	s			skel def, CH as b
ν_{36}	1361.7	1315.9	20.55	(0)	111.09	(157.34)			1386	s	skel def, CH s b
ν_{37}	1324.1	1280.6	6.01	(0)	78.48	(84.13)			1341	m	skel def, CH s b
ν_{38}	1320.2	1277.8	87.62	(85.48)	10.37	(0)	1333	m			skel def, CH as b
ν_{39}	1291.9	1249.4	3.58	(1.30)	32.85	(0.26)	1301	vw			skel def, CH as b
ν_{40}	1291.3	1248.8	0.77	(0)	119.86	(125.70)			1302	m	skel def, CH s b
ν_{41}	1263.8	1225.6	1.51	(0)	13.98	(24.15)			1275	m	CH s b, C7N11, C28N32, C8C9, C29C30 str
ν_{42}	1263.4	1222.7	37.25	(32.35)	1.74	(0)	1268	m			CH as b, C7N11, C28N32, C8C9, C29C30 str

Table 1: Continued.

	Calculated[a]						Observed				
	frequency[e] (cm^{-1})	frequency[f] (cm^{-1})	IR intensity[g] (km/mol)		Raman activity[g] (A^4/amu)		IR[b]		Raman[c]		Assignment[d]
ν_{43}	1239.0	1199.9	1.23	(24.33)	2.28	(0.02)			1251	w	NH and CH s b
ν_{44}	1236.5	1199.8	24.70	(0.11)	0.43	(4.81)	1243	m			NH and CH as b
ν_{45}	1199.6	1160.3	1.67	(0.57)	0.25	(0)	1210	w			CH as b, CC str cr
ν_{46}	1199.5	1159.7	0.03	(0)	1.27	(1.08)			1210	w	CH s b, CC str cr
ν_{47}	1180.7	1140.7	0.58	(16.59)	2.52	(0)			1193	w	CH s b, CC str
ν_{48}	1180.6	1138.8	15.28	(0)	0.09	(2.07)	1193	m			CH s b, CC str
ν_{49}	1123.7	1089.2	8.81	(10.81)	0.66	(0.01)	1133	m			CH17,18,19,20 and CH38,39,40,41 as b
ν_{50}	1123.5	1089.1	1.71	(0.03)	2.24	(2.15)			1132	w	CH17,18,19,20 and CH38,39,40,41 s b
ν_{51}	1112.3	1074.6	0.50	(25.90)	1.01	(0)					CH15,17,18,20 and CH36,38,39,41 and NH s b
ν_{52}	1110.6	1074.1	22.51	(0)	0.23	(4.96)	1121	m			CH15,17,18,20 and CH36,38,39,41 and NH as b
ν_{53}	1075.6	1041.7	0.14	(0)	3.42	(8.06)			1090	w	skel def, CH s b
ν_{54}	1071.0	1035.3	51.41	(69.84)	0.35	(0)	1082	s			skel def, CH as b
ν_{55}	1056.8	1026.7	0.02	(0)	30.98	(69.48)			1075	s	CH15,16,36,37 s b
ν_{56}	1055.9	1024.6	4.03	(3.50)	2.00	(0)	1065	w			CH15,16,36,37 s b
ν_{57}	1047.8	1015.9	0.86	(0)	53.49	(21.34)			1062	m	skel def, CH as b
ν_{58}	1046.4	1012.3	5.31	(11.68)	2.32	(0)	1058	w			skel def, CH as b
ν_{59}	1008.9	978.5	5.64	(6.69)	3.18	(0)	1025	w			skel def
ν_{60}	1008.6	975.5	0.60	(0)	24.42	(17.84)			1019	w	skel def
ν_{61}	968.6	931.8	1.25	(1.27)	0.15	(0)	972	vw	973	vw	CH19-21 and CH40-42 s “oop” twisting
ν_{62}	968.6	931.7	0.32	(0)	0.04	(0.24)	965	vw	969	vw	CH19-21 and CH40-42 as “oop” twisting
ν_{63}	944.2	909.4	0.03	(0)	0.26	(0.60)			951	w	CH17,18,21 and CH38,39,42 as “oop” wag
ν_{64}	944.1	909.4	0.11	(0.38)	0.13	(0)					CH17,18,21 and CH38,39,42 as “oop” wag
ν_{65}	938.9	887.5	0.86	(1.71)	0.40	(0.11)	946	w			CH17-19,21 and CH38-40,42 as “oop” twisting
ν_{66}	938.8	887.3	0.76	(0.28)	0.41	(0.66)			942	w	CH17-19,21 and CH38-40,42 as “oop” twisting
ν_{67}	888.4	857.1	51.13	(44.91)	2.84	(0)	899	m			as skel def pyr (N11-C12-C13)
ν_{68}	885.0	851.4	16.47	(0)	26.78	(25.25)			890	m	s skel def pyr (N11-C12-C13)
ν_{69}	872.9	841.8	10.51	(17.27)	4.86	(0)	882	m			skel def, NH s twisting
ν_{70}	871.3	839.8	16.74	(0)	1.46	(20.52)					skel def, NH as twisting
ν_{71}	860.9	809.0	9.07	(0)	13.06	(0.03)			853	w	CH15,16,36,37 and s “oop” wag
ν_{72}	857.2	808.8	2.82	(21.39)	0.83	(0)	860	vw			CH15,16,36,37 and s “oop” wag
ν_{73}	829.1	793.1	1.31	(43.69)	0.63	(0)					s skel “oop” def, NH, CH wag
ν_{74}	823.8	789.6	5.18	(0)	0.65	(1.24)					as skel “oop” def, NH, CH wag
ν_{75}	814.6	774.0	103.69	(76.52)	2.72	(0)	823	m	826	w	s NH “oop”
ν_{76}	805.0	771.8	9.08	(0)	0.45	(0.73)					as cr “oop” def, CH as wag
ν_{77}	804.3	735.0	29.08	(0)	0.76	(0.29)	801	s			s cr “oop” def, CH s wag
ν_{78}	782.9	733.5	5.92	(33.11)	0.03	(0)					as NH “oop”
ν_{79}	764.2	728.2	5.35	(0)	0.23	(32.85)					CH17-21,38-42 s “oop” wag
ν_{80}	763.1	727.2	0.29	(2.50)	0.05	(0)					CH17-21,38-42 s “oop” wag
ν_{81}	751.2	716.8	1.01	(57.55)	36.36	(0)			763	m	s “ip” skel def
ν_{82}	750.8	699.1	1.33	(0)	3.39	(0.26)	773	m	770	sh	as “ip” skel def
ν_{83}	727.8	688.3	17.14	(1.95)	0.14	(0)	738	m	739	w	CH15-18 and CH36-39 “oop” s wag
ν_{84}	726.3	669.7	2.58	(65.15)	0.02	(0)					CH15-18 and CH36-39 “oop” as wag
ν_{85}	696.2	668.3	61.18	(0)	1.87	(0.88)					s “oop” skel def, CH s wag
ν_{86}	696.1	656.9	13.35	(0)	0.05	(0.71)					as “oop” skel def, CH s wag

Table 1: Continued.

	Calculated[a]						Observed				
	frequency[e] (cm^{-1})	frequency[f] (cm^{-1})	IR intensity[g] (km/mol)		Raman activity[g] (A^4/amu)		IR[b]		Raman[c]		Assignment[d]
ν_{87}	678.6	653.4	0.03	(0)	64.70	(70.42)	684	vw	686	s	s cr and pyridine ring b (sym along N1-C4, C7-C10 axis)
ν_{88}	675.2	651.1	15.94	(14.61)	1.87	(0)	696	m	696	sh	as cr and pyridine ring b (sym along N1-C4, C7-C10 axis)
ν_{89}	610.6	589.1	5.28	(4.30)	0.01	(0)					as cr and pyridine ring b (asym along N1-C4, C7-C10 axis)
ν_{90}	607.0	587.8	1.15	(0)	6.13	(8.11)	615	vw	614	w	s cr and pyridine ring b (asym along N1-C4, C7-C10 axis)
ν_{91}	605.3	575.9	0.89	(14.68)	0.58	(0)					as "oop" skel def pyr
ν_{92}	604.5	572.2	6.17	(0)	2.14	(0.68)			602	w	s "oop" skel def pyr
ν_{93}	573.7	552.4	0.75	(2.39)	0.53	(0)					as "oop" skel def pyridine and cr
ν_{94}	573.5	547.6	0.55	(0)	0.98	(2.04)			571	w	s "oop" skel def pyridine and cr
ν_{95}	516.2	502.9	5.97	(7.19)	1.51	(0)					as "ip" skel def pyridine and cr
ν_{96}	516.1	500.6	0.74	(0)	8.04	(10.89)			524	m	s "ip" skel def pyridine and cr
ν_{97}	513.7	490.9	0.53	(0)	1.51	(1.03)			513	w	s "oop" skel def pyridine and cr
ν_{98}	511.6	485.2	0.17	(0.81)	0.72	(0)					as "oop" skel def pyridine and cr
ν_{99}	472.8	455.0	8.28	(0)	1.82	(9.13)					as "ip" skel def cr
ν_{100}	471.5	453.5	0.17	(8.39)	8.11	(0)			479	m	s "ip" skel def cr
ν_{101}	430.1	414.5	0.54	(8.03)	11.61	(0)			438	m	s "ip" skel def cr, CH17,19,38,40 "oop"
ν_{102}	429.9	414.3	7.54	(0)	2.59	(15.89)			432	sh	as "ip" skel def cr, CH17,19,38,40 "oop"
ν_{103}	426.3	411.4	0.52	(0)	1.64	(2.25)					as "oop" skel def cr, CH17,19,38,40 "oop"
ν_{104}	425.1	410.3	0.58	(2.00)	4.49	(0)			424	w	s "oop" skel def cr, CH17,19,38,40 "oop"
ν_{105}	284.4	273.3	1.89	(1.93)	0.81	(0)					as "oop" pyridine and cr rock
ν_{106}	283.5	270.9	1.37	(0)	1.34	(2.06)			300	w	s "oop" pyridine and cr rock
ν_{107}	252.8	244.7	0.65	(6.73)	0.04	(0)					as "oop" pyr and cr rock
ν_{108}	249.5	238.0	6.20	(6.29)	0.17	(0)					s "oop" pyr and cr rock
ν_{109}	248.8	237.5	3.53	(0)	0.52	(6.82)			267	w	as pyr and pyridine rings "ip" bend
ν_{110}	243.3	231.8	0.07	(0)	5.18	(0.05)			251	m	s pyr and pyridine rings "ip" bend
ν_{111}	163.0	141.8	0.01	(0.04)	0.27	(0)			169	w	as pyr and pyridine tor
ν_{112}	150.4	139.1	0.03	(0)	0.43	(1.24)			154	m	s pyr and pyridine tor
ν_{113}	122.3	117.0	6.27	(0)	0.23	(2.44)					as "oop" pyridine and pyr rock
ν_{114}	121.9	112.3	3.70	(6.00)	0.91	(0)					s "oop" pyridine and pyr rock
ν_{115}	80.2	75.9	3.58	(1.02)	3.54	(0)					dim rock
ν_{116}	78.2	71.4	0.02	(0)	1.54	(1.80)					dim b
ν_{117}	67.0	59.6	0.00	(0)	1.15	(3.12)					dim b
ν_{118}	43.4	21.3	0.18	(0.12)	9.82	(0)					dim rock
ν_{119}	26.1	9.2	0.27	(0)	4.96	(15.09)					dim rock
ν_{120}	21.3	−35.3	0.04	(0)	11.69	(0)					dim tor

[a]B3LYP/cc-pVTZ, C_2 symmetry group, scaling factor = 0.9682, as recommended in the literature [39].
[b]Polycrystalline sample, 293 K.
[c]Polycrystalline sample, 293 K, 785 nm laser (633 nm was used in the NH region).
[d]Abbreviations. s: symmetric; as: antisymmetric; str: stretch; b: bend; ip: in-plane; oop: out-of-plane; skel def: skeletal deformation; tor: torsion; pyrid: pyridine; pyr: pyrrole; cr: central ring.
[e]Twisted dimer.
[f]Planar dimer.
[g]In parentheses: values computed for the planar dimer.
[h]Very broad (~200 cm^{-1}).

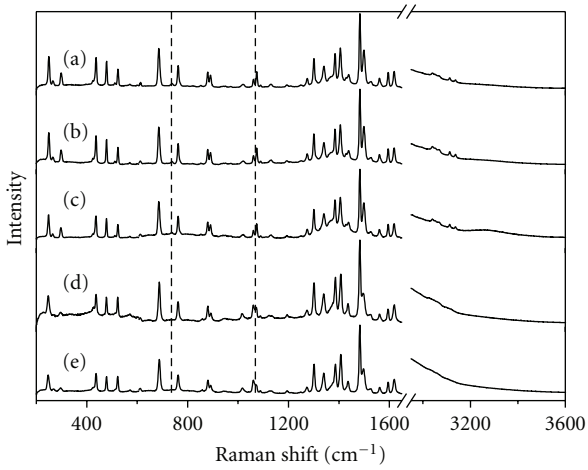

FIGURE 7: Raman spectra measured for samples crystallized from five different solvents: cyclohexane (a), methanol (b), toluene (c), dichloromethane (d), diethyl ether (e). Dashed vertical lines indicate regions with structure-sensitive transitions (see text).

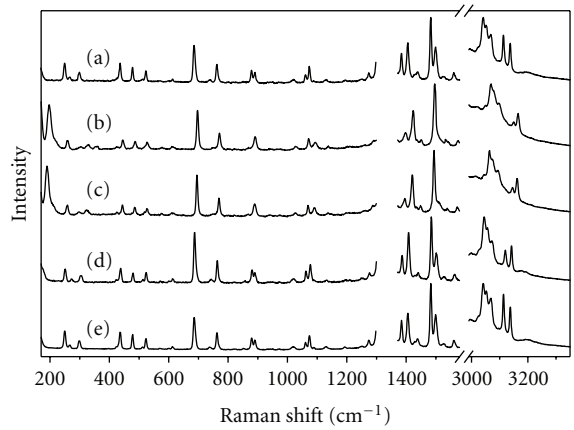

FIGURE 8: Raman spectra of crystalline PQ as a function of pressure: normal pressure, 1 atm (a); 2×10^3 atm (b); 22×10^3 atm (c); 35×10^3 atm (d); 1 atm (e), at the end of pressure cycle. The low and high frequency regions are normalized separately to their highest bands. A region between 1300–1370 cm^{-1}, exhibiting a strong Raman peak from diamond culets, was removed.

the red with increasing pressure. Such behavior is opposite to that of other modes and indicates the increase of the HB strength, most probably due to a shorter NH$\cdots$N distance. Unfortunately, the exact amount of the shift cannot be determined, as the band becomes buried under the transitions corresponding to CH stretches. Experiments are planned with either N- or C-deuterated PQ, to avoid interferences of NH/ND vibrations with other modes.

The second effect is the change in the relative intensity pattern with increasing pressure, observed for the peaks at 1062 and 1074 cm^{-1}. As discussed above, such behaviour can indicate a transition from a cyclic toward a twisted structure. For another mode diagnostic in this respect, 738 cm^{-1}, we observe decreasing intensity. However, it can still be detected at the highest pressures applied. It may be that what is

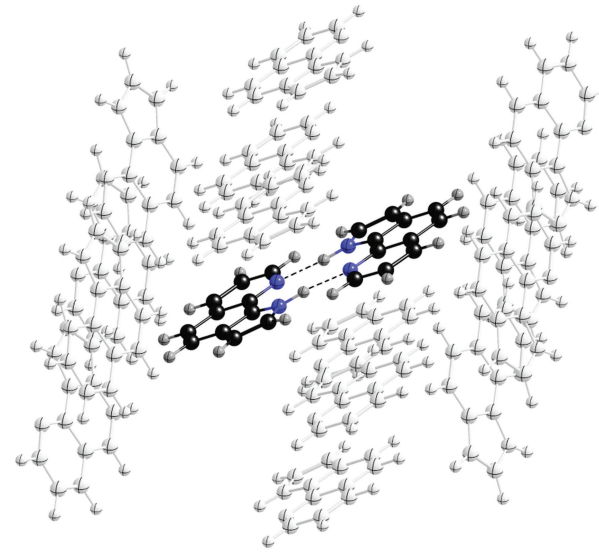

FIGURE 9: PQ dimer surrounded by identical neighbors (taken from X-ray data). The dimer in the middle was being distorted along the twisting coordinate, and then the whole structure was optimized.

observed is gradual twisting, not necessarily leading to the same angle between the monomeric units as observed for the nonplanar polymorph under normal pressure. More detailed investigations are planned once both planar and twisted dimeric samples are available. The experiments described in the previous section bode well for such studies.

3.7. Simulations of Polymorphic Structures. The existence of both planar and twisted dimers leads to the question of the energy barrier separating the two phases. Theoretical simulations have been carried out, in order to check the local minimum character of each structure and to estimate their relative stabilities. In this procedure, a dimer, surrounded by 14 identical neighbours (Figure 9), was distorted towards the structure of the other polymorph (twisted for the initially planar form, and vice versa). The whole ensemble was then optimized. Both planar and twisted structures relaxed back to the initial form, showing that they correspond to the minimum and providing additional independent confirmation of the existence of two crystal polymorphic forms of the PQ dimer. These results indicate that a collective rather than local distortion of the crystal is required for the phase change in PQ.

In agreement with the high pressure experiments, comparison of energies calculated for the slab consisting of 16 molecules for both planar and twisted dimers revealed a lower energy for the latter.

4. Summary and Conclusions

A combination of X-ray, IR and Raman spectroscopy, high pressure techniques, and quantum chemical calculations resulted in the detection of two polymorphic forms of dimeric PQ. Both types of dimer reveal a cyclic, doubly

hydrogen-bonded structure, but differ in the planar versus twisted arrangement of the monomeric units. The calculations predict a twisted dimer structure, whereas imposing planarity results in one negative vibrational frequency, corresponding to the twisting coordinate. These results show that the isolated dimer should be nonplanar and thus the polymorphism is due to the interplay of interactions between the two monomeric units forming the hydrogen bond and dimer-dimer interactions in the crystal. The experiments indicate that upon applying pressure the planar form can be converted into the twisted one.

The NH stretching and out-of-plane bending modes observed in the IR spectra were shown to be clear indicators of the HB formation. The analysis of the position of the latter could be used to determine the structure of the H-bonded dimer. With respect to the influence of HB formation on the Raman spectra, a large increase of the intensity was observed for the NH stretching band in the H-bonded dimers, indicating increase of polarizability. The Raman spectra were also diagnostic for structural assignments: even though the spectra are quite similar, the intensity ratio of two peaks observed at 1062 and 1074 cm^{-1} provides information whether the PQ dimer is planar or not.

Our future plans include testing a possibility of photoinduced double proton transfer in both forms of crystalline PQ. Both kinetics and thermodynamics of such a process should be strongly structure-sensitive. Moreover, we have selected PQ as one of the objects in the investigations of the influence of plasmonic structures on the spectral and photophysical characteristics of chromophores located in the vicinity of metallic environments. The results of vibrational and structural analysis presented in this work will provide a starting point for experiments in which monomers and dimers of PQ will be placed on, or close to metal surfaces.

Acknowledgments

The work was supported by the Grant 3550/B/H03/2011/40 from the Polish National Science Centre. The authors acknowledge the computing grant G17-14 from the Interdisciplinary Centre for Mathematical and Computational Modeling of the Warsaw University. They would like to thank bwGRiD (http://www.bw-grid.de), member of the German D-Grid initiative, funded by the Ministry for Education and Research (Bundesministerium für Bildung und Forschung) and the Ministry for Science, Research and Arts Baden-Württemberg (Ministerium für Wissenschaft, Forschung und Kunst Baden-Württemberg), for providing the opportunity to use parallel computing facilities and perform quantum chemical calculations. R. P. Thummel thanks the Robert A. Welch Foundation (E-621) and the National Science Foundation (CHE-0714751).

References

[1] J. Waluk, "Hydrogen-bonding-induced phenomena in bifunctional heteroazaaromatics," *Accounts of Chemical Research*, vol. 36, no. 11, pp. 832–838, 2003.

[2] J. A. Walmsley, "Self-association of 7-azaindole in nonpolar solvents," *The Journal of Physical Chemistry*, vol. 85, no. 21, pp. 3181–3187, 1981.

[3] P. Dufour, Y. Dartiguenave, M. Dartiguenave et al., "Crystal structures of 7-azaindole, an unusual hydrogen-bonded tetramer, and of two of its methylmercury(II)complexes," *Canadian Journal of Chemistry*, vol. 68, no. 1, pp. 193–201, 1990.

[4] H. Yokoyama, H. Watanabe, T. Omi, S. I. Ishiuchi, and M. Fujii, "Structure of hydrogen-bonded clusters of 7-azaindole studied by IR dip spectroscopy and ab initio molecular orbital calculation," *Journal of Physical Chemistry A*, vol. 105, no. 41, pp. 9366–9374, 2001.

[5] K. Sakota, Y. Kageura, and H. Sekiya, "Cooperativity of hydrogen-bonded networks in 7-azaindole$(CH_3OH)_n$ ($n = 2, 3$)clusters evidenced by IR-UV ion-dip spectroscopy and natural bond orbital analysis," *Journal of Chemical Physics*, vol. 129, no. 5, Article ID 054303, 2008.

[6] K. Sakota, Y. Komure, W. Ishikawa, and H. Sekiya, "Spectroscopic study on the structural isomers of 7-azaindole(ethanol)$_n$ ($n = 1 - 3$) and multiple-proton transfer reactions in the gas phase," *Journal of Chemical Physics*, vol. 130, no. 22, Article ID 224307, 2009.

[7] T. B. C. Vu, I. Kalkman, W. L. Meerts, Y. N. Svartsov, C. Jacoby, and M. Schmitt, "Rotationally resolved electronic spectroscopy of water clusters of 7-azaindole," *Journal of Chemical Physics*, vol. 128, no. 21, Article ID 214311, 2008.

[8] G. A. Pino, I. Alata, C. Dedonder, C. Jouvet, K. Sakota, and H. Sekiya, "Photon induced isomerization in the first excited state of the 7-azaindole-$(H_2O)_3$ cluster," *Physical Chemistry Chemical Physics*, vol. 13, no. 13, pp. 6325–6331, 2011.

[9] K. Sakota, C. Jouvet, C. Dedonder, M. Fujii, and H. Sekiya, "Excited-state triple-proton transfer in 7-azaindole$(H_2O)_2$ and reaction path studied by electronic spectroscopy in the gas phase and quantum chemical calculations," *Journal of Physical Chemistry A*, vol. 114, no. 42, pp. 11161–11166, 2010.

[10] K. Suwińska, "Crystal structure communications," *Acta Crystallographica C*, vol. 41, pp. 973–975, 1985.

[11] J. Waluk and B. Pakuła, "Viscosity and temperature effects in excited state double proton transfer: iuminescence of 1-azacarbazole dimers in solid state and solution," *Journal of Molecular Structure*, vol. 114, pp. 359–362, 1984.

[12] J. Waluk, A. Grabowska, B. Pakuła, and J. Sepioł, "Viscosity vs. temperature effects in excited-state double proton transfer. Comparison of 1-azacarbazole with 7-azaindole," *The Journal of Physical Chemistry*, vol. 88, no. 6, pp. 1160–1162, 1984.

[13] J. Waluk, J. Herbich, D. Oelkrug, and S. Uhl, "Excited-state double proton transfer in the solid state: the dimers of 1-azacarbazole," *Journal of Physical Chemistry*, vol. 90, no. 17, pp. 3866–3868, 1986.

[14] J. Catalán, "Photophysics of 1-azacarbazole dimers: a reappraisal," *The Journal of Physical Chemistry A*, vol. 111, no. 36, pp. 8774–8779, 2007.

[15] D. Marks, H. Zhang, P. Borowicz, J. Waluk, and M. Glasbeek, "(Sub)picosecond fluorescence upconversion studies of intermolecular proton transfer of dipyrido[2,3-a:3′,2′-i]carbazole and related compounds," *Journal of Physical Chemistry A*, vol. 104, no. 31, pp. 7167–7175, 2000.

[16] A. Kyrychenko, J. Herbich, M. Izydorzak, F. Wu, R. P. Thummel, and J. Waluk, "Role of ground state structure in photoinduced tautomerization in bifunctional proton donor-acceptor molecules: 1H-pyrrolo[3,2-*h*]quinoline and related

compounds," *Journal of the American Chemical Society*, vol. 121, no. 48, pp. 11179–11188, 1999.

[17] A. Kyrychenko and J. Waluk, "Excited-state proton transfer through water bridges and structure of hydrogen-bonded complexes in 1H-pyrrolo[3,2-*h*]quinoline: adiabatic time-dependent density functional theory study," *The Journal of Physical Chemistry A*, vol. 110, no. 43, pp. 11958–11967, 2006.

[18] Y. Nosenko, M. Kunitski, R. P. Thummel et al., "Detection and structural characterization of clusters with ultrashort-lived electronically excited states: IR absorption detected by femtosecond multiphoton ionization," *Journal of the American Chemical Society*, vol. 128, no. 31, pp. 10000–10001, 2006.

[19] Y. Nosenko, A. Kyrychenko, R. P. Thummel, J. Waluk, B. Brutschy, and J. Herbich, "Fluorescence quenching in cyclic hydrogen-bonded complexes of 1H-pyrrolo[3,2-*h*]quinoline with methanol: cluster size effect," *Physical Chemistry Chemical Physics*, vol. 9, no. 25, pp. 3276–3285, 2007.

[20] Y. Nosenko, M. Kunitski, C. Riehn et al., "Separation of different hydrogen-bonded clusters by femtosecond UV-ionization-detected infrared spectroscopy: 1H-pyrrolo[3,2-*h*] quinoline$\cdot(H_2O)_{n=1,2}$ complexes," *Journal of Physical Chemistry A*, vol. 112, no. 6, pp. 1150–1156, 2008.

[21] J. Herbich, J. Sepioł, and J. Waluk, "Determination of the energy barrier origin of the excited state double proton transfer in 7-azaindole: alcohol complexes," *Journal of Molecular Structure*, vol. 114, pp. 329–332, 1984.

[22] D. McMorrow and T. J. Aartsma, "Solvent-mediated proton transfer. The roles of solvent structure and dynamics on the excited-state tautomerization of 7-azaindole/alcohol complexes," *Chemical Physics Letters*, vol. 125, no. 5-6, pp. 581–585, 1986.

[23] J. Konijnenberg, A. H. Huizer, and C. A. G. O. Varma, "Solute-solvent interaction in the photoinduced tautomerization of 7-azaindole in various alcohols and in mixtures of cyclohexane and ethanol," *Journal of the Chemical Society, Faraday Transactions 2*, vol. 84, no. 8, pp. 1163–1175, 1988.

[24] R. S. Moog, S. C. Bovino, and J. D. Simon, "Solvent relaxation and excited-state proton transfer: 7-azaindole in ethanol," *Journal of Physical Chemistry*, vol. 92, no. 23, pp. 6545–6547, 1988.

[25] R. S. Moog and M. Maroncelli, "7-Azaindole in alcohols: solvation dynamics and proton transfer," *Journal of Physical Chemistry*, vol. 95, no. 25, pp. 10359–10369, 1991.

[26] A. V. Smirnov, D. S. English, R. L. Rich et al., "Photophysics and biological applications of 7-azaindole and its analogs," *Journal of Physical Chemistry B*, vol. 101, no. 15, pp. 2758–2769, 1997.

[27] S. Mente and M. Maroncelli, "Solvation and the excited-state tautomerization of 7-azaindole and 1-azacarbazole: computer simulations in water and alcohol solvents," *Journal of Physical Chemistry A*, vol. 102, no. 22, pp. 3860–3876, 1998.

[28] K. C. Ingham, M. Abu-Elgheit, and M. Ashraf El-Bayoumi, "Confirmation of biprotonic phototautomerism in 7-azaindole hydrogen-bonded dimers," *Journal of the American Chemical Society*, vol. 93, no. 20, pp. 5023–5025, 1971.

[29] S. N. Krasnokutskii, L. N. Kurkovskaya, T. A. Shibanova, and V. P. Shabunova, "Structure of 1H-pyrrolo[3,2-*h*]quinoline," *Zhurnal Strukturnoi Khimii*, vol. 32, p. 131, 1991.

[30] J. Herbich, M. Kijak, R. Luboradzki et al., "In search for phototautomerization in solid dipyrido[2,3-a:3′,2′-i]carbazole ," *Journal of Photochemistry and Photobiology A*, vol. 154, no. 1, pp. 61–68, 2002.

[31] F. Wu, C. M. Chamchoumis, and R. P. Thummel, "Bidentate ligands that contain pyrrole in place of pyridine," *Inorganic Chemistry*, vol. 39, no. 3, pp. 584–590, 2000.

[32] K. Takemura, S. Minomura, O. Shimomura, and Y. Fujii, "Observation of molecular dissociation of iodine at high pressure by X-ray diffraction," *Physical Review Letters*, vol. 45, no. 23, pp. 1881–1884, 1980.

[33] H. K. Mao, P. M. Bell, J. W. Shaner, and D. J. Steiberg, "Specific volume measurements of Cu, Mo, Pd, and Ag and calibration of the ruby R_1 fluorescence pressure gauge from 0.06 to 1 Mbar," *Journal of Applied Physics*, vol. 49, no. 6, pp. 3276–3283, 1978.

[34] G. M. Sheldrick, "Foundations of crystallography," *Acta Crystallographica A*, vol. 64, pp. 112–122, 2008.

[35] M. D. Segall, P. J. D. Lindan, M. J. Probert et al., "First-principles simulation: ideas, illustrations and the CASTEP code," *Journal of Physics Condensed Matter*, vol. 14, no. 11, pp. 2717–2744, 2002.

[36] J. P. Perdew, J. A. Chevary, S. H. Vosko et al., "Atoms, molecules, solids, and surfaces: applications of the generalized gradient approximation for exchange and correlation," *Physical Review B*, vol. 46, no. 11, pp. 6671–6687, 1992.

[37] D. Vanderbilt, "Soft self-consistent pseudopotentials in a generalized eigenvalue formalism," *Physical Review B*, vol. 41, no. 11, pp. 7892–7895, 1990.

[38] H. J. Monkhorst and J. D. Pack, "Special points for Brillouin-zone integrations," *Physical Review B*, vol. 13, no. 12, pp. 5188–5192, 1976.

[39] J. P. Merrick, D. Moran, and L. Radom, "An evaluation of harmonic vibrational frequency scale factors," *Journal of Physical Chemistry A*, vol. 111, no. 45, pp. 11683–11700, 2007.

Hindawi Publishing Corporation
Journal of Atomic, Molecular, and Optical Physics
Volume 2012, Article ID 217932, 10 pages
doi:10.1155/2012/217932

Review Article

Proton Transfer Equilibria and Critical Behavior of H-Bonding

L. Sobczyk, B. Czarnik-Matusewicz, M. Rospenk, and M. Obrzud

Faculty of Chemistry, University of Wrocław, Joliot-Curie 14, 50-383 Wrocław, Poland

Correspondence should be addressed to L. Sobczyk, lucjan.sobczyk@chem.uni.wroc.pl

Received 23 February 2012; Revised 25 April 2012; Accepted 26 April 2012

Academic Editor: Marek J. Wojcik

Copyright © 2012 L. Sobczyk et al. This is an open access article distributed under the Creative Commons Attribution License, which permits unrestricted use, distribution, and reproduction in any medium, provided the original work is properly cited.

The aim of the present paper is an analysis of the hydrogen bond properties for the acid-base systems depending on the ability to the proton transfer in the formulation of the Brönsted approach. After definition of the proton transfer equilibrium expressed by using the equation $\log K_{\mathrm{PT}} = \xi \Delta pK_N$, various examples of different physical properties, such as dipole moments, IR spectra, and nuclear magnetic resonances, are presented which correlate with the ΔpK_N value. In such a way, a critical state of hydrogen bonding can be defined that corresponds to the potential of the proton motion for either single minimum or double minimum with low barrier. A particular attention in this paper found electronic spectra which have not been analysed so far and the quantitative analysis of the vibrational polarizability which can reach very high values of the order of electronic polarizability.

1. Introduction

The subject of our interest in the present review is hydrogen bonds which can be expressed as A–H$\cdots$B. It is an acid-base system in the Brönsted formulation when the A–H group is treated as an acid while the B atom or group of atoms as proton acceptor (base). The potential energy curves for the proton motion can reach various shapes, as shown in Figure 1.

The extreme curves (1) and (6) correspond to states either without proton transfer (1) or to the complete ionization when the proton is attached to B while atom A is negatively charged (6). Among the intermediate states take place those when the proton is located in the central position either with two minima (3) and a low barrier or with one single minimum (4).

There is a rich literature [1–16] with various approaches to the hydrogen bonding corresponding to different definitions, showing an increase of systems analyzed with comprehensive theoretical treatments, and containing different rich chemical characteristic features of hydrogen bonds. Most actual comprehensive review was recently published by G. Gilli and P. Gilli [16].

From the point of view of the approach based on the acid-base interaction, the substantial, parameter is the proton transfer degree which evokes changes of further physico-chemical parameters. The main quantity is the ΔpK_a value which can be expressed in the form:

$$\Delta pK_a = pK_{\mathrm{B^+H}} - pK_{\mathrm{AH}}. \tag{1}$$

This quantity was introduced by Huyskens and Zeegers-Huyskens [17]. We introduced normalized parameter defined as

$$\Delta pK_N = \Delta pK_a - \Delta pK_a\,(\mathrm{crit}), \tag{2}$$

where ΔpK_a(crit) is related to ΔpK_a region when the proton transfer degree reaches 50% [18].

The dependence of proton transfer degree on the ΔpK_N value needs a correction connected with "softness/hardness" of interaction by using parameter $\xi < 1$ [19]. The value of this parameter is the higher, the harder is the interaction reaching maximal value equal to unity. As will be seen, this quantity is well correlated with the polarizability in the transition state of hydrogen bonds. The general equation presenting the dependence of proton transfer degree on ΔpK_N possesses the form:

$$\log K_{\mathrm{PT}} = \xi \Delta pK_N. \tag{3}$$

One should remember that physicochemical parameters measured depending on ΔpK_N and connected with the

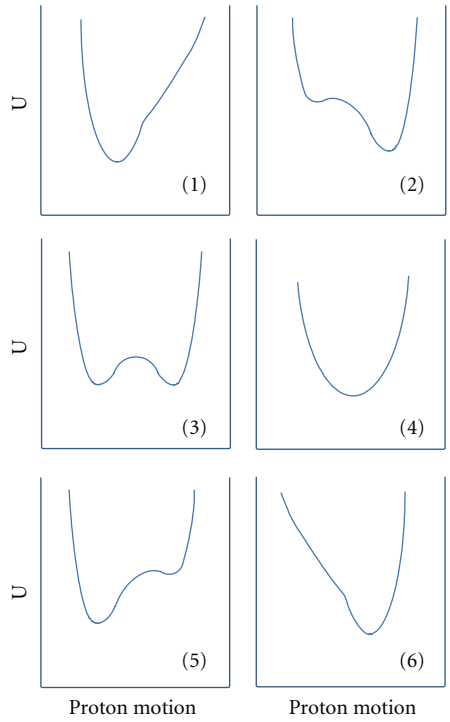

Figure 1: Postulated potential energy curves for the proton motion starting from nonproton-transfer state (1) up to fully ionized state (6).

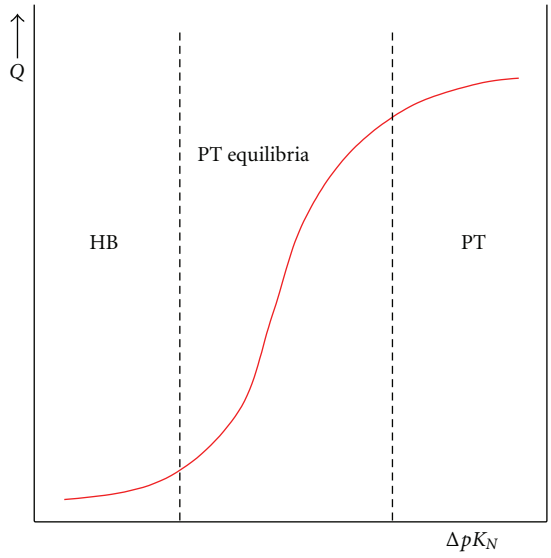

Figure 2: Three regions of physical properties depending on ΔpK_N: HB-related to nonproton-transfer states, PT-related to proton transfer state and HB + PT proton transfer equilibrium.

softness of interaction are related not only to ΔpK_N as has been shown in Figure 2.

There exist three regions; the central one with the equilibria of the proton transfer and side regions without proton transfer (HB) and with full ionization (PT).

Finally, as will be shown, it is necessary to mention the role of medium such as electric permittivity of the solvent

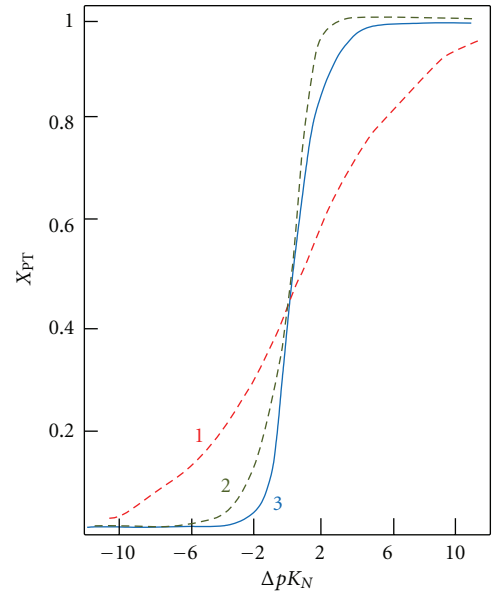

Figure 3: Proton transfer degree from NQR measurements for complexes composed of chlorine containing proton donors plotted versus ΔpK_N: (1) CCl_3COOH complexes ($\xi = 0.12$), (2) $CHCl_2COOH$ complexes ($\xi = 0.42$), and (3) C_6Cl_5OH complexes ($\xi = 0.74$) [20].

and specific interaction between the solute and solvent molecules.

For characterization of the role of the ξ parameter we present in Figure 3 dependencies of the proton transfer degree deduced from the measurements of nuclear quadruple resonance (NQR) for complexes of CCl_3COOH (1) ($\xi = 0.12$), $CHCl_2COOH$ (2) ($\xi = 0.42$), and C_6Cl_5OH (3) ($\xi = 0.74$) [20]. It is well seen the property of the curves in the critical region when approaching to $\Delta pK_N = 0$.

It is justified to mention in the introduction that curves expressing dependencies of physicochemical parameters on ΔpK_N possess various shapes [18]. One can distinguish two types of correlations between the physical quantity and ΔpK_N, namely, of the sigma and delta type. The examples of such correlations will be presented in the next chapter.

2. Examples of Correlation between Physicochemical Parameters and the ΔpK_N Quantity

So far a most precisely investigated phenomenon is the dependence of the increase of dipole moment $\Delta\mu$ for complexes of phenols with N-bases. In Figure 4, we present correlation between $\Delta\mu$ and ΔpK_N obtained for a number of systems in nonpolar solvents, particularly in benzene [18]. The experimental points are adjusted to the equation [21]:

$$\Delta\mu = \frac{\Delta\mu_{HB} + b_{HB}\Delta pK_N}{1 + \exp\left(2.303\xi\Delta pK_N\right)} + \frac{\left(\Delta\mu_{PT} + b_{PT}\Delta pK_N\right)\cdot \exp\left(2.303\xi\Delta pK_N\right)}{1 + \exp\left(2.303\xi\Delta pK_N\right)}, \quad (4)$$

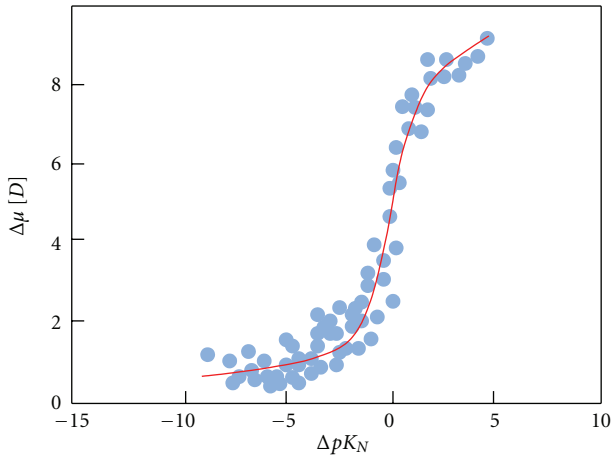

Figure 4: The increase of dipole moment $\Delta\mu$ plotted versus normalized parameter ΔpK_N [18].

where $\Delta\mu_{HB}$ and $\Delta\mu_{PT}$ mean the increase of the dipole moment without proton transfer (HB) and after the proton transfer (PT). These quantities depend nearly linearly on ΔpK_N with coefficients b_{HB} and b_{PT}. When approaching the critical region around $\Delta pK_N = 0$, a stepwise change of the dipole moment connected with the increase of the proton degree takes place. The proton transfer degree x_{PT} defines the equilibrium:

$$X_{PT} = \frac{\exp(2.303\xi\Delta pK_N)}{1+\exp(2.303\xi\Delta pK_N)}. \quad (5)$$

To obtain the agreement with the experiment, it is necessary to introduce the coefficient ξ which, as has been formulated, characterizes softness/hardness of interactions. It can be, on the other hand, connected with the barrier height for the proton transfer. The value of the ξ coefficient for the case of the situation in Figure 4 equals 0.65.

Very similar run of the dependence on ΔpK_N shows the value of the ^{15}N resonance chemical shift with the ξ value equal to 0.56 [22]. However, one should remember that the results are related to markedly different experimental conditions. Thus, the results obtained for ^{15}N chemical shift were obtained for complexes of carboxylic acids with pyridine in liquefied freons.

Sigmoidal type of the relationship of physical quantity on ΔpK_N is also observed for complexes of pentachlorophenol with amines by using the nuclear quadrupole resonance (NQR) [23] that is presented in Figure 5. In addition to experimental points, there are indicated values corresponding to neat pentachlorophenol, H-bis-phenolate, as well as to Na^+ and tributylamine salts. One should remember that NQR measurements are performed for solid state that reflects observed behavior.

The similar shape of the plot with that in Figure 5 is observed between geometrical parameters of complexes and ΔpK_N and particularly between C–O bond length and ΔpK_N [25].

An example of correlation between the measured quantity and ΔpK_N of the delta type relates first of all to the proton magnetic resonance δ^1H. It is presented for the

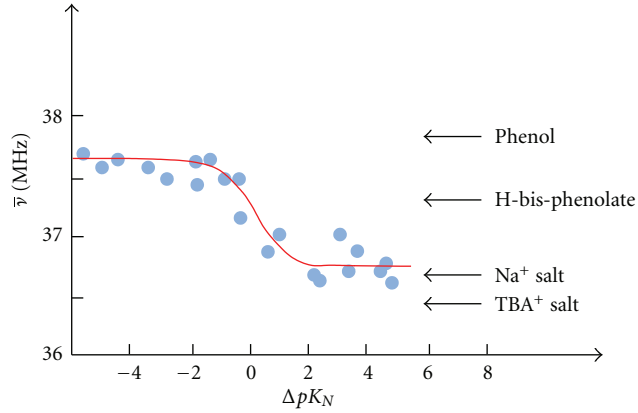

Figure 5: The dependence of average NQR ^{35}Cl frequency upon ΔpK_N for complexes of pentachlorophenol [24].

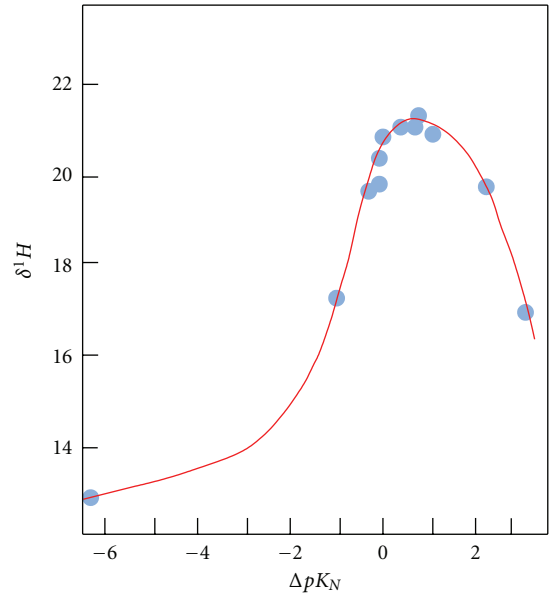

Figure 6: The dependence of δ^1H for complexes of carboxylic acids with pyridine in liquid freon [22].

systems analogues to the δ^{15}N resonance [18]. The experimental points of δ^1H presented in Figure 6 were obtained in the same conditions as for δ^{15}N. The value of the ξ parameter is, however, somewhat lower (0.46) that we are not able to explain. From already done numerous experiments it follows that methods applied do not possess marked influence on the ξ value.

In the analysis of the correlation plots exhibiting an extremum in the critical region as in the case of δ^1H, a modified approach can be used. Thus, for the description of the dependence of given physical property Q showing an extremum, the following simple procedure can be employed. The reference value of a given physical property Q is its extremum; that is, maximum or minimum. In the case of δ^1H for the systems composed of carboxylic acids and pyridine in liquid freons the maximum value equals 21.5 ppm. The delta type correlation can be transformed to the sigmoidal one by assuming that $Q(\text{crit}) = 0$, while $\Delta Q_{HB} < 0$ and $\Delta Q_{PT} > 0$ as has been done in Figure 7.

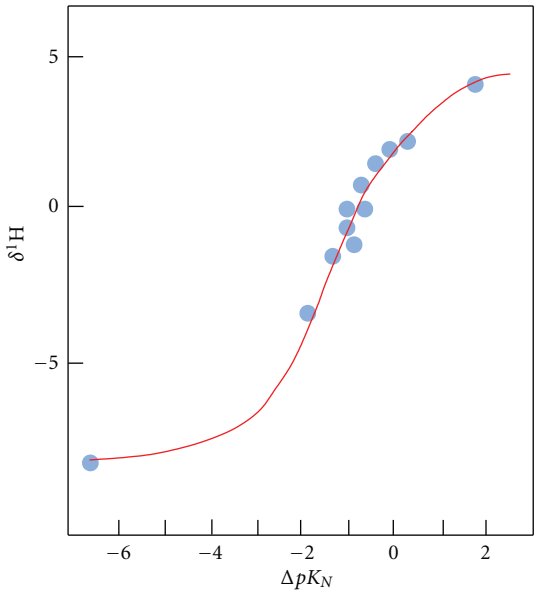

FIGURE 7: Correlation between δ^1H and ΔpK_N for complexes of carboxylic acids with pyridine in liquid freon according (6).

The correlation between ΔQ and ΔpK_N is presented in the following equation [18]:

$$\Delta Q = \frac{\Delta Q_{\mathrm{HB}} + \Delta Q_{\mathrm{PT}} \exp(2.303\xi\Delta pK_N)}{1 + \exp(2.303\xi\Delta pK_N)}. \quad (6)$$

The parameters for best fitting are $Q_{\max} = 21.5$ ppm $\Delta Q_{\mathrm{HB}} = -8.3$ ppm while $\Delta Q_{\mathrm{PT}} = 4.4$ ppm and $\xi = 0.46$ as has been already mentioned.

The properties of infra-red spectra are commonly accepted for the hydrogen bonded systems. This relates first of all to the absorption band ascribed to the stretching vibrations of either AH group (HB state) or BH^+ group (PT state). The evolution of broad absorption ascribed to the ν(AH) or $\nu(NH^+)$ vibrations is illustrated in Figure 8 taking as an example complexes of pentachlorophenol with amines [26]. In the infra-red spectra the correlated quantity is the center of gravity of protonic vibrations (ν_{cg}) versus the ΔpK_N value. Figure 9 represents numerous data related to ν_{cg} collected for various O–H$\cdots$N hydrogen bridges [27]. The scattering of experimental points is very large that seems to be understandable taking into account various experimental conditions and differences in the acid-base interaction for various components. One of the reasons of scattering is a difficulty connected with precise assessment of the position of broad bands. As follows from the results collected by Albrecht and Zundel [28] for the complexes of phenols with octylamine, the maximal absorbance in the range of continuous absorption corresponds to 50% of proton transfer that is shown in Figure 10.

3. Electronic Spectra and the Proton Transfer Degree

The UV-Vis spectroscopy is a very useful method of studies on the proton transfer degree in the Brönsted acid-base

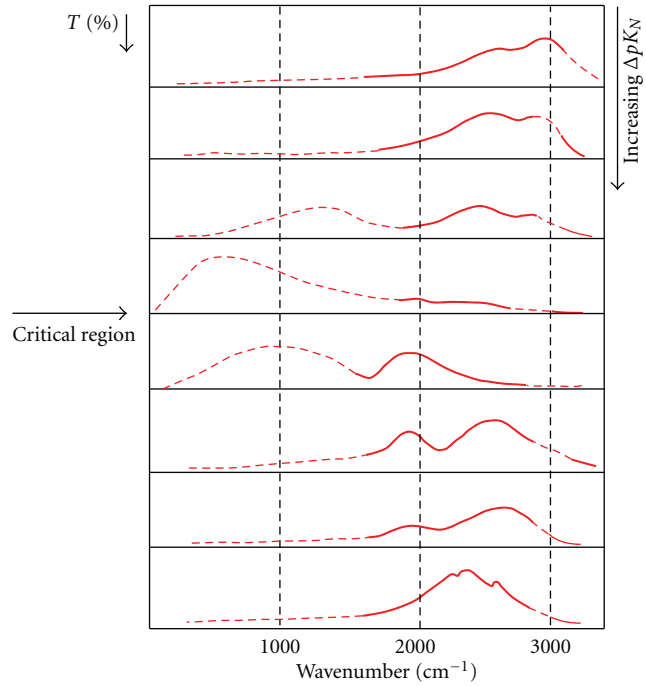

FIGURE 8: The evolution of infra-red absorption ascribed to ν(OH) when increasing ΔpK_N for complexes of pentachlorophenol with amines [26].

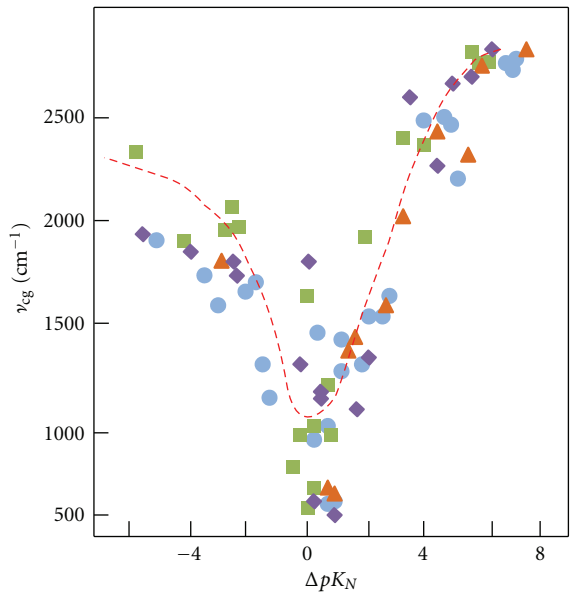

FIGURE 9: The center of gravity ν_{cg} for protonic vibrations as a function of ΔpK_N for various complexes of carboxylic acids [27].

system for the diluted solutions. The majority of quantitative data related to the proton transfer equilibria relates mainly to the complexes between phenols and amines [24, 29–35]. In the UV spectra, the tautomeric equilibrium is characterized by appearance of a new band corresponding to the $\pi \rightarrow \pi^*$ transition in the phenolate ion. After careful quantitative separation of the HB and PT bands the proton transfer equilibrium $c_{\mathrm{PT}}/c_{\mathrm{HB}}$ can be evaluated. As an example of the UV spectra with the proton transfer equilibrium, we use

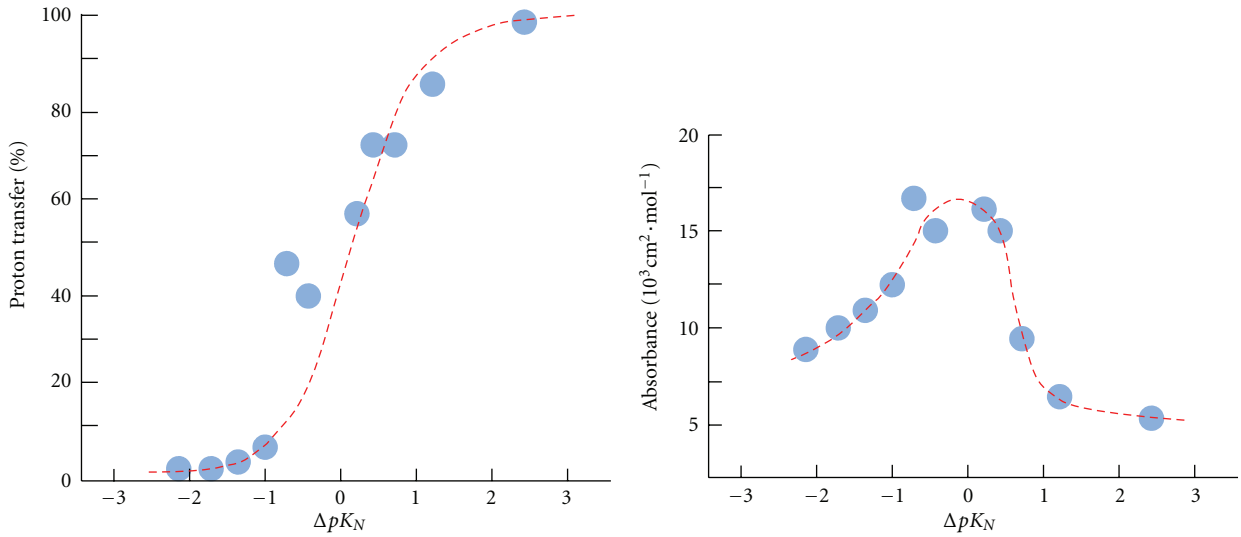

Figure 10: The proton transfer degree (a) and intensity of continuous absorption (b) for complexes of phenols with octylamine [28].

the system of 2,4,6-trichlorophenol in tributylamine (TBA) [29] presented in Figure 11 which shows the overlapping of HP and PT bands. From the equilibrium constant, other thermodynamic parameters can be determined according to equation:

$$\ln K = \frac{\Delta S^\circ}{R} - \frac{\Delta H^\circ}{RT}, \tag{7}$$

where K is calculated by using intensities of bands and molar absorption coefficients of corresponding forms:

$$K = \left(\frac{I_{PT}}{I_{HB}}\right)\left(\frac{\varepsilon_{HB}}{\varepsilon_{PT}}\right). \tag{8}$$

The first quantitative studies by using the electronic absorption spectra were performed by Baba et al. [30] for complex of 4-nitrophenol with triethylamine in 1,2-dichloroethane who found $\Delta H^\circ = -13\,\mathrm{kJ\cdot mol^{-1}}$ and $\Delta S^\circ = -49.8\,\mathrm{J\cdot mol^{-1}\cdot K^{-1}}$. Similarly, Crooks and Robinson [31] investigated complexes of bromophenol with methyl derivatives of pyridine in chlorobenzene. The obtained data correspond to $-\Delta H^\circ$ in the range 12–38 $\mathrm{kJ\cdot mol^{-1}}$ and $-\Delta S^\circ$ in the range 29–55 $\mathrm{J\cdot mol^{-1}\cdot K^{-1}}$. The values of thermodynamic parameters for the complexes of chlorophenols with TBA [29] are comparable with those of nitrophenol.

From the studies [29, 37–44] it follows that the concentration of the PT form, independently of the H-bonding type, increases with an increase of ΔpK_a value of interacting components, as well as with increase of the solvent activity and the drop of temperature.

For the systems with negative or close to zero ΔpK_a values, it was not possible to find traces of the PT band even in the most active solvents at temperatures as low as below −190°C [38]. Thus, for observation in UV spectrum participation of the PT form even in favorable conditions (low temperature and high polarity of solvent), some boundary ΔpK_a value is necessary.

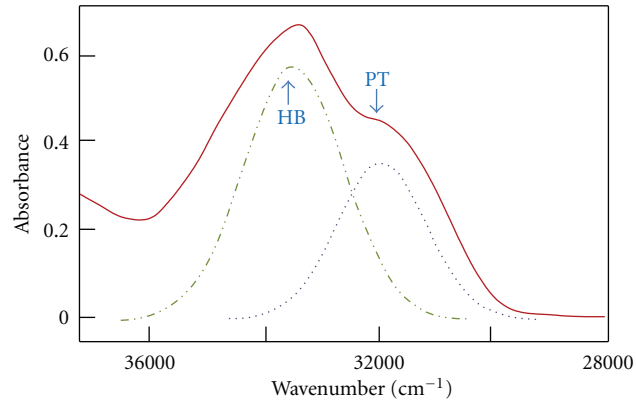

Figure 11: The plot of the absorbance versus wavenumber for 2,4,6-trichlorophenol in tributylamine at room temperature, $c = 5 \cdot 10^{-4}\,\mathrm{mol\cdot dm^{-3}}$; $d = 5\,\mathrm{mm}$.

Figure 12 shows the UV spectra for the series of complexes formed by TBA with various chlorophenols of increasing acidity. It can be seen that 2,4-dichlorophenol and 2,4,5-trichlorophenol do not show any contributions of PT species, only 2,6-dichlorophenol shows traces of the ionic PT form. For 2,4,6-trichlorophenol, a considerable amount (ca. 25%) of the PT form was estimated from the UV spectrum. Pentachlorophenol appears entirely in the zwitterionic state, whereas in a case of 2,6-dichloro- and 2,4,5-trichloro derivatives, characterized by almost the same ΔpK_a values, some contribution of the PT state shows only the former one. The ΔpK_a value is not, however, a completely satisfactory measure of the proton donor-acceptor properties in nonaqueous media.

In several papers, for example, [45–48] one considers the attention that one should apply another scale of proton donor and acceptor properties for defining the proton

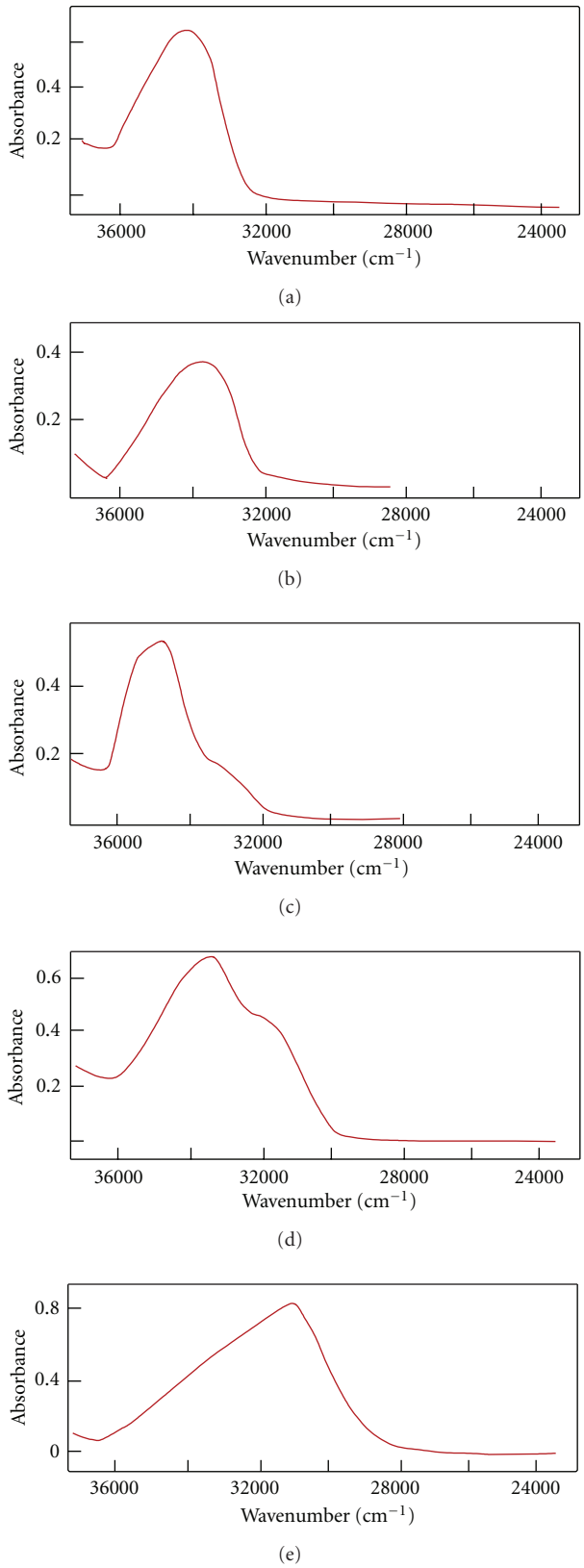

Figure 12: UV spectra of chlorophenols: (a) 2,4-dichlorophenol, (b) 2,4,5-trichlorophenol, (c) 2,6-dichlorophenol, (d) 2,4,6-trichlorophenol, (e) pentachlorophenol in TBA at room temperature, $c = 5 \cdot 10^{-4}$ mol·dm^{-3}; $d = 5$ mm [29].

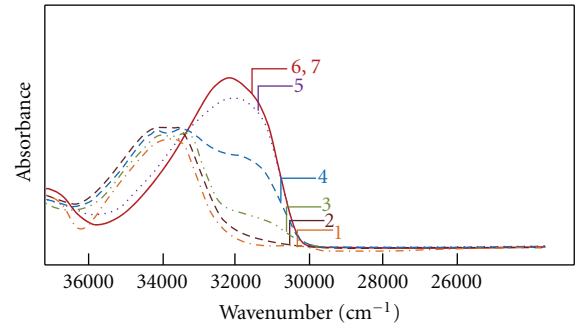

Figure 13: UV spectra of 2,4-dichlorophenol in TBA as a function of temperature: 298 K (1), 223 K (2), 203 K (3), 186 K (4), 165K (5), 143 K (6), 128 K (7). $C = 4 \times 10^{-4}$ mol dm^{-3}, $d = 5$ mm, wavenumber of PT form ≅ 32160 cm^{-1} and HB form ≅ 33840 cm^{-1} [29].

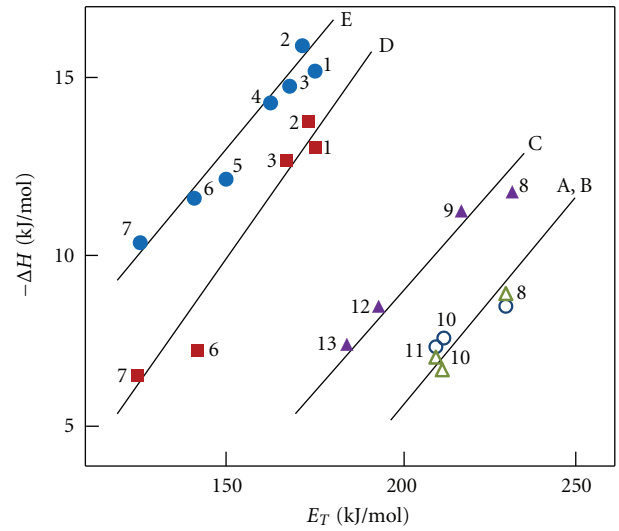

Figure 14: Comparison of the ΔH°_{PT} with E_T parameters for Mannich bases: (A) 2-(N,N-dimethylaminomethyl)-4,6-dibro- mophenol, (B) 2-(N,N-diethylaminomethyl)-4-nitro-phenol, (C) 2-(N,N-diethylaminomethyl)-3,4,6-trichlorophenol, (D) 2-(N,N-diethylaminomethyl)-3,4,5,6-tetrachlorophenol, (E) 2-(N,N-diethylaminomethyl)-4-nitronaphthol-1, in 1,2-dichloroethane (1), dichloromethane (2), n-butylchloride (3), chloroform (4), 1,4-dioxane (5), isopropylbenzene (6) squalane (7), methanol (8), ethanol (9), butan-1-ol (10), propan-1-ol (11), acetonitrile (12), and N,N-dimethylformamide (13) [36].

position in hydrogen-bonded complexes. In the analysis, one takes into account the proton affinity and deprotonation enthalpy based on calculations by using DFT methods. However, in the present article, we limited our considerations to experimental methods leading to evaluation of the pK_a values.

A strong influence of cooling on the increase of concentration of the PT form indicates on negative change of enthalpy effect on the proton transfer process. In Figure 13, the UV spectra of 2,4-dichlorophenol in TBA are shown as a function of temperature [29]. The 2,4-dichlorophenol—TBA system at room temperature does not show any

contribution of the PT state. Similar to other systems of this type, we observe a very strong influence of cooling on the contribution of the PT state. At the temperatures 203, 186, and 165 K, the values of K_{PT} are 0.33, 0.82, and 5.70, respectively. The complete proton-transfer state is reached at about 143 K and further cooling does not affect the intensity of the phenolate band.

By using electronic spectroscopy in the UV range, the PT equilibrium constants have been measured as a function of temperature in various solvents for various H-bonded systems. They allowed to determine the thermodynamic parameters of the PT process and correlate with various empirical parameters of the solvent activity. The results for Mannich bases [36, 39, 40] correlated with the Dimroth-Reichardt E_T parameter [49, 50] are presented in Figure 14. These correlations present individual straight lines with similar slope for particular Mannich bases. Such clear differentiation shows that the differences in the proton affinity of particular acid-base centers contribute essentially to the stabilization of both forms. The observed effect of solvent activity shows that the proton transfer process is characterized by two factors. Simultaneously, with previous ΔpK_a effect that can be classified as inter one, an additional factor, called an external, takes place, which correlates with the solvent activity expressed by the E_T parameter. Formally, one can express

$$\Delta H^{\circ}_{PT} = \Delta H^{\circ}_{int}\left(\Delta pK_a\right) + \Delta H^{\circ}_{ext}(E_T), \tag{9}$$

however, quantitative estimation of both components is not an easy task.

The attempt has been undertaken to correlate the ΔH°_{PT} values with other parameters characterized the solvent activity, but the best correlation was obtained with E_T. Thus, the external factor contains two effects, that is, the electrostatic stabilization of the ionic form and the donor-acceptor interaction of solvent molecules with the free electron pair of the phenolate oxygen atom. So far, no proton transfer equilibrium was observed in the gas phase that prooves decisive role of the solvent for observation of the proton transfer. This is confirmed by relatively high values of entropy effect, ΔS°_{PT} from -30 up to $-70\,\mathrm{J\,K^{-1}\,mol^{-1}}$ [36, 39, 40] that confirms a considerable redistribution of molecules and high increase of ordering of solvent molecules under influence of intramolecular proton transfer.

The UV spectra were used to locate the position of 50% proton transfer in chloranilic acid-amine complexes; the similar result was deduced from IR and NMR studies [51]. Chranina et al. [52] studied the proton transfer equilibria between hydroxyanthraquinone dyes and aliphatic amines in low-polarity solvents by UV spectroscopy. The shift of this equilibrium in an external electrical field has been observed by the method of electrochromism in the visible region. Also, the mechanism of proton transfer reactions between various acids and amines was studied kinetically by applying UV spectroscopy, when the order and the isotopic ratio effect were discussed [53, 54].

4. Vibrational Polarization of Hydrogen Bonded Systems

It has been broadly postulated by Zundel [55] that for the characteristic dependences of the important physical parameters on ΔpK_N, with the anomalous behavior in the critical region, the large proton polarizability of the hydrogen bonds is responsible. The extraordinary increase in proton polarizability with increased strength of the hydrogen bonds in heteroconjugated systems was the aim of detailed infrared studies conducted by Hawranek's group. For six systems of pentachlorophenol (PCPh) dissolved in different basis, the molar vibrational polarization (P^{vib}, called also atomic polarization as it arises from atomic motions) and molar electronic polarization were determined according to the procedure sketched below. Names of the basis are given in Table 1. The PCPh-base complexes were studied in binary solutions, that is, the proton donor (PCPh) was directly dissolved in an excess of the proton acceptor. Such conditions facilitated accurate determination of optical quantities necessary for calculations of the P^{vib} values, according to the following scheme.

Table 1 shows the P_2^{vib} values along with the position (ν_{max}) and the half width ($\Delta\nu_{1/2}$) of the ν_s(OH) band. The spectral parameters were obtained only for H-bonded systems related to the nonproton-transfer state, their values cannot be estimated with a sufficient accuracy for systems corresponding to other two states (see Figure 2). The plot of the P_2^{vib} values versus ΔpK_a, shown in Figure 15, possess the delta type character with a maximum.

It has to be mentioned here that the measurements in binary system have many advantages that facilitate the used procedure of determination of the molar vibrational polarization. However, there is also one disadvantage: the P^{vib} values are obtained for H-bonded systems differently polarized by their environment. The PCPh-base complexes are immersed in various media that have different macroscopic parameters and more or less strongly polarize the hydrogen bonds. For each system, the ξ and ΔpK_a (crit) parameters should be determined whenever the ΔpK_a values are subjected to the normalization procedure. Due to the lack of such data, the P^{vib} values on Figure 15 are plotted against ΔpK_a parameter. We can guess that the normalization and the different influence of solvents on the vibrational polarization should not meaningfully change the delta-type relation between P^{vib} and strength of the hydrogen-bonded systems.

According to Table 1, the molar vibrational polarization increases from a very small value for TMPh in inert CCl_4 solution, to a slightly larger for the OH group involved in a weak OH$\cdots$Cl intramolecular hydrogen bond in PCPh. Noticeable increase is observed for OH group engaged in a weak intermolecular hydrogen bonds in the PCPh-CH_3CN and PCPh-dioxane systems. Their P^{vib} values compared with that for the 2,4,6-TMPh-CCl_4 indicate on the 17- and 20-fold increase. The changes are strictly correlated with the typical spectral features of H-bond formation, that is, the shift of ν_s(OH) bands towards lower frequencies and the increase in its bandwidth. In relation to the system with intramolecular

Table 1: Spectral parameters related to the ν_s(OH) band and P^{vib} of the H-bond complexes of PCPh.

Acceptor	ν_{max} (cm^{-1})	$\Delta\nu_{1/2}$ (cm^{-1})	P^{vib} (cm^3 mol^{-1})	Reference
CCl_4	3525	21.6	0.048	[56]
CH_3CN	3322	275.5	0.294	[57]
Dioxane-D_8	3162	316.5	0.333	[58]
3-Chloropyridine	2737	945	1.182	[59]
Pyridine	—	—	12.5	[60]
2,4,6-Trimethylpyridine	—	—	17. 8	[61]
Tri-*n*-octylamine	—	—	9.0	[62]
2,4,6-TMPh-CCl_4	3622		0.017	[56]

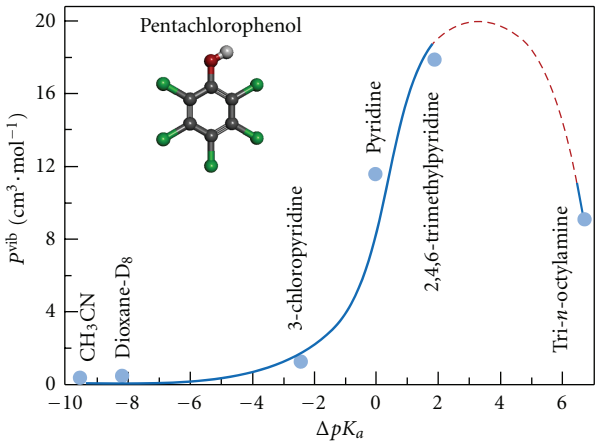

Figure 15: P^{vib} plotted versus ΔpK_a of complexes formed by PCPh with various proton acceptors.

hydrogen bonds (PCPh-CCl_4), the increase is 6-fold for the PCPh-CH_3CN and 7-fold for the PCPh-dioxane complex. It reveals that formation even rather weak intermolecular H-bond, when the proton is located in a relatively narrow single-minimum proton potential near the acid (Figure 1 (1)), leads to a drastic increase in P^{vib} of the OH group.

The PCPh-3-chloropyridine system, with still relatively asymmetrical hydrogen bond, is close to a border between the HB and the PT equilibrium states (see Figure 2). However, its P^{vib} value, compared with that obtained for the system with intramolecular H-bonded, shows almost 25- and 70-fold increase in comparison with the free OH-group in the 2,4,6-TMPh-CCl_4 system. Despite this, the molar vibrational polarization of the PCPh-3-chloropyridine system is still markedly less than its molar electronic polarization.

The complex of PCPh with pyridine with symmetrical O···H···N hydrogen bond is classified to the proton transfer state. The molar vibrational polarization of the OH group rises to 12.5 cm^3·mol^{-1}. This value compared with that obtained for free (2,4,6-TMPh-CCl_4) and for the intramolecularly bonded (PCPh-CCl_4) OH group shows almost 600- and 200-fold increase, respectively.

According to [28], the complex of PCPh with 2,4,5-trimethylpyridine is close to the border between the PT equilibrium and the PT states. Its molar vibrational polarization is more than 370 and 1000 times higher than in the PCPh-CCl_4 and 2,4,6-TMPh-CCl_4 system, respectively. For the PCPh-2,4,6-trimethylpyridine complex hydrogen bond possess largest proton polarizability. The last complex of PCPh with tri-*n*-octylamine belongs to the PT state. According to Figure 15, its P^{vib} value drops almost twice when compared with the previous system. For such large change of P^{vib}, a characteristic evolution of the infrared spectra corresponding to the PT state, shown in Figure 8, is responsible.

Summing up, the very large P^{vib} values determined for PCPh complexes with pyridine and 3-chloropyridine are excellent confirmation of the extraordinary properties of hydrogen bonds from the transition region with symmetrical potential. Moreover, they confirm very well Zundel's concept that an extreme broadening of the OH band occurs for hydrogen bonds showing the largest proton polarizability [55].

References

[1] D. Hadži and H. W. Thompson, Eds., *Hydrogen Bonding*, Pergamon Press, London, UK, 1959.

[2] L. Pauling, *The Nature of the Chemical Bond and the Structure of Molecules and Crystals: An Introduction to Modern Structural Chemistry*, Cornell University Press, Ithaca, NY, USA, 1960.

[3] G. C. Pimentel and A. L. McClellan, *The Hydrogen Bond*, W. H. Freeman, San Francisco, Calif, USA, 1960.

[4] S. N. Vinogradov and R. H. Linnel, *Hydrogen Bonding*, Van Nostrand-Reinhold, New York, NY, USA, 1971.

[5] M. D. Joesten and L. J. Schaad, *Hydrogen Bonding*, Marcel Dekker, New York, NY, USA, 1974.

[6] P. Schuster, G. Zundel, and C. Sandorfy, Eds., *The Hydrogen Bond. Recent Developments in Theory and Experiments*, vol. 1–3, North Holland, Amsterdam, The Netherlands, 1976.

[7] H. Ratajczak and W. J. Orwille-Thomas, Eds., *Molecular Interactions*, John Wiley & Sons, New York, NY, USA, 1980.

[8] P. L. Huyskens, W. A. P. Luck, and Th. Zeegers-Huyskens, Eds., *Intermolecular Forces: An Introduction to Modern Methods and Results*, Springer, Heidelberg, Germany, 1991.

[9] S. Scheiner, Ed., *Hydrogen Bonding. A Theoretical Perspective*, Oxford University Press, Oxford, UK, 1997.

[10] G. A. Jeffrey, *Introduction to Hydrogen Bonding*, Oxford University Press, Oxford, UK, 1997.

[11] D. Hadži, Ed., *Theoretical Treatments of Hydrogen Bonding*, Oxford University Press, Oxford, UK, 1997.

[12] G. R. Desiraju and T. Steiner, *The Weak Hydrogen Bond in Structural Chemistry and Biology*, Oxford University Press, Oxford, UK, 1999.

[13] Th. Elsaesser and H. J. Bakker, Eds., *Ultrafast Hydrogen Bonding Dynamics and Proton Transfer Processes in the Condensed Phase*, Kluwer Academic Publishers, Dordrecht, The Netherlands, 2002.

[14] S. J. Grabowski, Ed., *Hydrogen Bonding—New Insights*, Springer, Dordrecht, The Netherlands, 2006.

[15] Y. Maréchal, *The Hydrogen Bond and the Water Molecule: The Physics and Chemistry of Water Aqueous and Bio-Media*, Elsevier, Amsterdam, The Netherlands, 2007.

[16] G. Gilli and P. Gilli, *The Nature of The Hydrogen Bond: Outline of a Comprehensive Hydrogen Bond Theory*, Oxford University Press, Oxford, UK, 2009.

[17] P. L. Huyskens and Th. Zeegers-Huyskens, "Associations moleculaires et equilibres acide-base," *Journal de Chimie Physique*, vol. 61, aticle 84, 1964.

[18] P. Huyskens, L. Sobczyk, and I. Majerz, "On a hard/soft hydrogen bond interaction," *Journal of Molecular Structure*, vol. 615, no. 1–3, pp. 61–72, 2002.

[19] L. Sobczyk, "Softness of hydrogen bond interaction," *Khimicheskaya Fizika*, vol. 24, article 31, 2005.

[20] L. Sobczyk, "Quasi-symmetric O–H$\cdots$N hydrogen bonds in solid state," *Molecular Physics Reports*, vol. 14, pp. 19–31, 1996.

[21] R. Nouwen and P. Huyskens, "Dipole moments and structure of the complexes of phenols with pyridines," *Journal of Molecular Structure*, vol. 16, no. 3, pp. 459–471, 1973.

[22] S. N. Smirnov, N. S. Golubev, G. S. Denisov, H. Benedict, P. Schah-Mohammedi, and H. H. Limbach, "Hydrogen/deuterium isotope effects on the NMR chemical shifts and geometries of intermolecular low-barrier hydrogen-bonded complexes," *Journal of the American Chemical Society*, vol. 118, no. 17, pp. 4094–4101, 1996.

[23] E. Grech, J. Kalenik, and L. Sobczyk, "^{35}Cl nuclear quadrupole resonance studies of pentachlorophenol-amine hydrogen-bonded complexes," *Journal of the Chemical Society, Faraday Transactions 1*, vol. 75, pp. 1587–1592, 1979.

[24] J. P. Castaneda, G. S. Denisov, and V. M. Schreiber, "Structure of 1 : 1 and 1 : 2 complexes formed by aromatic NH and OH proton donors with aliphatic amines. Possibility of homoconjugated NHN^+ cation formation," *Journal of Molecular Structure*, vol. 560, no. 1–3, pp. 151–159, 2001.

[25] I. Majerz, Z. Malarski, and L. Sobczyk, "Proton transfer and correlations between the C–O, O–H, N–H and O$\cdots$N bond lengths in amine phenolates," *Chemical Physics Letters*, vol. 274, no. 4, pp. 361–364, 1997.

[26] Z. Malarski, M. Roepenk, E. Grech, and L. Sobczyk, "Dielectric and spectroscopic studies of pentachlorophenol-amine complexes," *Journal of Physical Chemistry*, vol. 86, no. 3, pp. 401–406, 1982.

[27] J. Kalenik, I. Majerz, L. Sobczyk, E. Grech, and M. M. M. Habeeb, "Infra-red and ^{35}Cl nuclear quadrupole resonance studies of hydrogen bonded adducts of 2-chlorobenzoic acid derivatives," *Collection of Czechoslovak Chemical Communications*, vol. 55, no. 1, pp. 80–90, 1990.

[28] G. Albrecht and G. Zundel, "Phenol–amine hydrogen bonds with large proton polarizabilities. Position of the OH$\cdots$N $\rightleftharpoons$ $O^{--}\cdots H^+N$ equilibrium as a function of the donor and acceptor," *Journal of the Chemical Society, Faraday Transactions 1*, vol. 80, no. 3, pp. 553–561, 1984.

[29] V. M. Schreiber, A. Kulbida, M. Rospenk, L. Sobczyk, A. Rabold, and G. Zundel, "Temperature effect on proton-transfer equilibrium and IR spectra of chlorophenol-tributylamine systems," *Journal of the Chemical Society, Faraday Transactions*, vol. 92, no. 14, pp. 2555–2561, 1996.

[30] H. Baba, A. Matsuyama, and H. Kokubun, "Proton transfer in *p*-nitrophenol-triethylamine system in aprotic solvents," *Spectrochimica Acta Part A*, vol. 25, no. 10, pp. 1709–1722, 1969.

[31] J. E. Crooks and B. H. Robinson, "Hydrogen-bonded and ion-pair complexes in aprotic solvents," *Faraday Symposia of the Chemical Society*, vol. 10, pp. 29–40, 1975.

[32] H. Romanowski and L. Sobczyk, "Ultraviolet spectra and proton-transfer equilibria in 2,6-dichloro-4-nitrophenol-amine systems," *Journal of Physical Chemistry*, vol. 79, no. 23, pp. 2535–2542, 1975.

[33] M. M. Habeeb and M. A. Kharaba, "Intermolecular hydrogen bonds and proton transfer equilibrium in some nitro cresols-aliphatic amines-acetonitrile or methanol systems," *Journal of Molecular Liquids*, vol. 107, no. 1–3, pp. 205–219, 2003.

[34] M. M. Habeeb and R. M. Alghanmi, "Spectrophotometric study of intermolecular hydrogen bonds and proton transfer complexes between 1,2-dihydroxyanthraquinone and some aliphatic amines in methanol and acetonitrile," *Journal of Chemical and Engineering Data*, vol. 55, no. 2, pp. 930–936, 2010.

[35] Z. Dega-Szafran, E. Dulewicz, and M. Szafran, "Spectroscopic studies of N-methylpiperidine betaine complexes with phenols," *Journal of Molecular Structure*, vol. 704, no. 1–3, pp. 155–161, 2004.

[36] M. Rospenk, "The influence of steric effects of proton-transfer equilibrium in intramolecular hydrogen bonds," *Journal of Molecular Structure*, vol. 221, pp. 109–114, 1990.

[37] V. M. Schreiber, M. Rospenk, A. I. Kulbida, and L. Sobczyk, "Shaping of broad IR absorption in proton transfer equilibrating OH$\cdots$N hydrogen bonded systems," *Spectrochimica Acta—Part A*, vol. 53, no. 12, pp. 2067–2078, 1997.

[38] V. M. Schreiber, A. Koll, and L. Sobczyk, "Effect of temperature on the proton transfer equilibrium in the intramolecular hydrogen bond hydroxyl$\cdots$nitrogen," *Bulletin de l'Academie Polonaise des Sciences, Serie des Sciences Chimiques*, vol. 26, article 651, 1978.

[39] A. Koll, M. Rospenk, and L. Sobczyk, "Thermodynamic parameters for the proton-transfer reaction in Mannich bases," *Journal of the Chemical Society, Faraday Transactions 1*, vol. 77, no. 10, pp. 2309–2314, 1981.

[40] M. Rospenk, I. G. Ruminskaya, and V. M. Schreiber, "Elektronnye spektri i wnutrimolekularnij perekhod protona v osnovanyakh Mannikha v zhidkikh i tverdikh stekloobraznikh rastvorakh," *Journal of Applied Spectroscopy*, vol. 36, article 756, 1982.

[41] M. Rospenk, L. Sobczyk, A. Rabold, and G. Zundel, "Low temperature studies on ultraviolet and infrared spectra of ortho Mannich bases," *Spectrochimica Acta—Part A*, vol. 55, no. 4, pp. 855–860, 1999.

[42] I. Król-Starzomska, M. Rospenk, Z. Rozwadowski, and T. Dziembowska, "UV-visible absorption spectroscopic studies of intramolecular proton transfer in N-(R-salicylidene)-alkylamines," *Polish Journal of Chemistry*, vol. 74, no. 10, pp. 1441–1446, 2000.

[43] M. Rospenk, I. Król-Starzomska, A. Filarowski, and A. Koll, "Proton transfer and self-association of sterically modified Schiff bases," *Chemical Physics*, vol. 287, no. 1-2, pp. 113–124, 2003.

[44] A. Koll, M. Rospenk, L. Sobczyk, and T. Glowiak, "Properties of a strong intramolecular OHO hydrogen bond in 2-(N,N-diethylamino-N-oxymethyl)-4,6-dichlorophenol," *Canadian Journal of Chemistry*, vol. 64, no. 9, pp. 1850–1854, 1986.

[45] S. Kong, I. G. Shenderovich, and M. V. Vener, "Density functional study of the proton transfer effect on vibrations of strong (short) intermolecular O–H$\cdots$N/O$^-\cdots$H–N$^+$ hydrogen bonds in aprotic solvents," *Journal of Physical Chemistry A*, vol. 114, no. 6, pp. 2393–2399, 2010.

[46] T. Lankau and C. H. Yu, "Solubility of methane in water: The significance of the methane-water interaction potential," *Chemical Physics Letters*, vol. 424, article 264, 2006.

[47] P. Gilli, L. Pretto, and G. Gilli, "PA/pKa equalization and the prediction of the hydrogen-bond strength: a synergism of classical thermodynamics and structural crystallography," *Journal of Molecular Structure*, vol. 844-845, pp. 328–339, 2007.

[48] T. Lankau and C. H. Yu, "Correlated proton motion in hydrogen bonded systems: tuning proton affinities," *Physical Chemistry Chemical Physics*, vol. 9, no. 2, pp. 299–310, 2007.

[49] C. Reichardt, "Empirical parameters of the polarity of solvents," *Angewandte Chemie International Edition in English*, vol. 4, no. 1, pp. 29–40, 1965.

[50] C. Reichardt and K. Dimroth, "Solvents and empirical parameters for characterization of their polarity," *Fortschritte der Chemischen Forschung*, vol. 11, article 1, 1968.

[51] M. Habeeb, H. Alwakil, A. El-Dissouky, and H. Abdel-Fattah, "Spectroscopic studies of 1:1 chloranilic acid-amine complexes," *Polish Journal of Chemistry*, vol. 69, article 1428, 1995.

[52] O. V. Chranina, F. P. Czerniakowski, and G. S. Denisov, "UV-vis electrochromism due to proton transfer," *Journal of Molecular Structure*, vol. 177, pp. 309–315, 1988.

[53] W. Galezowski and A. Jarczewski, "Kinetics, isotope effects of the reaction of 1-(4-nitrophenyl)-1-nitroalkanes with DBU in tetrahydrofuran and chlorobenzene solvents," *Canadian Journal of Chemistry*, vol. 68, no. 12, pp. 2242–2248, 1990.

[54] A. Jarczewski, G. Schroeder, and K. T. Leffek, "The proton transfer reaction between bis(2,4-dinitrophenyl)methane and nitrogen bases in dimethyl sulfoxide and toluene solvents," *Canadian Journal of Chemistry*, vol. 69, no. 3, pp. 468–473, 1991.

[55] G. Zundel, "Hydrogen bonds with large proton polarizability and proton transfer processes in electrochemistry and biology," *Advances in Chemical Physics*, vol. 111, 2000.

[56] J. P. Hawranek and B. Czarnik-Matusewicz, "Infrared dispersion of H-bonded systems. The dielectric function for weak complexes," *Chemical Physics Letters*, vol. 109, no. 2, pp. 166–169, 1984.

[57] J. P. Hawranek and B. Czarnik-Matusewicz, "Infrared dispersion of the H-bonded pentachlorophenol-acetonitrile complex," *Chemical Physics Letters*, vol. 138, no. 5, pp. 397–400, 1987.

[58] J. P. Hawranek and B. Czarnik-Matusewicz, "IR dispersion of hydrogen bonded systems III. Pentachlorphenol—dioxane-D8 complex," *Journal of Molecular Structure*, vol. 143, no. C, pp. 337–340, 1986.

[59] B. Czarnik-Matusewicz and J. P. Hawranek, "Infrared dispersion of the hydrogen-bonded pentachlorophenol—3-chloropyridine complex," *Journal of Molecular Structure*, vol. 219, pp. 221–226, 1990.

[60] J. P. Hawranek, B. Czarnik-Matusewicz, and W. Wrzeszcz, "Infrared dispersion of the hydrogen-bonded pentachlorophenol-pyridine complex," *Journal of Molecular Structure*, vol. 322, pp. 181–186, 1994.

[61] J. P. Hawranek, J. Z. Flejszar-Olszewska, and A. S. Muszynski, "Infrared dispersion of the pentachlorophenol-sym-collidine complex," *Journal of Molecular Structure*, vol. 448, no. 2-3, pp. 149–159, 1998.

[62] J. P. Hawranek and A. S. Muszynski, "Infrared dispersion of the pentachlorophenol-trioctylamine complex," *Journal of Molecular Structure*, vol. 552, no. 1–3, pp. 205–212, 2000.